



Forschungszentrum Karlsruhe
Technik und Umwelt

Wissenschaftliche Berichte
FZKA 6215

**Proceedings of the
Workshop ANI 98**

**Current Topics of Cosmic Ray
Research with EAS Observations**

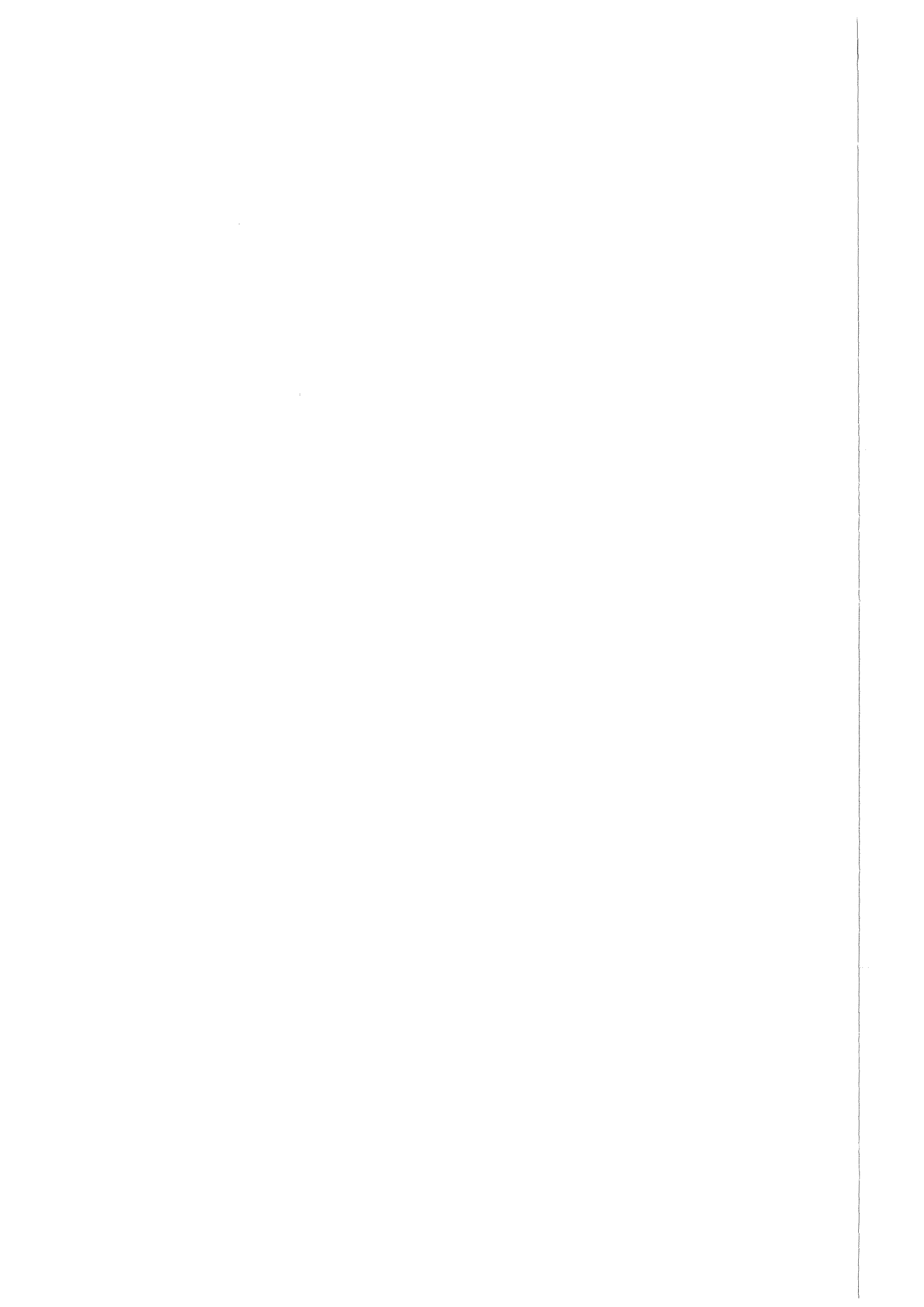
**Nor-Amberd Station of the Mt. Aragats
Cosmic Ray Observatory, Armenia
May 29 – June 5, 1998**

Editors:

**A. A. Chilingarian, H. Rebel, M. Roth,
M. Z. Zazyan**

Institut für Kernphysik

Dezember 1998



FORSCHUNGSZENTRUM KARLSRUHE
Technik und Umwelt

Wissenschaftliche Berichte
FZKA 6215

Proceedings of the Workshop ANI 98

Current Topics of Cosmic Ray Research
with EAS Observations

Nor-Amberd Station of the Mt. Aragats Cosmic Ray
Observatory
Armenia
May 29 – June 5, 1998

Editors: A.A. Chilingarian¹, H. Rebel, M. Roth and M.Z. Zazyan¹

Institut für Kernphysik

¹*Yerevan Physics Institute, Cosmic Ray Division, Yerevan, Armenia*

Forschungszentrum Karlsruhe GmbH, Karlsruhe
1998

Als Manuskript gedruckt
Für diesen Bericht behalten wir uns alle Rechte vor

Forschungszentrum Karlsruhe GmbH
Postfach 3640, 76021 Karlsruhe

Mitglied der Hermann von Helmholtz-Gemeinschaft
Deutscher Forschungszentren (HGF)

ISSN 0947-8620

Preface

The energy spectrum of primary cosmic rays, which covers 11 orders of magnitudes and extends to energies beyond 10^{20} eV is remarkably structureless and boring. In fact, the power-law fall-off with increasing energies, giving witness of the nonthermal character of the processes producing and accelerating nuclei in the cosmos, shows merely with the so called knee a conspicuous change in the spectral index, i.e. an almost abrupt steepening of the spectrum at about ca. $3 \cdot 10^{15}$ eV. This phenomenon has been first observed in the shower size spectrum by Kulikov and Khristiansen in 1958. In spite of a lapse of time of 40 years the origin of the knee has not yet clarified and even the details of the knee region, how the slope is changing and where the knee position (in whatever way defined) is located, are open questions. Various alternative current theories about the astrophysical origin of the knee predict not only details of the shape of energy distribution, but also specific variations of mass composition of the primary spectrum in the knee region. With these aspects various extended detector arrays, observing the development of Extensive Air Showers (EAS), have been put in operation in recent years. The approach of the KASCADE experiment (located 110m a.s.l.) is of particular interest due to its basic concept of observing simultaneously the electron-photon, the muon and hadron components and determining a larger number of EAS observables for each individual shower and a correlation analysis based on detailed Monte-Carlo EAS simulations, invoking as generator hadronic interaction models. In this way the influence of intrinsic shower fluctuations and the model dependence are expected to get minimised. Adequate methods for such analyses, based on techniques of advanced statistical approaches, have been developed in the Cosmic Ray Department of the Yerevan Physics Institute and have been successfully applied to the interpretation of the experimental data. The Yerevan Physics Institute is also leadingly operating the Cosmic Ray Observatory ANI with two detector arrays (GAMMA and MAKET) located on Mt. Aragats (3250m a.s.l.), which are showing up with first experimental data about the shower size spectrum and the muon component. Accurate data of EAS observations of high mountain altitudes are of great interest, since the fluctuations of the shower development are less pronounced and do less obscure the nature of the initiating primary. Thus, there are prospects for a future combined consideration of KASCADE and ANI data with increased information potential.

The present proceedings are the outcome of a workshop of scientists participating in the investigations of ANI and KASCADE, partly in collaborative groups. The main focus has been a discussion of the relevant EAS observables and of the methods of analyses in terms of the primary energy spectrum and mass composition, illustrated by recent results of the different detector setups. Special emphasis has been put on methodical aspects and the clarification of experimental problems in determining EAS observables. Various contributions stressed clearly the preliminary character of the results and point to open problems. A proposal with technical details has been presented to extend the muon observation of the underground GAMMA detectors by measurements of the muon arrival time distributions. A scholar presentation about the frontier status of our understanding of the high-energy hadronic interaction and experimental tests of the Monte-Carlo EAS simulation program CORSIKA did flank the illustrations of the application of the advanced analysing methods.

A particular event embedded in the meeting of about 35 scientists in the Nor-Amberd Station of the Mt. Aragats observatory has been the academic celebration of the anniversary of the Academician Prof. Dr. Tina Asatiani with a special session of the workshop. With an extremely nice and warm laudatio Prof. Egyan (Yerevan Physics Institute) introduced the audience into the great merits of Tina Asatiani for cosmic ray and particle physics, illustrating - also with personal anecdotes - her engagement for the experimental facilities on Mt. Aragats. Many developments of contemporary cosmic ray and hadronic interaction physics, theoretically and experimentally - like the recent arguments of studies of muon charge ratio in the atmospheric flux - originate from her early ideas. Tina's reply to the attentive audience, with lively interest in the current scientific problems and encouragement for the younger physicists - corroborated the impression of her exceptional personality as scientist and human being of high social responsibility. Remarkably the amiable Grande Dame of the field advocated strongly just larger experimental efforts to improve the reliability, accuracy and statistical relevance of the experimental data as reasonable prerequisite of interpretation attempts. In fact, that recommendation is one of the results of the workshop, which has prompted various new ideas and did clarify the present standings and future necessities. We are looking forward with hope to the initiated progress.

Finally we would like to thank all participants and contributors for the fruitful discussion atmosphere, Mrs. Susanna Safaryan and the staff of the Nor-Amberd station for the valuable help in organising the meeting and the Yerevan Physics Institute for sponsoring the workshop. The participants from abroad acknowledge the kind hospitality in Armenia and the travel support from various funding agencies: Osteuropa -Verbindungsbüro des Bundesministeriums für Wissenschaft und Bildung (Deutschland), Volkswagen Foundation (Deutschland) and Centre d'Etudes Nucléaires de Bordeaux-Gradignan (France). We would like to thank the Ministries of Industry and Science of Armenian Government for the support of the investigations on Mt. Aragats high altitude mountain station (grants 96-752, 96-852, and 94-964).

Yerevan - Karlsruhe in December 1998

The editors



Tina L. Asatiani, born in March, 12, 1918 in Tbilisi (Georgia), Professor Emeritus of the Yerevan State University and member of the National Academy of Sciences of Armenia, celebrated her anniversary in an academic session in the frame of the ANI 98 meeting. With her scientific activities of broad horizon, with more than two hundred publications in international journals of considerable impact in particle and cosmic ray physics, Tina, holder of many honourable awards and prizes, has distinctly influenced the development of the field, in Armenia, in particular. We admire her exceptional engagement, being active till today in science and social life, initiating and guiding aid programmes with her great public reputation, and we love her warm and amiable personality.

MANY HAPPY RETURNS !

PARTICIPANTS

IK - KASCADE, Forschungszentrum Karlsruhe, Germany

J. Hörandel
H. Mathes
H. Rebel
S. Riess
M. Roth

Centre d'Études Nucléaires de Bordeaux -Gradignan, France

P. Aguer
J. Procureur

National Institute for Physics and Nuclear Engineering, Bucharest, Romania

I.M. Brancus

Institute of Nuclear Physics, Moscow State University, Russia

S. Ostapchenko

International Science and Technology Center, Moscow, Russia

Y.I. Malakhov

Yerevan Physics Institute, Armenia

T.L. Asatiani	E.V. Korkotyan
V.Kh. Babayan	R.M. Martirosov
H.G. Bakhshetyan	L.G. Melkumyan
N.Kh. Bostandjyan	R.L. Mkrtchyan
A.A. Chilingarian	E.A. Mnatsakanyan
K.Sh. Eryan	V.A. Sahakyan
A.P. Garyaka	S.V. Safaryan
G.V. Gharaguozyan	K.E. Sogoyan
A.S. Hairapetyan	S.M. Sokhoyan
L.S. Haroyan	S.V. Ter-Antonyan
A.P. Hovhanissyan	A.A. Vardanyan
G.G. Hovsepyan	M.Z. Zazyan
V.A. Ivanov	

Proceedings of the Workshop ANI 98

Current Topics of Cosmic Ray Research with EAS Observations

Nor-Amberd Station of the Mt. Aragats Cosmic Ray Observatory, Armenia,
May 29 – June 5, 1998

Editors: A.A. Chilingarian, H. Rebel, M. Roth and M.Z. Zazyan

CONTENT

Preface	iii
Tina L. Asatiani	v
Participants	vi
EAS signatures for mass discrimination of cosmic rays investigated by the KASCADE experiment <i>H.Rebel - KASCADE collaboration, Forschungszentrum Karlsruhe</i>	1
Cosmic ray mass composition in the PeV region estimated from the hadronic EAS component <i>J.R.Hörandel - KASCADE collaboration, Forschungszentrum Karlsruhe</i>	15
Nonparametric determination of energy and elemental composition of cosmic rays from EAS observables <i>A. Vardanyan, M. Roth, A.A. Chilingarian - KASCADE collaboration, Yerevan Physics Institute and Forschungszentrum Karlsruhe.....</i>	19
Application of nonparametric methods to the analysis of EAS observables for determining energy and elemental composition of cosmic rays <i>M. Roth, A. Vardanyan, A.A. Chilingarian - KASCADE collaboration, Forschungszentrum Karlsruhe and Yerevan Physics Institute</i>	23
Measurements of the characteristics of the soft EAS component with the GAMMA array <i>A.P. Garyaka - ANI collaboration, Yerevan Physics Institute</i>	31
The EAS muon characteristics measured by the GAMMA installation <i>A.A. Chilingarian, A.V Darian, V.S.Eganov, A.P. Garyaka, V.A. Ivanov, E.A. Mamidjanian, R.M. Martirosov, N.M. Nikolskaya, J. Procureur, V.A. Romakhin, B.V. Subbotin, Yerevan Physics Institute - Lebedev Institute Moscow - Centre d'Etudes Nucléaires Bordeaux.....</i>	27
Studies of the muon detector response of the GAMMA installation with the simulation	

program ARES <i>M.Z. Zazyan - ANI collaboration, A. Haungs, Yerevan Physics Institute and Forschungszentrum Karlsruhe</i>	37
Determination of the measurement accuracy of the GAMMA array <i>L.S. Haroyan, Yerevan Physics Institute</i>	41
The measurement of the EAS charged particle component using a logarithmic ADC <i>G.G. Hovsepyan - ANI collaboration, Yerevan Physics Institute</i>	45
EAS size spectrum for $1 \cdot 10^5 \leq N_e \leq 5 \cdot 10^7$ measured by the MAKET installation <i>G.V. Gharagozyan - ANI collaboration, Yerevan Physics Institute</i>	51
Investigation of the integral EAS size spectra in the knee region <i>S.H. Sokhoyan - ANI collaboration, Yerevan Physics Institute</i>	55
Expected cosmic ray background flux at Aragats level <i>S.V. Ter-Antonyan, R.S. Ter-Antonyan, Yerevan Physics Institute</i>	61
The alpha parameter is model independent <i>M. Brankova, R.M. Martirosov, N.M. Nikolskaya, V. Pavlyuchenko, J. Procureur, J.N. Stamenov, Institute for Nuclear Research and Nuclear Energy Sofia - Yerevan Physics Institute - Lebedev Institute Moscow - Centre d'Etudes Nucléaires Bordeaux</i>	69
Studying a new possibility of EAS selection <i>L.G. Melkumyan - ANI collaboration, Yerevan Physics Institute</i>	73
Correlation features of muon arrival time and angle of incidence distributions from EAS simulations at sea level and high mountain altitude <i>A.F. Badea, I.M. Brancus, M. Duma, A. Haungs, H.J. Mathes, H. Rebel, B. Vulpescu, A.A. Chilingarian, NIPNE Bucharest - Forschungszentrum Karlsruhe and Yerevan Physics Institute</i>	77
Extension of the GAMMA muon underground detectors for studies of the longitudinal air shower development <i>H.-J. Mathes, H.J. Gils, H. Rebel, A.F. Badea, H. Bozdog, I.M. Brancus, M. Petcu, A.A. Chilingarian, G. Hovsepian, V. Ivanov, R. Martirosov, Forschungszentrum Karlsruhe - NIPNE Bucharest and Yerevan Physics Institute</i>	91
The universal approach to superhigh energy hadron production <i>H.J. Drescher, M. Hladik, K. Werner, S. Ostapchenko, Université de Nantes and Moscow State University</i>	99
On the differences in high energy hadronic interaction models and their influence on the calculated EAS characteristics <i>N. Kalmykov, S. Ostapchenko, Moscow State University</i>	103

Test of high-energy hadronic interaction models using the hadronic shower core measured with the KASCADE calorimeter <i>J.R. Hörandel - KASCADE collaboration, Forschungszentrum Karlsruhe</i>	107
Verification of the CORSIKA code in the 0.01-500 TeV energy range <i>S.V. Ter-Antonyan, L.S. Haroyan, Yerevan Physics Institute</i>	115
The charge ratio of cosmic ray muons <i>I.M. Brancus, B. Vulpescu, J. Wentz, H. Rebel, A.F. Badea, H. Bozdog, M. Duma, A. Haungs, H.-J. Mathes, M. Petcu, M. Roth, NIPNE Bucharest and Forschungszentrum Karlsruhe</i>	121
Collaborations	131



EAS signatures for mass discrimination of cosmic rays investigated by the KASCADE experiment

Heinigerd Rebel for the KASCADE collaboration

*Forschungszentrum Karlsruhe, Institut für Kernphysik
P.O.B.3640 - D 76021 Karlsruhe, Germany*

The extensive air shower experiment KASCADE which investigates the features of the dominant components (hadrons, muons and electromagnetic particles) of extensive air showers (EAS) aims at a determination of the elemental composition of high-energy cosmic rays in a region around and above the so-called knee of the energy spectrum. A sufficiently detailed knowledge of the chemical composition provides key information about the astrophysical sources and acceleration mechanisms of cosmic rays, in particular about the origin of the knee. Various signatures of the EAS observables, explored by the KASCADE measurements for mass discrimination of the EAS primaries, and the methodical concept of the KASCADE approach are discussed in detail. The present status of current results and our knowledge about the elemental composition in the knee region are briefly reviewed.

Introduction

"Multum non multa" (C. Plinius Secundus, 23-79 p.Ch.n.)

This lecture addresses the EAS signatures on the mass composition of cosmic rays in the knee region, which we are currently investigating in the KASCADE experiment [1], the present status of information and our actual understanding of the problem. The current experimental results illustrate the concepts, but they must be considered to be still preliminary, due to lack of sufficient statistical accuracy, in addition to the fact that we are still in the process of elaborating adequate data evaluating and analysing procedures of statistical relevance, and of refining the quality of the experimental apparatus.

Signatures of Mass Composition

"Omnium rerum principia parva sunt" (Marcus Tullius Cicero, 106-43 a.Ch.n.)

The identification of hadronic interaction effects and of the nature of the primary by extensive air shower studies requires a detailed modeling of the shower development by Monte - Carlo methods, following each individual particle from production to destruction, decay or passage through the plane of observation, and displaying the fluctuations arising from the stochastic mechanisms governing the processes. The most important features of the hadronic interactions to be taken into account are :

- the number of secondary particles produced in high-energy collisions increases with the primary particle energy, but less than in linear proportion,
- the average fraction of energy converted into secondary particles is about 50% and nearly energy - independent,

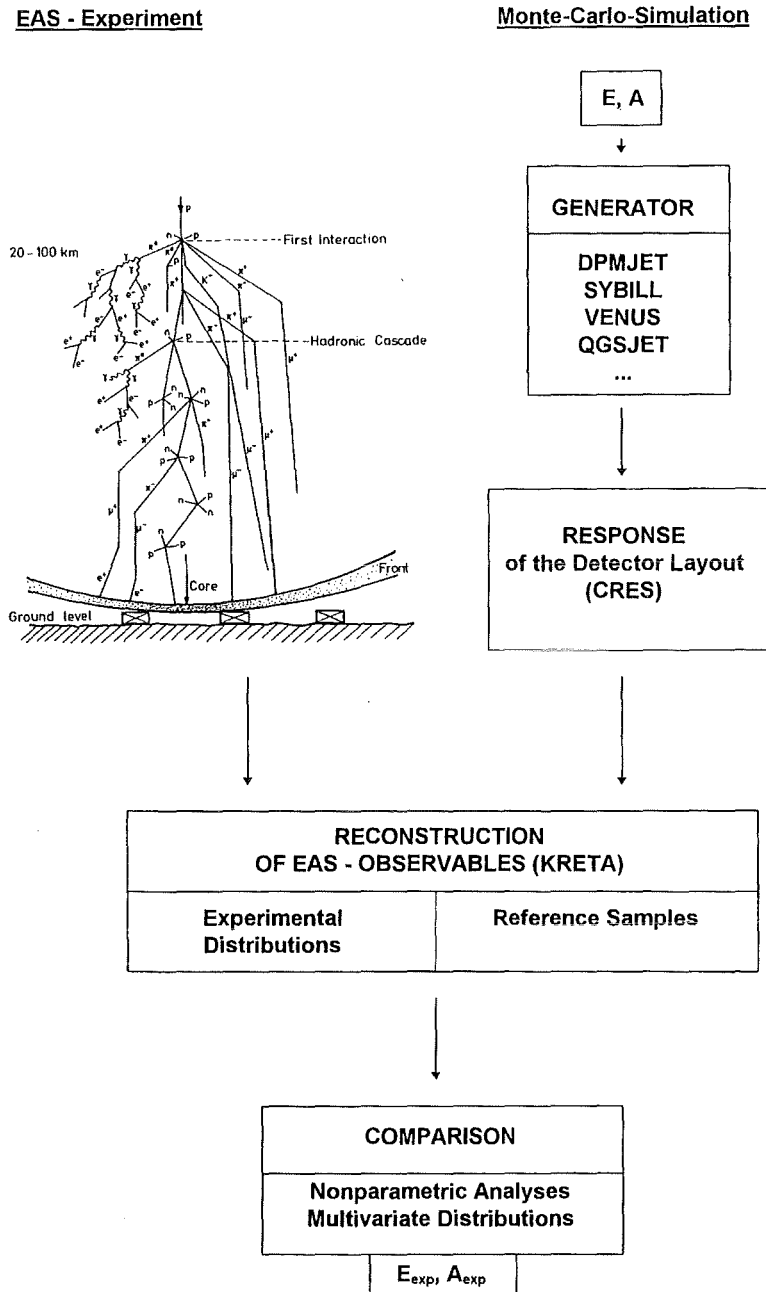


Fig. 1: *General Scheme of the Analysis.*

- as a consequence the average energy of secondary particles increases faster than proportional to the primary energy,
- the mean transverse momentum of the secondaries increases only slowly with energy.

In adequate formulations as Monte Carlo generators various models, based on the Regge -

Gribov theory, together with proper algorithms, are the basis of our code CORSIKA (Cosmic Ray Simulations for KASCADE) [2] for guiding the extrapolations of accelerator results to ultrahigh energies.

The general scheme of the procedures analysing the EAS observation is sketched in the diagram (Fig. 1). Using the Monte-Carlo simulations we construct pseudo-experimental data (folding with the apparatus response by the programs CRES), which correspond to the real data and from which we can reconstruct (by KRETA) equivalent distributions of any shower variable, we would like to compare. The "king way" of such a comparison procedure is the application of statistical techniques of multivariate analyses of non-parametric distributions [3, 4]. On this way we are able to specify various kinds of uncertainties and to quantify the relevance of the results. An inherent difficulty of this way, however, is the model dependence and the necessity of a sufficient statistical accuracy, also in the Monte-Carlo simulations, in an extent, sufficient to represent realistically the fluctuations of the shower variables. When looking for observables, discriminating the mass of the primary, we should realize that the appearance of an extensive air shower at the observation level is critically influenced by the first interactions at the beginning of the cascade, reflected by the longitudinal development.

Fig. 2 displays the longitudinal development of the electromagnetic and muonic components, the total number of electrons and photons (the shower size N_e) and the muon number N_μ , for showers initiated by 1 PeV protons and 1 PeV Fe, respectively. The "error bars" represent the range of fluctuations. The faster development of the heavy primary induced shower reflects not only the smaller interaction length, but also the smaller energy of the secondaries at the same primary energy.

a. N_μ - N_e correlation

"Omnia praeclara rara sunt" (Marcus Tullius Cicero, 106-43 a.Ch.n.)

The inspection of the longitudinal shower development immediately reveals a signature for mass differences: the muon content N_μ at a certain observation level as compared to N_e . A heavy mass shower of the energy E is approximately borne out by the superposition of A leading nucleons of the energy E/A . Due to the weak increase of the multiplicity with energy, A nucleons produce more secondaries than one single nucleon with the higher energy E . Most secondaries are π -mesons. Charged π -mesons (and K-mesons) decay in muons.

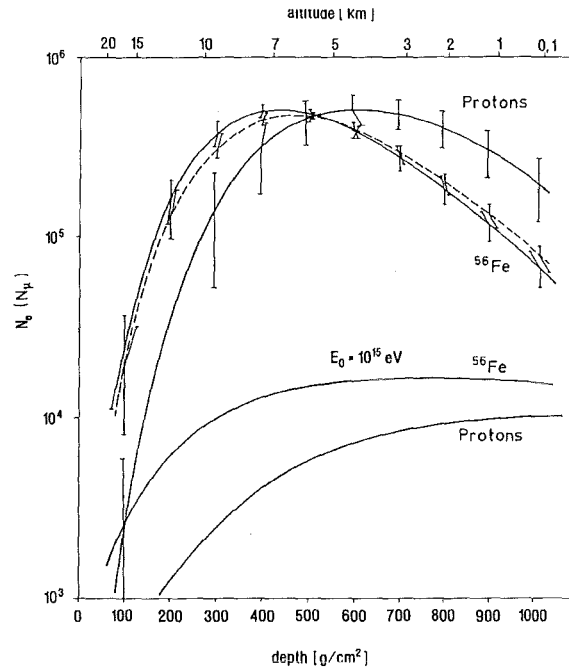


Fig. 2: *Simulated Longitudinal Development of the Electron-Photon and of the Muon Component (The Dashed Line for the N_e Development of the Fe-showers represents the Prediction by a Fragmentation Model).*

- **Shower Size N_e - Muon Content N_μ - Correlation**

Reason: Weak dependence of the multiplicity n_p of the secondaries on the energy of the interacting nucleon

$$n_p(E) \propto \ln E$$

$$n_A(E) \propto A \ln(E/A)$$

- **Structure of the Energy and Lateral Distributions of Hadrons and Muons in the Shower core**

Reason: Smaller deflection angles and larger energies of the secondaries in proton induced showers than in heavy ion induced showers of the same primary energy

- **Distributions of the Relative Arrival Time and Angles-of-Incidence of the EAS-Muon Components**

Reason: Mapping the longitudinal shower profile and differences in the development of the muonic component (height of maximum) of EAS of different primary sources

Table 1: *EAS Observables with Signatures of the Mass of the Primary*

This is the basis of the $N_\mu - N_e$ correlation method and its variants. The signal is actually enhanced by the comparatively smaller electromagnetic content at observation level due to an earlier development of the "heavy" cascade, i.e. at the same primary energy the shower size is significantly smaller for iron induced showers than for showers of proton primaries. Thus, an important signature can be obtained by the study of frequencies of muon numbers for fixed N_e , e.g.

Theoretically a mass-sensitive correlation of the muon number with the electron number can be worked out by detailed Monte-Carlo simulations, displayed in Fig. 3 for proton and iron induced showers of the energy 10^{14} and 10^{15} eV, respectively. The contour lines represent the half-width maximum of the distribution (CORSIKA-VENUS generator pronounced). The predicted correlation is dependent from the particular interaction model. The variation due model dependence is shown. Actually the $N_\mu - N_e$ correlation is the most powerful discriminator, and all other signatures just help to shrink the fluctuations and model dependence, especially the hadronic observables do so.

In detail the mass discrimination of the $N_\mu - N_e$ correlation results from a complicated competition of various features. It depends not only on the multiplicity spectra, but also on the energy spectra and thus from the detection thresholds, due to the fact that the proton induced showers have harder energy spectra of the secondaries than Fe induced showers. This feature is important for deep - underground observations of muon bundles. It is also relevant for installations like KASCADE with a hadron calorimeter, since the hadron spectra show the same effect.

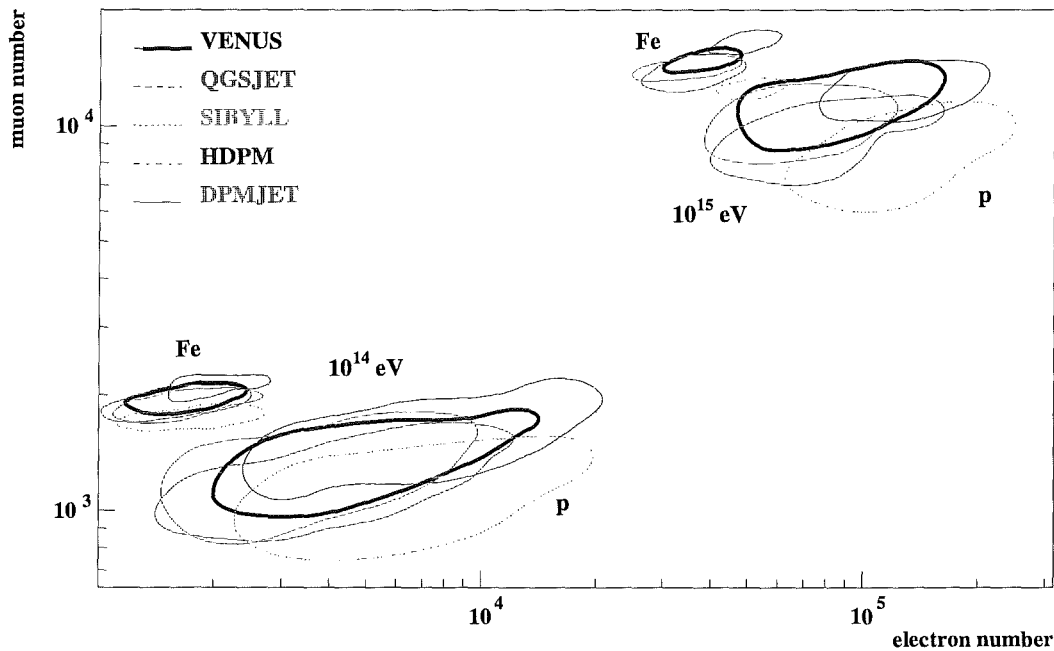


Fig. 3: The N_μ - N_e Correlation as predicted by Monte-Carlo Simulations (CORSIKA) on Basis of Different Interaction Models.

Unfortunately the experimental application of the N_μ - N_e correlation implies some difficulties. In most detector setups, if the muon detectors are not extremely shielded, the punch-through of the electromagnetic component in the shower center spoils the discrimination of muons there. In addition, due to the large lateral extension and fluctuations of the muon component at large distances from the shower center the extrapolations of the lateral distribution appear rather uncertain. As a consequence the total number N_μ is rather difficult to determine in an unbiased way, and it might have been never correctly done. In cases, quoting a measured total muon number, an extrapolation of an adequate parametrisation like the Greisen form has been invoked, fitted in an experimentally well determined, but a restricted range of the lateral distribution. From these reasons the KASCADE applies the correlation method in a modified variant, using as observable the *truncated muon number* N_μ^{tr} , the inte-

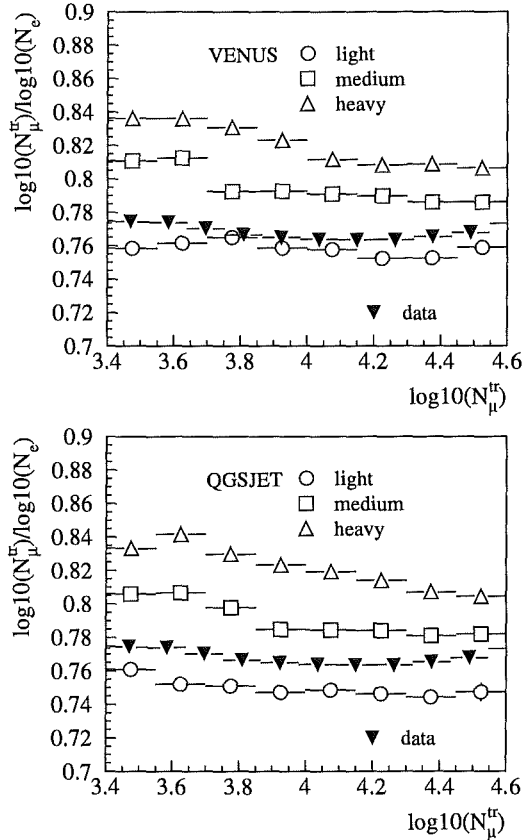


Fig. 4: N_μ^{tr}/N_e Ratio versus N_μ^{tr}

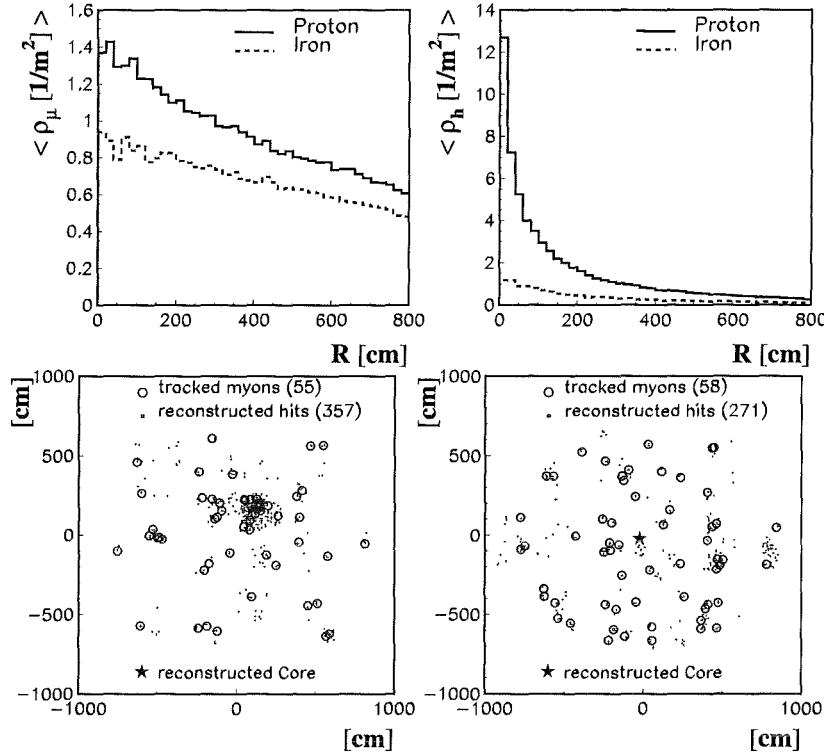


Fig. 5: *Density Distributions in the EAS Core*

grated muon intensity between 40 and 200

m from the shower core. As evidenced by simulations and as consequence of a fortunate interference of effects arising from different shapes, energy distributions and intensities for the KASCADE conditions, this quantity proves to be nearly independent from the mass of the primary and is proportional to primary energy in range of 10^{14} to 10^{16} eV. Hence by introducing N_μ^{tr} as nearly mass independent energy identifier we lose the sensitivity of the muon number to the primary mass, and the mass discrimination is completely based on the different development of the electromagnetic EAS component and its fluctuations. For a first orientation the experimental findings can be displayed by comparing the theoretical expectations of the N_μ^{tr}/N_e ratio versus N_μ^{tr} (i.e. approximately the energy) with the data (Fig. 4). The trend to a heavier composition beyond the knee ($N_\mu^{tr} = 4.1$) is indicated. A methodically more consistent analysis of the N_μ^{tr}/N_e ratio together with other EAS observables using advanced statistical methods will be discussed in detail in the presentation by M. Roth and A.Vardanyan [4].

b. Appearance of the shower core

" Medio tutissimus ibis " (Publius Ovidius Naso, 43 a.Ch.n. - 18 p. Ch.n.)

Additional effects arise from the transverse momentum distribution of the secondaries. The smaller deflection angles in proton induced showers lead to a steeper lateral distribution. This is particularly pronounced for the penetrating muon component, which is less absorbed and less deflected by Coulomb scattering and carries original information about the air shower cascade. Consequences of these features of the lateral distributions together with the differences in the energy spectra are observable differences, in particular, in the **appearance of the muonic and hadronic components in shower center of**

EAS of different mass primaries.

The upper part of Fig.5 displays the average distributions of muons and hadrons ($E_{\mu,h} > 2$ GeV), simulated for the primary energy spectrum above 1 PeV. The lower part shows the two-dimensional patterns observed for single EAS with the position sensitive MWPC under the iron sampling calorimeter of KASCADE. Comparing with simulations, fully taking into account the detector response, these hit distributions can be analysed by an adequate pattern recognition procedure. The observed patterns contain also secondaries produced in the central detector itself:

in addition to muons, hadrons of the high energy tails of the hadron spectra, δ -electrons, small electromagnetic showers following pair- and bremsstrahlung production by high energy muons. All features are discriminative, and in this sense we may say: We use the central detector of KASCADE as an active spectrometer enhancing the spectral differences by secondary effects [5, 6]. The characteristics of the distributions can be quantified by a parametrisation in terms of multifractal moments, which have been shown by the simulation studies [5] to be significant in view of mass information.

We shall not discuss in detail this type of analysis and classification of seemingly irregular patterns. In brief, we derive from these patterns three mass sensitive parameters: the total intensity N_{μ}^ and two so-called generalised multifractal dimensions D_6 and D_{-6} which are added to other shower parameters as input of a neural network trained with corresponding simulated results. To derive the multifractal quantities the area (R) around the estimated shower core is divided in M circular rings of equal size (in area): $M=2,4,8,16... 2^N$, and the moments G_q from the number of hits in the ring are calculated. It can be shown that these multifractal moments follow a power law relation, what is in fact the basic condition for self-similar behaviour and justifies this type of analysis.*

The output of the analysis is displayed in Figs. 6 and 7.

(i) The variation of the average of the net parameter which indicates the average mass with some unspecified calibration. We notice a slight increase beyond the knee ($\log N_{\mu}^{tr} \approx 4.1$) in the data.

(ii) The relative abundances deduced with the assumption of different mass groups indicate the same feature.

This result indicates a derichment of the light nuclei in cosmic rays at the knee [5] (see "Haungs" in the compilation of Fig.11d). Of course, such a single result has still to be detailed by a more specific determination of primary energy, by improving the statistical and systematic accuracy and by correlating with further significant shower parameters. Actually this result has been the first KASCADE indication about the general trend and is now going to be further refined by other observations of KASCADE, especially with the $N_{\mu} - N_e$ correlation. The KASCADE central detector, which consists basically of an iron sampling calorimeter for identification and energy measurements of hadrons (10 GeV - 20 TeV) in the EAS core allows a detailed experimental study of the lateral and energy distributions of the EAS

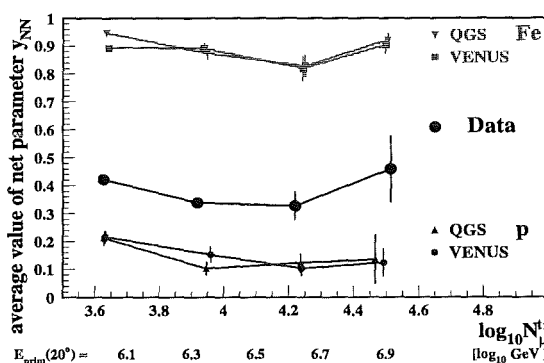


Fig. 6: Variation of the Mass Indicative Net Parameter with $\log N_{\mu}^{tr}$

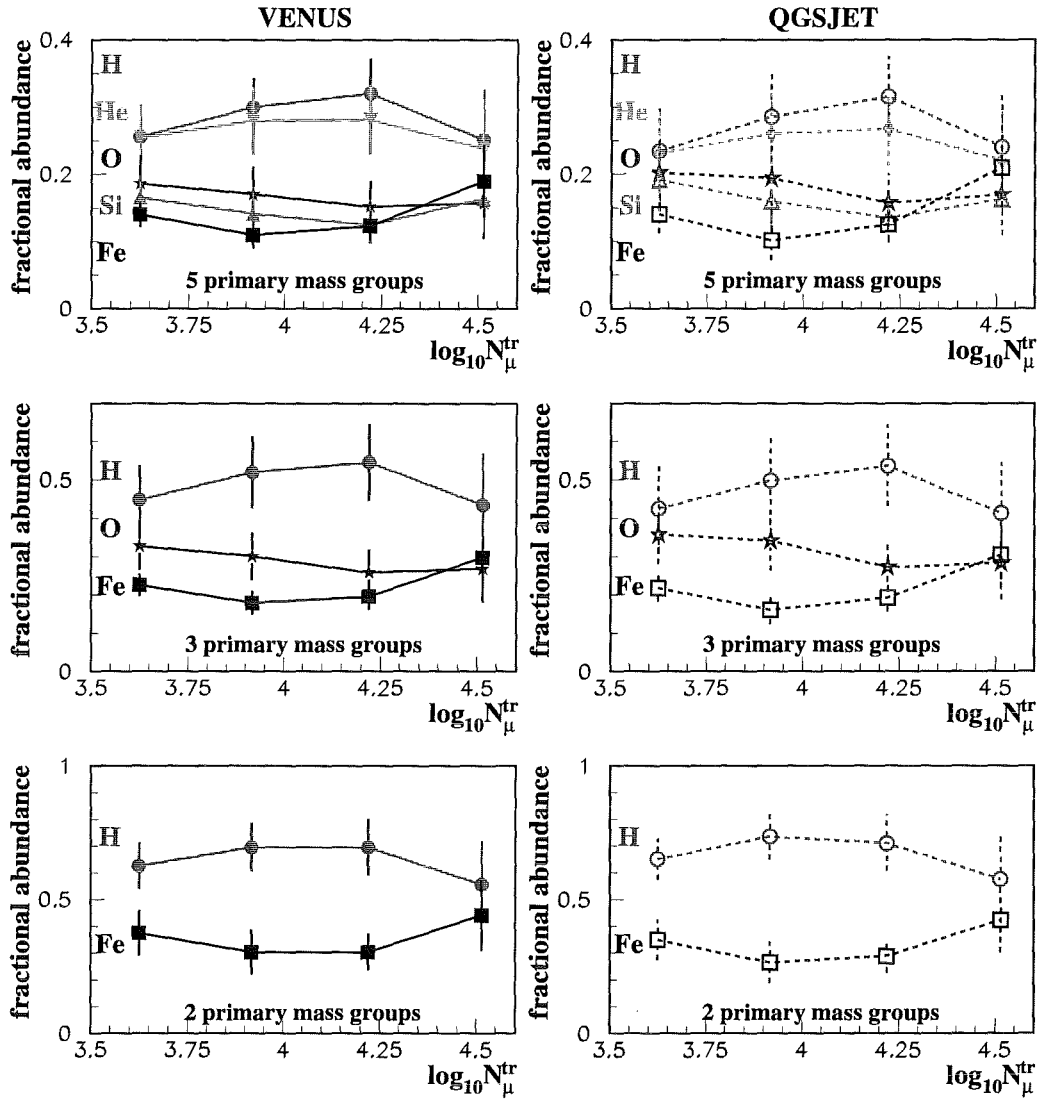


Fig. 7: *Relative Abundances of Various Composition Groups.*

hadrons. They carry information on the mass composition, whose analysis and results (see also Fig. 11) will be discussed in the contribution of J.Hörandel [7].

c. Muon arrival time distributions

"Utere tempore" (Epikur, 341-270 a.Ch.n.)

In fact, our problem about interaction and nature of the primary would be more accessible, if we could observe the longitudinal development of the cascade, and not only the lateral appearance at a certain observation level. In this respect the angle - of - incidence and the arrival - time distributions of higher energy muons provide interesting information.

The time profile (the time dispersion) of the muon shower disc is a coded picture of the longitudinal shower development, and observed at larger distances, it can be approximately related to the production height of muons (Fig. 8).

The basic idea of the "time-of-flight" observation and its interpretation is indicated by the triangulation procedure, ignoring velocity dispersion and scattering of muons in air. We expect that arrival time of Fe appears with an earlier distribution than that for protons, which probe deeper and with larger fluctuations into the atmosphere (Fig. 9).

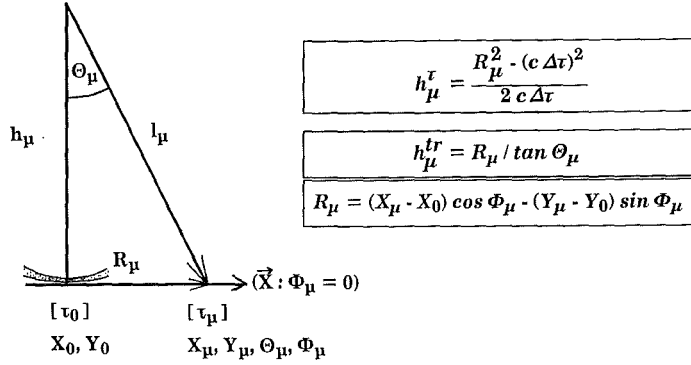
Advantages of muons:

- Enhanced sensitivity to earlier stages of the EAS cascade
- Directly coupled to the nuclear cascade and not mediated by the e/γ component like \dot{C} -photons
- "Seen" all the day, not only in clear and moonless nights

$$\tau_\mu = f(E_0, E_\mu, R_\mu, \Theta)$$

Muon delay time:

$$\begin{aligned} \Delta\tau_\mu &= \tau_\mu(R_\mu) - \tau_{\text{core}} \\ &= l_\mu / \beta_\mu c - h_\mu / c \end{aligned}$$



Mean arrival time $\Delta\tau$ and dispersion σ

Relative arrival time of the foremost muon

$$\Delta\tau_\mu^1 = \tau_\mu^1 - \tau_{\text{core}}$$

Fig. 8: Geometric Mapping of the Longitudinal Development [8].

This is reproduced by realistically simulated distributions of the mean values of relative arrival times for two different primaries and for different energies or shower sizes, respectively, observed in 150- 200 m distance from the shower center. Thus muon arrival time distribution carry some information about the mass of the primaries (Fig. 10).

In our experimental studies of the EAS muon component we represent the EAS time structure by the distribution of various moments: mean, median values , the quartile of the single distributions. Fig. 10 shows an example of the results of systematic measurements of the EAS muon profile. Specified with more details (angle of EAS incidence, N_μ^{tr} , N_e etc.) they can be analysed with an nonparametric analysis procedure [8, 9].

Trends of the first results of KASCADE in context of the information of other experiments

"Quis deus incertum est, habitat deus" (Aen. 8,30)

Summarising the present status of the information about the mass composition from KASCADE measurements (Fig. 11), we have to consider five different independently derived results, whose consistency remains an open problem, indeed :

- from an analysis of N_e and N_μ (Fig. 11a);
- from the analysis of the shower core appearance of "central" showers, including the $N_e - N_\mu$ information (Fig. 11b);

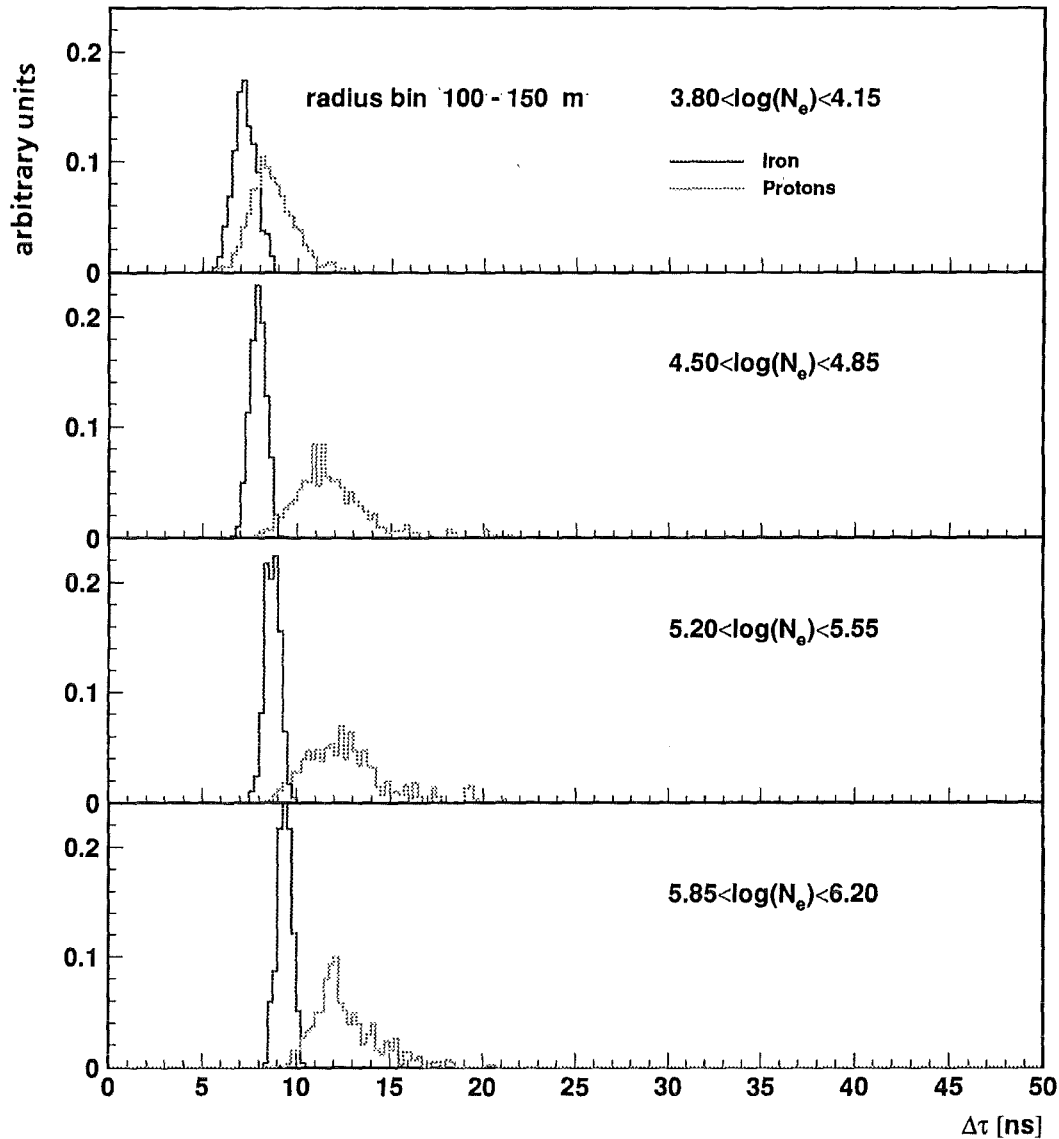


Fig. 9: *Distribution of Mean Values of Arrival Time Distributions* [8].

- from the analysis of the muon arrival time distribution including the $N_e - N_\mu$ information (Fig. 11c);
- from the analysis of the lateral and energy distributions of the hadrons in the shower core (Fig. 11d);
- from a multivariate analysis of different observables ($N_e, N_\mu, N_h, E_h, \dots$), finally of all three shower components (Fig. 11e);

A comparison of these results and consistency considerations are hampered since different observables carry a different mass discriminative power, which is presently not quantified. In addition different methodical procedures use different kind of mass parameters of qualitative nature, whose relative calibration in terms of a composition is not seriously explored.

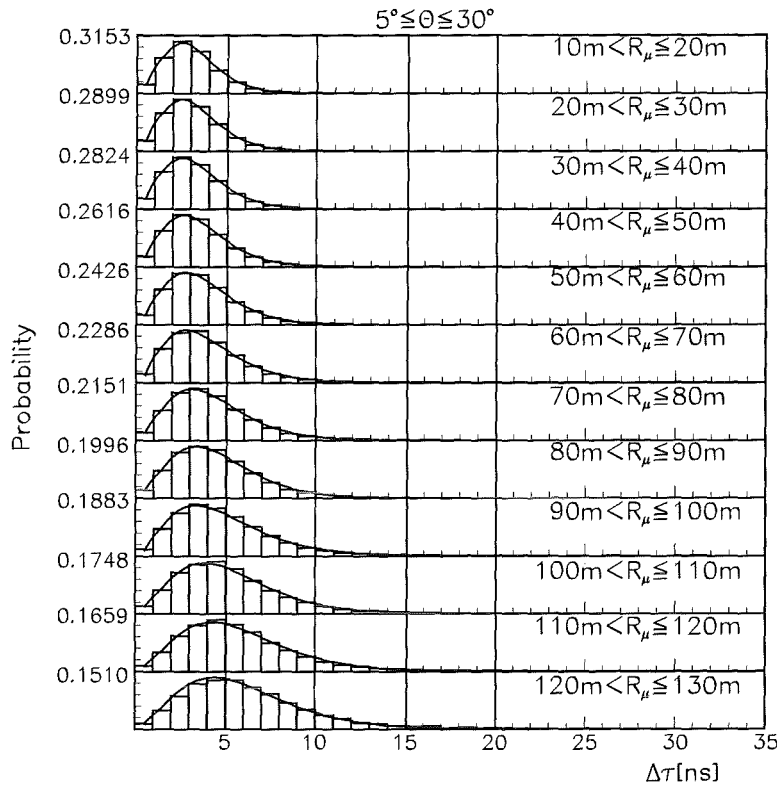


Fig. 10: *Average Radial Variation of the Distribution of the Median Values of the EAS Muon Arrival Time Distributions, measured Relative to the Arrival of the Foremost Muon [10].*

Obviously, whenever the N_μ/N_e ratio is involved, it dominates the result, and as we realize it leads to a relatively "light" composition. This is in contrast to the result derived by the analysis of observables only of the hadron component, though qualitatively the same trend with the energy is displayed, but on a higher level of the average mass. The clarification of this puzzling inconsistency is the greatest challenge of our present status. I shall not speculate about possible reasons, whereby even a basically wrong theoretical description of the EAS development, in particular of the fluctuations of the EAS observables, could not be excluded.

At the 25th International Cosmic Ray Conference in Durban a number of new results with preliminary character has been presented [11] (Fig. 12). The compilation may give an impression about the present situation. There is shown the variation of the mean of the logarithmus of mass number (this is a very crude indicator of the composition, but many experiments can be reduced to such an indicator). Like within the KASCADE approach there are two groups of results. One group: "Heavy composition results" finds a contribution of heavier nuclei increased relative to the hydrogen contribution, increasingly with higher energies. Other results show a more complicated variation, with a larger contribution of lighter elements. The DICE experiment, which extracts information from the observation of the Cerenkov light and the determination of the height of maximum of the shower development, favours a light component in its observation range. Within the quoted uncertainties this feature agrees with preliminary results of KASCADE.

In Durban two methodically independent analyses of the data have been presented. They

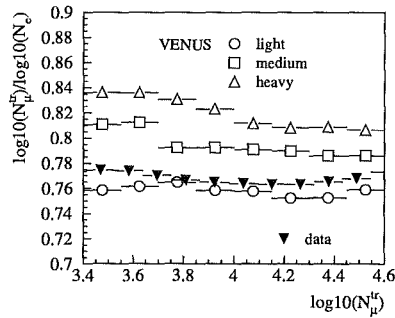


Figure 11 a)

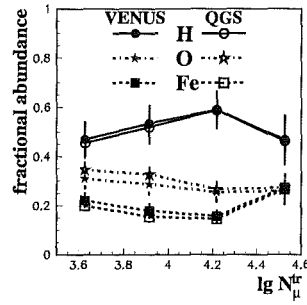


Figure 11 b)

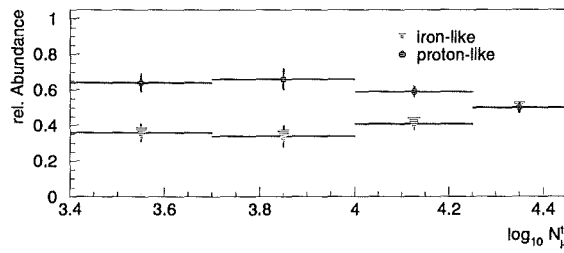


Figure 11 c)

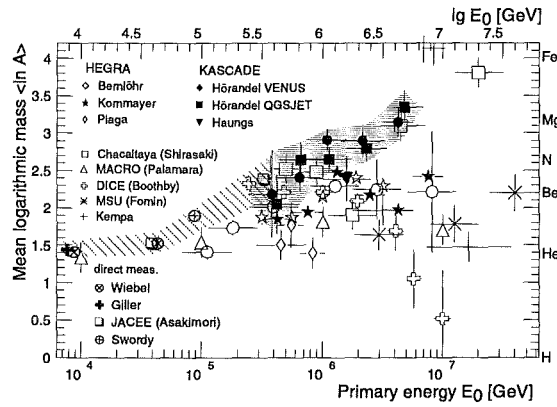


Figure 11 d)

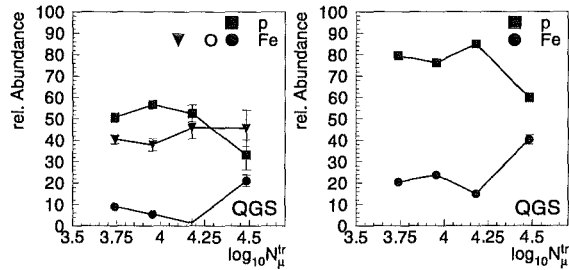


Figure 11 e)

Fig. 11: Mass Composition Messages of the KASCADE Experiment.

use essentially only data about the $N_e - N_\mu$ correlation. The result indicates a light composition in a narrow band around the knee, with a distinct increase of heavier elements

just beyond, perhaps at ultrahigh energies again with proton dominance. This tendency is common to all signatures in the KASCADE experiment.

Concluding remarks

"Tales versus facio, qualae vinum bibo"

Though the issue of mass composition of cosmic rays arose already in the sixties, we know only a little definite. But we understand at least better why we have so uncertain messages:

- The uncertainties in high - energy interaction models, necessarily involved in interpretations of the EAS experiments, are reflected in the experimental answers.
- The fluctuations of the stochastic shower development cover largely mass discriminative signals.
- Experimental procedures, biasing the result by selective, less understood cuts, and using statistically unjustified analysing methods have led to confusing and contradictory results.

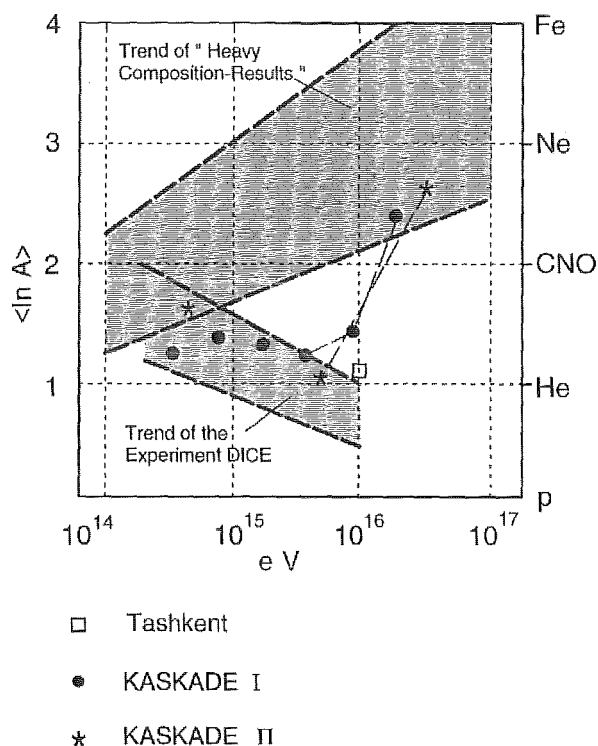


Fig. 12: *Compilation of Composition Results presented at the 25th International Cosmic Ray Conference in Durban [11].*

The concept of KASCADE is to bypass largely these problems i.e. to minimise the influence of the fluctuations and of the uncertainties of the interaction models by combining a larger number of various different signatures in multiparameter analyses. This lecture tried to convince you, how this way is traced.

The lecture is based on current results and communications of the KASCADE collaboration. I acknowledge, in particular, the scientific discussions with Ashot Chilingarian, the organiser of the workshop ANI 98, with Iliana Brancus, Andreas Haungs, Jörg Hörandel, Hermann Mathes and Markus Roth. I enjoyed the kind hospitality of the Armenian colleagues of the Yerevan Physics Institute.

References

- [1] H.O. Klages et al. -KASCADE Collaboration, Nucl. Phys. (Proc.Suppl.) 52B (1997)

- [2] J.N. Capdevielle et al., KFK-Report 4998, Kernforschungszentrum Karlsruhe (1990); D. Heck, J. Knapp, J.N. Capdevielle, G. Schatz and T. Thouw, FZKA-Report 6019, Forschungszentrum Karlsruhe (1998)
- [3] A.A. Chilingarian for the KASCADE Collaboration, Proc. 16th ECRS, Alcala de Henares, Spain, H.E. 8.1 1998
- [4] M. Roth, A.A. Vardanyan, A.A. Chilingarian, Proceed. ANI workshop (1998); M. Roth for the KASCADE Collaboration, Proc.16th ECRS, Alcala de Henares, Spain, H.E. 8.2 1998
- [5] R. Glasstetter for the KASCADE Collaboration, 25th ICRC (Durban, South Africa) 1997 Vol. 6,157; J.H. Weber for the KASCADE Collaboration, 25th ICRC (Durban, South Africa) 1997, Vol. 6, 153
- [6] A. Haungs, J. Kempa, H. Rebel, H.J. Mathes, J. Wentz, Nucl. Instr. and Meth. A 372 (1996) 515 - Nucl. Phys. B (Proc. Suppl.) 52B (1997) 169
- [7] A. Haungs, J. Kempa, H. Rebel et al. - KASCADE collaboration, FZKA-Report 6105, Forschungszentrum Karlsruhe (1998)
- [8] H. Rebel, G. Völker, M. Föller and A.A. Chilingarian, Journ. Phys. G: Nucl. Part. Phys.21 (1995) 451; H. Rebel, in: The Cosmic Ray Mass Composition, Proc. XV Cracow Summer School of Cosmology, 15-19 July, 1996, Lodz, Poland, Uniwersytetu Lodzkiego,1997, ed. W. Tkaczyk, p. 91
- [9] M. Föller, U. Raidt for the KASCADE Collaboration, 25th ICRC (Durban, South Africa) 1997, Vol. 6, 149
- [10] I.M. Brancus, F. Badea, R. Haeusler, H. Rebel -KASCADE Collaboration, FZKA-Report 6151, Forschungszentrum Karlsruhe (1998)
- [11] A.A. Watson, Rapporteur Talk, Proc. 25th ICRC, (Durban, South Africa) 1997, Vol. 8, 257

Cosmic-ray mass composition in the PeV region estimated from the hadronic component of EAS

J.R. Hörandel* for the KASCADE collaboration

Universität and Forschungszentrum Karlsruhe, P.O. Box 3640, 76021 Karlsruhe, Germany

The primary cosmic-ray mass composition is estimated for the first time using the hadronic component of extensive air showers measured by the large hadron calorimeter of the KASCADE experiment. Methods for evaluation of the mean mass are described and first results are presented. The data indicate an increase of the mean mass with rising primary energy.

Introduction

Important information concerning the sources of charged cosmic rays in the energy range from 0.1 PeV to 100 PeV are measurements of the primary energy spectrum and the determination of the cosmic-ray mass composition. Due to the strongly decreasing particle flux only ground-based measurements with large detector areas and long exposure times are possible above 0.5 PeV. The development of extensive air showers (EAS) in the earth's atmosphere is determined by the primary's energy and mass. In the past several experiments estimated the mass composition by detecting the electromagnetic and muonic component of EAS or by measuring the shower propagation in the atmosphere with Čerenkov or fluorescence photons. The Karlsruhe experiment KASCADE [1] is able to estimate the mass composition using the hadronic component as measured in a large and fine grained sampling calorimeter.

Experimental set-up and measurements

KASCADE detects the electromagnetic, muonic and hadronic component of EAS simultaneously. The experiment consists of 252 detector stations spread over an $200 \times 200 \text{ m}^2$ array. Each station contains scintillation counters to probe the electromagnetic and, under an iron and lead shielding, the muonic component. In addition, a 300 m^2 hadron calorimeter equipped with eight layers of liquid ionisation chambers detects the hadrons. The fine spatial segmentation of the calorimeter of $25 \times 25 \text{ cm}^2$ allows to separate hadrons from each other within a distance of 0.4 m and to determine their energy and angle of incidence individually.

From October 1996 up to May 1998 about $7 \cdot 10^7$ events were collected. In $4 \cdot 10^6$ events we reconstructed at least one hadron. Events accepted for the present analysis had to fulfill the following requirements: At least three hadrons with a threshold energy of 50 GeV had been reconstructed. The zenith angle of the shower was less than 30° , and the shower core was located inside the calorimeter. After this cuts 28000 events remained for the further analysis.

Simulations

EAS simulations are performed with the program CORSIKA [2], versions 5.2 and 5.62.

*corresponding author, e-mail: joerg@ik1.fzk.de

In order to investigate systematic uncertainties within the high-energy hadronic interaction models we used the models VENUS, QGSJET and SIBYLL as implemented in CORSIKA. We calculated 2000 proton and iron induced showers for SIBYLL and 7000 p and Fe events for QGSJET. For VENUS 2000 showers were generated, each for p, He, O, Si and Fe primaries. The showers were distributed in the energy range 0.1 PeV up to 31.6 PeV according to a power law with an index of 2.7. All secondary particles at ground level are passed through a detector simulation program using the GEANT package to determine the signals in the individual detectors. Consequently, the simulation results are analysed in the same way as the experimental data.

Method

Goal of the investigations is to determine the number of primary particles as a function of their energy and mass. As an energy estimator we are using the number of muons in a radius range from 40 m to 200 m around the shower core, *the truncated muon number* N'_μ [3]. It has been demonstrated that this observable is nearly independent of the primary's mass [4].

To estimate the primary's mass, different observables of the hadronic component are used. Our investigations proved six observables to be particularly sensitive: The lateral distribution of hadrons, the lateral distribution of the hadronic energy density, the differential hadron energy spectrum and the energy of the most energetic hadron in each shower. A further observable is the distance distribution in a so called *minimum spanning tree*. To construct the latter, the points of incidence of all hadrons are connected by straight lines to each other under the condition that the sum of all connections is minimized. The resulting frequency distribution of the distances in the minimum spanning tree is sensitive to the primary's mass. It is particularly sensitive if an energy-weighted geometrical distance d is used, defined as $d_{ij} = \frac{\sqrt{(x_i-x_j)^2+(y_i-y_j)^2}}{E_H^i+E_H^j}$. The last observable concerns the partition of the hadronic energy to individual hadrons, obtained as the fraction of the energy of each individual hadron normalized to the maximum hadron energy in each shower.

As an example, these frequency distributions of the energy fraction E_H/E_H^{max} are plotted in Figure 1 for a particular muonic shower size interval. Results from simulations using the model VENUS are presented for five different types of primaries. The distributions exhibit with increasing mass a continuous transition from the proton to the iron curve.

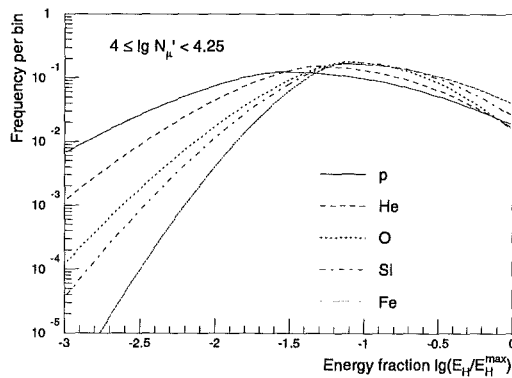


Fig. 1: Frequency distribution of energy fraction for different primaries.

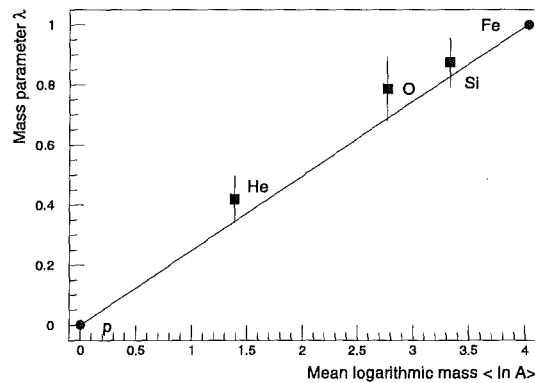


Fig. 2: Mass parameter λ versus mean logarithmic mass.

To quantize this observation we define a mean relative distance λ of a curve f_D with an unknown composition relative to the curves for primary protons f_p and iron induced showers f_{Fe} as $\lambda(a, b) = \frac{1}{b-a} \int_a^b \frac{f_D(x) - f_p(x)}{f_{Fe}(x) - f_p(x)} dx$. The integral yields a mean distance within this interval from a to b and smooths out statistical fluctuations.

Defining a mean logarithmic mass by $\langle \ln A \rangle = \sum r_i \ln A_i$, where r_i is the relative fraction of particles with mass number A_i , one obtains from simulations the relation $\lambda \approx \frac{\langle \ln A \rangle}{\ln A_{Fe}}$ between the mean logarithmic mass and the distance parameter λ as can be inferred from Figure 2, where λ is plotted as a function of $\ln A$ calculated from distributions as shown in Figure 1. Simulations has shown, that this relation is approximately fulfilled for mixed compositions too. The calibration curves for the other five hadronic observables show a similar behaviour. Hence, λ can be assumed to be a good estimator for the primary's mass.

Results

Using all six hadronic observables as described, we compare the measured data with the simulation results. To obtain a reasonably good energy classification, we bin the showers in intervals of N'_μ . Within these intervals the mean relative distance λ is calculated between the data curves and the distributions for primary protons and iron nuclei using VENUS and QGSJET. The results are shown in Figure 3. The parameter λ is plotted versus N'_μ for the observables investigated. Within statistical fluctuations the results obtained with the models VENUS and QGSJET agree with each other. Never the less one observes systematical deviations between the observables, which may be a hint to inconsistencies in the models. We do not present the calculations with SIBYLL due to problems in it's muon number generation. All observables indicate an increase of λ as a function of N'_μ .

Finally, we calculate a mean λ from the six observables and after corrections for efficiency we obtain $\langle \ln A \rangle$. The latter is plotted in Figure 4 versus the primary energy. The grey shadow covers the error range as given by the two hadronic interaction models used. We observe an increase of the mean mass with rising energy. Results from direct measurements are summarized in the hatched area indicating an increase of the mean mass

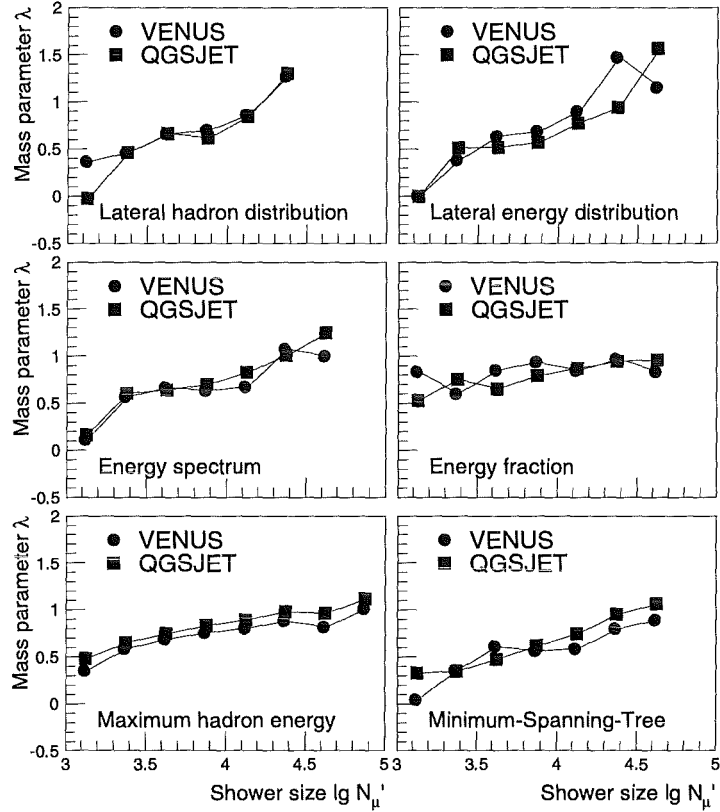


Fig. 3: Mass parameter λ (not corrected for efficiency) for six observables estimated by using the models VENUS and QGSJET.

with energy. This increase persists in our data and in the overlapping region the results agree with each other. In addition, results from other authors are included in the graph as presented at the two latest ICRC's in Rome 1995 and Durban 1997. One notices a strong scattering of the data even among the most recent experiments ranging from a pure proton, e.g. DICE, to a very heavy composition, e.g. Chacaltaya. This may originate from different detection techniques and experimental methods. In any case, the inconsistencies should be settled as soon as possible.

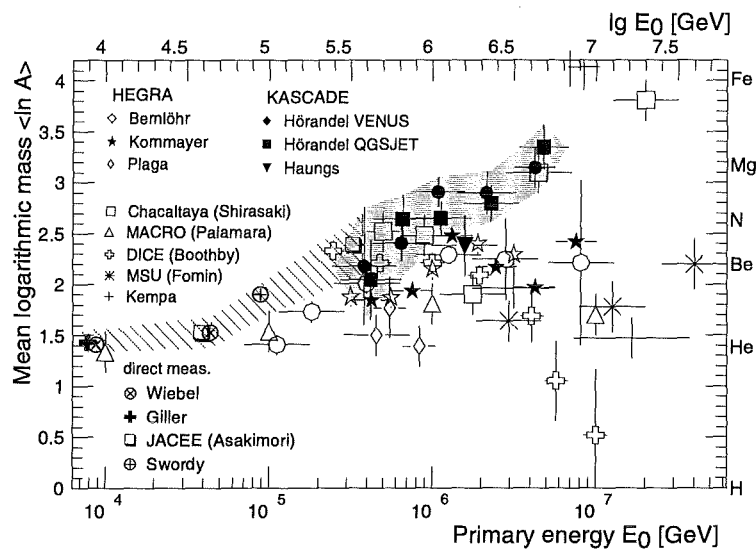


Fig. 4: Measured mean logarithmic mass of primary cosmic rays versus primary energy for several experiments.

References

- [1] H.O. Klages et al., *Nucl. Phys. B (Proc. Suppl.)* 52B (1997) 92
- [2] D. Heck, J. Knapp et al., FZKA 6019 Forschungszentrum Karlsruhe (1998)
- [3] R. Glasstetter et al., *Proc. 25th ICRC.* (1997) 157
- [4] J. Hörandel et al., *Proc. 25th ICRC.* (1997) 93
- [5] K. Bernlöhrt et al., *Proc. 25th ICRC.* 4 (1997) 65
- [6] H. Kornmayer et al., *Proc. 25th ICRC.* 4 (1997) 69
- [7] R. Plaga et al., *Proc. 24th ICRC.* 2 (1995) 693
- [8] Y. Shirasaki et al., *Proc. 25th ICRC.* 4 (1997) 53
- [9] O. Palamara et al., *Proc. 24th ICRC.* 2 (1995) 689
- [10] K. Boothby et al., *Proc. 25th ICRC.* 4 (1997) 33
- [11] Y.A. Fomin et al., *Proc. 25th ICRC.* 4 (1997) 17
- [12] J. Kempa et al., *Proc. 24th ICRC.* 2 (1995) 681
- [13] J. Hörandel, FZKA 6015 Forschungszentrum Karlsruhe (1998)
- [14] A. Haungs et al., *Nucl. Phys. B (Proc. Suppl.)* 52B (1997) 169
- [15] B. Wiebel, WUB 94-08, Bergische Universität Wuppertal (1994)
- [16] M. Giller, *Nucl. Phys. B (Proc. Suppl.)* 52B (1997) 164
- [17] K. Asakimori et al., *Proc. 23th ICRC.* 2 (1993) 25
- [18] K. Asakimori et al., *Proc. 24th ICRC.* 2 (1995) 707
- [19] S. Swordy, *Proc. 23th ICRC. Invited Papers* (1993) 243

Nonparametric determination of energy and elemental composition of cosmic rays from EAS observables

A. Vardanyan^{1*}, A.A. Chilingarian¹ and M. Roth² for the KASCADE collaboration

¹*Yerevan Physics Institute, Cosmic Ray Division, Armenia*

²*Institut für Kernphysik, Forschungszentrum Karlsruhe, Germany*

The problem of an event-by-event analysis of Extensive Air Showers (EAS) observations is addressed, developing a unified methodology of nonparametric multivariate statistical inference and providing tools for the estimation of type and energy of the primary cosmic particle. The methods are illustrated on basis of detailed CORSIKA simulations of the EAS development in the atmosphere and calculating the full detector response of the KASCADE experiment with the GEANT code. The observed reconstructed EAS observables are classified in different categories by Bayesian decision making and neural net approaches.

Introduction

Recent developments of composition studies around the "knee" [1] proved, that only the determination of the energy spectra for different species will solve the problem of specifying "true" models of the charged flux sources and acceleration mechanisms.

The KASCADE experiment [2] has several advantages to address this problem:

- The measurement of large number of mass and energy sensitive parameters with better accuracy than in other comparable experiments, due to the greater coverage of the sensitive area and reduction of the instrumental uncertainties [2].
- The development of the appropriate multivariate statistical methods for EAS data analysis on event-by-event (shower-by-shower) basis [3, 4].
- The detailed simulation of KASCADE response function for various primaries in a wide energy range.
- The investigation of the nontrivial correlations of measured EAS parameters allow to outline the nonlinear multidimensional regions corresponding to different primaries.

Bayesian decision making

The basis of statistical decision on the particle type and energy is the information on the EAS particular characteristics means and fluctuations, corresponding to the different trials of CORSIKA simulations [5] with subsequent KASCADE response and parameter reconstruction calculations.

*corresponding author: e-mail: aro@crdlx5.yerphi.am

The best summary of accumulated in simulation trials knowledge are the nonparametric multidimensional probability density functions. Due to the stochastic nature of the cascade development in the atmosphere we can't expect that analytic families (Gaussian) will describe any measurable EAS parameter. Moreover, very long (usually unregular) tails of the parameter distributions require considerable large amount of simulations to map all possible misclassifications and errors.

Proceeding from these knowledge (prior or conditional probability density distributions) and considering the experimentally measured values we've to make statistical decision on the primary particle type and energy. The applied Bayesian approach of the statistical inference provides the optimal way of combination of prior and experimental knowledge and the Bayes theorem specifies how such modification should be made [6].

The Nonparametric Bayesian decision rule takes the form

$$\tilde{\mathcal{A}} = \operatorname{argmax}_i \{c_i \hat{p}(\mathcal{A}_i/\mathbf{v})\}, i = 1, \dots, L. \quad (1)$$

where \mathcal{A} is the space of possible states of nature – $\mathcal{A} \equiv (P, He, O, Si, Fe)$ - groups of primary nuclei; $\tilde{\mathcal{A}}$ - the space of possible statistical decisions – $\tilde{\mathcal{A}} \equiv (\tilde{P}, \tilde{He}, \tilde{O}, \tilde{Si}, \tilde{Fe})$ where $\tilde{p}, \dots, \tilde{Fe}$ are the decisions that the examined event is caused by a primary proton, or ... , iron nuclei. c_i are the losses connected with $\tilde{\mathcal{A}}$ decision, \mathbf{v} is the multidimensional measurement, $\hat{p}(\mathcal{A}_i/\mathbf{v})$ is the nonparametric estimate of the a posteriori density connected with conditional ones by Bayes theorem:

$$\hat{p}(\mathcal{A}_i/\mathbf{v}) = \frac{\hat{P}_i \hat{p}(\mathbf{v}/\mathcal{A}_i)}{\hat{p}(\mathbf{v})}. \quad (2)$$

where \hat{P}_i is the a priori measure, e.g. what is assumed about the states of nature before experiment. And finally, substituting the a posteriori densities by the conditional ones we get the Bayesian decision rule in the form

$$\tilde{\mathcal{A}} = \operatorname{argmax}_i \{c_i P_i \hat{p}(\mathbf{v}/\mathcal{A}_i)\}, i = 1, \dots, L. \quad (3)$$

As one can easily see from above formulae, the Bayesian statistical decision is dependent on multiplier $c_i P_i$. Therefore we can't separate the influence of losses (cost) measure and prior measure on decision making. Changes in losses can be compensated by changes in a priori measure to keep constant the Bayesian decisions. We think, that it is reasonable to treat $c_i P_i$ as a single entity and denote it as a priori losses.

Nonparametric Probability Density Estimators

To estimate conditional densities we use Parzen and KNN methods with automatic parameter (the kernel width for Parzen estimate and the number of neighbours for KNN estimate) adaptation [3].

Several probability density values corresponding to different values of parameters are calculated simultaneously. Then the obtained sequence is ordered and the median of this sequence is chosen as the final estimate (so called L-estimate). Depending on the intrinsic probability density in the vicinity of point \mathbf{v} , where the density is estimated, due to stabilising properties of the median, each time the best estimate will be chosen.

The Neural Classification and Estimation

The Feed-Forward Neural Network (FFNN) provides the mapping of a complicated input signal to the class assignments in the classification case and to the regressand value (energy) in the estimation case [7, 8]. The network training is performed by minimising a special quality function. The figure of merit to be minimised is simply the discrepancy of apparent and target outputs over all training samples (so called classification score):

$$Q = \sum_{k=1}^K \sum_{j=1}^{M_k} \left(\text{OUT}_{j,k} - \text{OUT}_{j,k}^{\text{goal}} \right)^2 \quad (4)$$

where $\text{OUT}_{j,k}$ is the actual output value for the j -th training event from the k -th category, and the $\text{OUT}_{j,k}^{\text{goal}}$ is the goal value of the j -th event from the k -th category, where K is number of categories and M_k is the number of events in the k -th training set.

Results

The techniques described above were applied to simulation data for calculating the accuracies of mass discrimination and energy estimation [9, 10]. Approximately 10000 events for 5 groups of primary nuclei (P , He , O , Si , Fe) were simulated by CORSIKA code (including the detector response function), in the energy range $10^{14} - 10^{16}$ eV. Four EAS parameters were used: N_e , N_{μ}^{tr} , N_h and $\sum E_h$.

As a measure of separability between different types of nuclei we use the geometrical mean of diagonal elements of misclassification matrices, which is the measure of the mean portion of correct classifications. The root mean square deviation (RMS) was used as energy estimation accuracy measure.

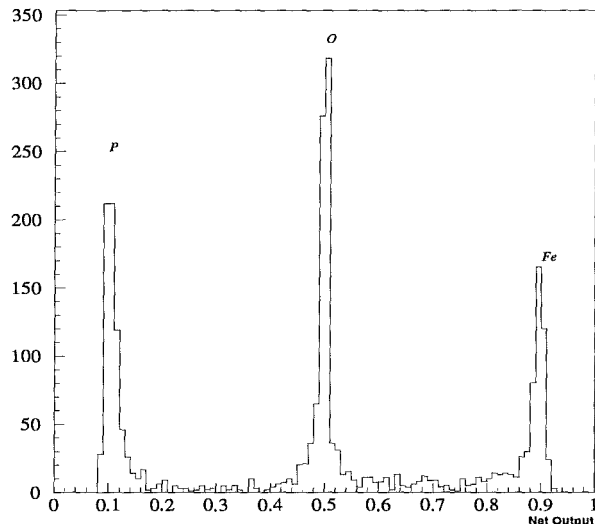


Fig. 1: 3-way classification by neural network

Conclusions

Present status of a priori knowledge accumulated in simulations and available experimental data does not support the attempts to make 5-way classification. The situation with 3-way classification is much better, as we need

Table 1: Separability measure for the KASCADE experiment

	Bayes method	Neural Network
5-way classification	0.380	0.401
3-way classification	0.626	0.662
2-way classification	0.894	0.856

much less a priori information, compared with classification into 5 nuclei groups (Fig.1).

The 2-way classification in "heavy" and "light" nuclei can be done with greater accuracy. Also from table 1 it is seen that alternative classification techniques gives very close results.

Fig. 2, where the "true" versus estimated energies are plotted (EAS electron and muon numbers were used) demonstrates the unbiasedness and consistency of energy estimates. The spread of estimated energies is relatively large in low energy region due to the large fluctuations of the used features for this energy range, and a small underestimation in the highest energy range can be explained by the deficiency of training events with larger energy.

The handling of EAS simulation data prove, that the methods proposed allow for KASCADE experiment:

To determine with 60-70% efficiency the type of the primary.

To estimate primary energy with an accuracy of 20%.

To obtain the energy spectra for 3 groups of primary nuclei.

To calculate the along with the statistical also the methodical and model errors.

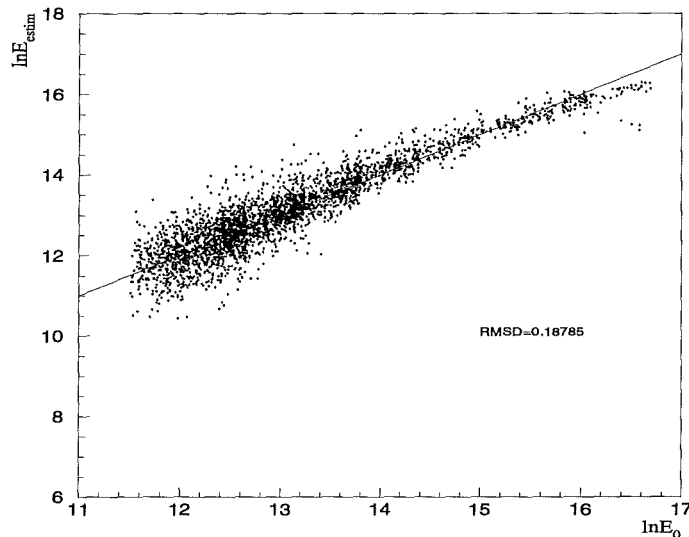


Fig. 2: Primary energy estimation by Neural network

Acknowledgements

The work has been partly supported by a research grant (No.94964) of the Armenian Government and by the ISTC project A116. The collaborating group of the Cosmic Ray Division of the Soltan Institute of Nuclear Studies in Lodz and of the University of Lodz is supported by the Polish State Committee for Scientific Research (grant No. 2P03B 160 12). The collaborating group of the National Institute of Nuclear Engineering is supported by the Romanian Ministry of Research and Technology. The KASCADE collaboration work is embedded in the frame of scientific-technical cooperation (WTZ) projects between Germany and Romania (No.RUM-014-97), Armenia (No.002-98) and Poland (No.92-94).

References

- [1] A.A. Watson, Raporteur talk, 25th ICRC, Durban 8 (1998) 257
- [2] H.O. Klages et al., *Nucl. Phys. B (Proc. Suppl.)* **52B** (1997) 92
- [3] A.A. Chilingarian, *Computer Physics Communications* **54** (1989) 381
- [4] A.A. Chilingarian, H.Z.Zazyan, *Pattern Recognition Letters* **11** (1990) 781
- [5] D. Heck et al, FZKA Report 6019, Forschungszentrum Karlsruhe (1998)
- [6] H. Raifa, R. Schlaifer, *Applied Statistical Decision Theory*, Boston (1961)
- [7] A.A. Chilingarian, *Neurocomputing* **6** (1994) 497
- [8] A. Chilingarian et al., *Nucl. Instr. and Meth. A* **1063** (1997) 230
- [9] M. Roth, et al, *Proc. 25th ICRC*, Durban 4 (1997) 157
- [10] A.A. Chilingarian et al., *Nucl. Phys. B (Proc.Suppl.)* **52B** (1997) 237

Application of nonparametric methods to the analysis of EAS observables for determining energy and elemental composition of cosmic rays

M. Roth^{1*}, A.A. Chilingarian², A. Vardanyan² for the KASCADE collaboration

¹*Institut für Kernphysik, Forschungszentrum Karlsruhe, Germany*

²*Yerevan Physics Institute, Cosmic Ray Division, Armenia*

The KASCADE experiment measuring a larger number of EAS observables with an improved sampling of the electron-photon, hadron, and muon components than previous experiments provides data accurate enough for an event-by-event analysis of the energy dependence of the primary cosmic ray flux in the energy range of $10^{14} - 10^{16}$ eV. Bayesian nonparametric and neural network approaches enable to estimate the primary cosmic ray flux and the elemental composition. The major feature in the observed PeV energy region, the so called knee seems to be reproduced. The investigated EAS data indicate a tendency to a heavier composition above the knee.

Introduction

The knowledge of the energy spectra of different components of primary cosmic rays in the knee region is of vital importance for testing alternative hypotheses of the cosmic ray (CR) origin and acceleration. The manifold interpretations of CR experiments have their causal connection in the inadequate knowledge about the characteristics of hadronic interactions above accelerator energies. Moreover uncertainties in the CR composition, caused by strong fluctuations of the shower parameters give rise to this ambiguities.

The presented detailed analysis of EAS benefits from the simultaneous measurement of a large number of observables for each individual event. Specific EAS parameters measurable by the experiment KASCADE [1] are used, like the number of electrons N_e , the truncated number of muons N_μ^{tr} [2, 3], the number of hadrons with an energy larger than 100 GeV N_h^{100GeV} , the deposited energy in the iron sampling calorimeter [4] $\sum E_h$, and the number of muons N_μ^x with an energy threshold of $E_\mu \geq 2$ GeV measured below the central calorimeter [5]. The techniques presented by Chilingarian [6] on the basis of nonparametric multivariate methods (neural networks, Bayesian decision making) are developed and applied to infer the mass and the energy of primary particles on an event-by-event analysis.

Simulations

Simulations have been performed with the models VENUS, and QGSJet in the energy range $10^{14} - 3.16 \cdot 10^{16}$ eV using the CORSIKA code version 5.2 [7]. The zenith angle was chosen between 15° and 20° . For each primary (p, He, O, Si, and Fe) approximately 2000 EAS events have been simulated, distributed in the energy range with an decreasing particle flux. The core of the EAS lies within a 5 m radius away from the centre of the central detector. The response of all detector components is taken into account in

*corresponding author: e-mail:roth@ik3.fzk.de

great detail using the GEANT code. The number of simulated events is limited by the available computer power.

Energy and mass sensitive observables

The number of electrons as a classical EAS measure provide a very good ability to distinguish between light and heavy particles. Just so in analyses done for different other sin-

Table 1: The classification rates $P_{j \rightarrow i}$ for three groups of primary nuclei using different sets of observables (VENUS model).

	$N_\mu^*, \sum E_h.$			$N_\mu^{tr}, N_e.$			$N_\mu^{tr}, N_e, N_\mu^*, \sum E_h.$				
	p	O	Fe	p	O	Fe	p	O	Fe		
$P_{p \rightarrow i}$	0.58	0.27	0.15	$P_{p \rightarrow i}$	0.68	0.26	0.06	$P_{p \rightarrow i}$	0.71	0.24	0.05
$P_{O \rightarrow i}$	0.34	0.33	0.32	$P_{O \rightarrow i}$	0.21	0.49	0.30	$P_{O \rightarrow i}$	0.18	0.52	0.30
$P_{Fe \rightarrow i}$	0.22	0.30	0.48	$P_{Fe \rightarrow i}$	0.09	0.31	0.60	$P_{Fe \rightarrow i}$	0.07	0.26	0.67

Table 2: Geometric mean of correct classification as a measure of separability for different groups of primaries (VENUS model).

	5 groups	3 groups	2 groups
$N_\mu^*, \sum E_h$	0.154	0.462	0.708
N_μ^{tr}, N_e	0.341	0.584	0.887
$N_\mu^{tr}, N_e, N_\mu^*, \sum E_h$	0.38	0.626	0.894

gle detector components (see refs above) it is shown that in general the signatures obtained by the central part of the KASCADE detector arrangement are mass sensitive parameters ($N_h^{100GeV}, \sum E_h, N_\mu^*, \dots$).

The truncated number of muons N_μ^{tr} (the integration of the lateral distribution function limited to the range of the fit region caused by the array layout), however, is considered as a good energy estimator as it shows only marginal sensitivity

to the mass of the primary particle according to simulations [3]. Due to the limited statistics

of simulated and measured events (approximately 2500 events according to the simulations) the analysis of measured data using information in the centre of the EAS core is restricted to at most three types of primaries: light (p), medium (O), and heavy (Fe).

Table 1 shows, as an example, the nearly energy independent classification rates from the Bayesian analysis for three groups of primaries, which are calculated for different sets of observables. They represent the possibility of correct classification $P_{i \rightarrow i}$ (or misclassification $P_{i \rightarrow j}$). As expected the combination of all observables together provides the

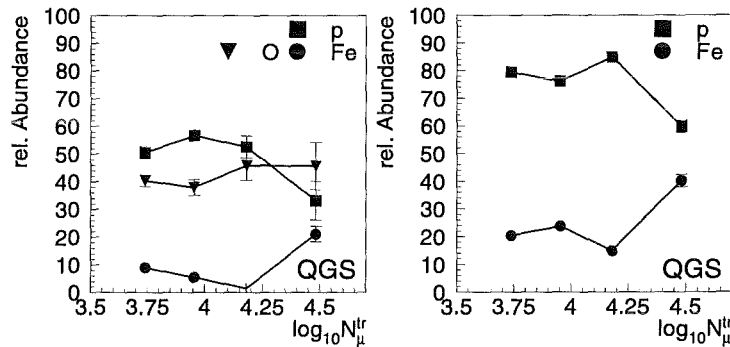


Fig. 1: QGSJet model: Relative abundance of primary particles vs. truncated muon size N_μ^{tr} . A Bayesian analysis was applied using two (right) and three (left) classes.

best classification. However, even the increase of the $P_{i \rightarrow i}$ from the set $\{N_\mu^{tr}, N_e\}$ to the set $\{N_\mu^{tr}, N_e, N_\mu^*, \sum E_h\}$ is not very large, because the correlations of these parameters are strongly model dependent. Hence, applying different models in a nonparametric analysis can lead to different results. The geometric mean $\sqrt[N]{\prod_{i=1}^N P_{i \rightarrow i}}$ of the diagonal elements $P_{i \rightarrow i}$ in Table 2 reflects once more the increasing separability by taking into account more than two observables. Even when taking the full information into consideration the separability for five groups is a crucial point and must be studied in more detail.

Mass and energy estimation

As shown in Figures 1 and 2 there is a tendency to have a lighter composition in the knee region ($\log_{10} N_\mu^{tr} \approx 4.1$) using the Bayesian decision making procedure independently of the applied model and the number of chosen groups to divide in (2 or 3). At higher energies the composition is getting heavier. In the case of VENUS the composition seems to be in general lighter than in the QGSJet case. Results of different combinations of observables (N_μ^{tr} , N_e , N_μ^* , $\sum E_h$, and E_h^{max}) which show similar behaviour are combined to average values. The result for three

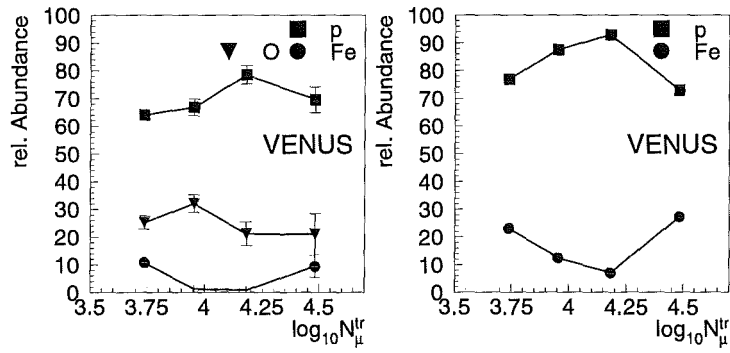


Fig. 2: **VENUS model:** Relative abundance of primary particles vs. truncated muon size N_μ^{tr} . A Bayesian analysis was applied using two (right) and three (left) classes.

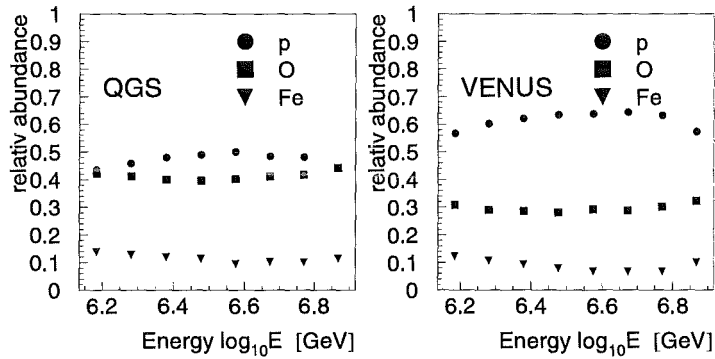


Fig. 3: Relative abundance of primary particles vs. estimated energy of a neural network analysis for three classes (QGSJet and VENUS model).

groups applying the neural network (Figure 3) method corroborates the Bayesian one. The error of the misclassification is taken into consideration only by the Bayesian procedure. Instead of only 2400 events in the Bayesian case in the neural net case there were ca. 460.000 events processed by using only the N_μ^{tr} , N_e observables. This provides the opportunity to use the large amount of data taken by the KASCADE detector field. The abscissa scale is the estimated energy which is calculated by a neural network. The lack of Monte-Carlo simulations in the high-energy region prevents the estimation of energies larger than $8 \cdot 10^{15}$ eV. Therefore, the increase of the heavier components in Figure 3 is not as strong as indicated in Figures 2 and 3 ($\log_{10} N_\mu^{tr} = 4.5 \approx 1 \cdot 10^{16}$ eV). The errors

given in the Figures 1,2, and 3 are of statistical nature only. Systematic errors like finite number of groups and efficiencies are of the order of 5-15%. The all-particle energy spectrum resulting from different networks shows strong model dependence ($\gamma_{QGSJet} = -2.61$ and $\gamma_{VENUS} = -2.77$). The slope difference 0.16 between the models below the knee is even larger than the methodical errors of 0.05.

Conclusion

The presented results on the energy dependence of the elemental composition are of preliminary character. The major feature of the observed energy region (the abrupt change of the composition) seems to be reproduced. The two models indicate the same tendency on different scales of relative abundances.

Acknowledgements

The work has been partly

supported by a research grant (No.94964) of the Armenian Government and by the ISTC project A116. The collaborating group of the Cosmic Ray Division of the Soltan Institute of Nuclear Studies in Lodz and of the University of Lodz is supported by the Polish State Committee for Scientific Research (grant No. 2P03B 160 12). The collaborating group of the National Institute of Nuclear Engineering is supported by the Romanian Ministry of Research and Technology. The KASCADE collaboration work is embedded in the frame of scientific-technical cooperation (WTZ) projects between Germany and Romania (No.RUM-014-97), Armenia (No.002-98) and Poland (No.92-94).

References

- [1] H.O. Klages et al., *Nucl. Phys. B (Proc. Suppl.)* **52B** (1997) 92
- [2] R. Glasstetter et al., *Proc. 25th ICRC*, Durban **6** (1997) 157
- [3] J. Weber et al., *Proc. 25th ICRC*, Durban **6** (1997) 153
- [4] J. Hörandel et al., *Proc. 25th ICRC*, Durban **6** (1997) 93
- [5] A. Haungs et al., *Nucl. Inst. and Meth. A* **372** (1996) 515
- [6] A.A. Chilingarian, M. Roth, A. Vardanyan et al., *Proc. 16th ECRS*, Madrid **HE-8.1** (1998)
- [7] D. Heck et al, FZKA Report 6019, Forschungszentrum Karlsruhe (1998)

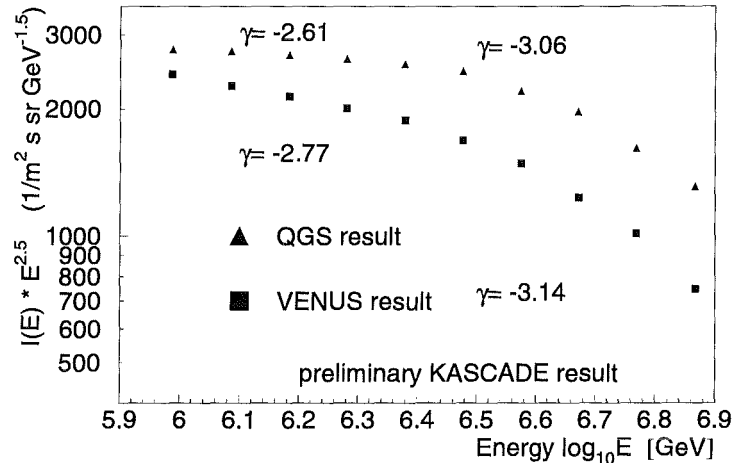


Fig. 4: All-particle energy spectrum as a result of a neural net analysis (QGSJet and VENUS data trained networks were used).

The EAS muon characteristics measured by the GAMMA installation

A.A. Chilingarian¹, A.V Darian¹, V.S. Eganov¹, A.P. Garyaka¹, V.A. Ivanov¹, E.A. Mamidjanian², R.M. Martirosov^{1*}, N.M. Nikolskaya², V.A. Romakhin², B.V. Subbotin² for the ANI collaboration and J. Procureur³

¹Yerevan Physics Institute, Cosmic Ray Division, Armenia

²P.N. Lebedev Institute, Leninsky pr., 56, Moscow, Russia

³Centre d'Etudes Nucleaires de Bordeaux-Gradignan, France

The EAS muon component is studied in the range of shower size $N_e > 10^5$ with the GAMMA installation of the ANI Cosmic Ray Observatory (Mt. Aragats, Armenia). First experimental data are presented and compared with the Tien-Shan experiment and CORSIKA simulations.

Introduction

An accurate measurement of the mass composition and energy spectra of the primary cosmic radiation in the energy region $10^{14} - 10^{17}$ eV has extremely important aspects. The current methods applied for investigations are mainly based on the experimental study of the EAS electron and muon component characteristics and on the analysis of the corresponding fluctuations and correlations. A new installation designed for these aims is the GAMMA array [1]. GAMMA is located at Mt. Aragats in Armenia (3200 m a.s.l., 700 g/cm² atmospheric depth) and is the most developed part of the ANI Cosmic Ray Observatory.

GAMMA is a central type array and consists in two main parts (figure 1):

- the surface part for the registration of the EAS soft component;
- the large muon underground detector to register the muon component.

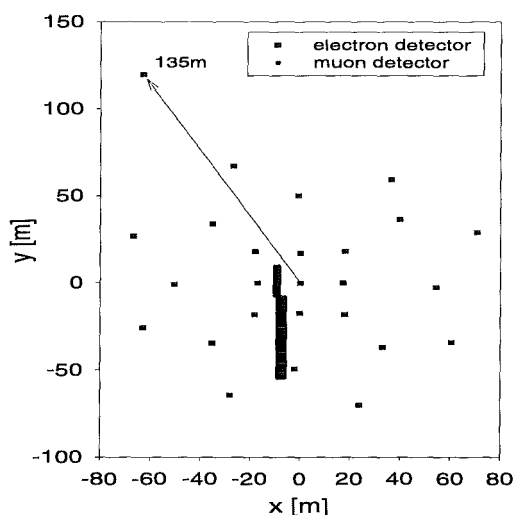


Fig. 1: The GAMMA installation: the black bars indicate the underground part.

25 groups of 3 scintillation detectors are placed on concentric circles with radius 17, 28, 50 and 70m. They are distributed on the area of $\approx 1.5 \cdot 10^4 m^2$. This surface part involves also 25 timing channels. Such a com-

*corresponding author: e-mail: martir@lx2.yerphi.am

bination allows to register showers with particle number $N_e > 5 \cdot 10^5$ within 40m from the array centre with 100% efficiency;

The accuracy of the EAS parameters determination is

- for the total soft component particles number: ca. 10%;
- for the coordinates of shower axis: ca. 3m;
- for the total muon number: ca. 20%;
- for the zenith angle of shower axis for $\theta < 45^\circ$ ca. : 1.5° .

Up to now the operation time of the installation is 1.600 hours. The number of EAS with $N_e > 10^5$ is ≈ 170000 .

Experimental conditions and results

The muon detector (figure 2) consists of two parts: 60 muon detectors are placed in the underground hall and other 90 detectors distributed on the tunnel. We have two problems connected with study of muons:

1. The surface detectors are placed on the hillside and sometimes the difference between the z coordinates of different detectors is 18 meters. On the other side, the position of muon detectors is very asymmetric in respect to the installation geometric centre. So, it is necessary to check the event reconstruction programs to avoid effects connected with the installation geometry.

2. The second problem is the existence of different muon energy threshold in the hall and in the tunnel. The thresholds in the hall is $\approx 5\text{GeV}/\cos\theta$ and in the tunnel $\approx 2.5\text{GeV}/\cos\theta$. For analysis we selected showers with $N_e > 10^5$, $\theta \in [0 - 30]^\circ$ and axes inside [0-40] meters from the installation centre. To check the influence of the azimuth angle to the muon lateral distribution, we divided the observed events into four groups with azimuth angles $\varphi \in [0 - 180]^\circ$, $[90 - 270]^\circ$, $[180 - 360]^\circ$ and $[270 - 90]^\circ$.

Fig. 3 shows that the measured muon lateral distributions for each group show practically no difference between these distributions. The same situation is observed for the tunnel detectors, (figure 3b). The error bars are statistical only.

Fig. 4a shows the muon lateral distributions for a different shower sizes N_e . The dotted lines are the Tien-Shan experimental data [2] obtained for the same observation level and the same muon energy threshold 5 GeV. For $\langle N_e \rangle = 1.34 \cdot 10^5$ there is a good agreement with the Tien-Shan data. But for higher values of N_e , our experimental data appear with a steeper fall-off than observed for the Tien-Shan experiment. The situation at small distances from the shower centre, (< 5 m), requires a special study with taking into account the punch through of particles (high energy electrons and hadrons).

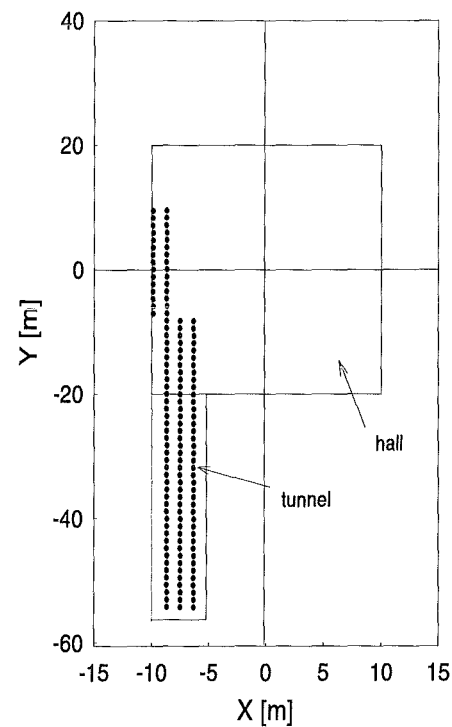


Fig. 2: Underground muon detector array of the GAMMA installation

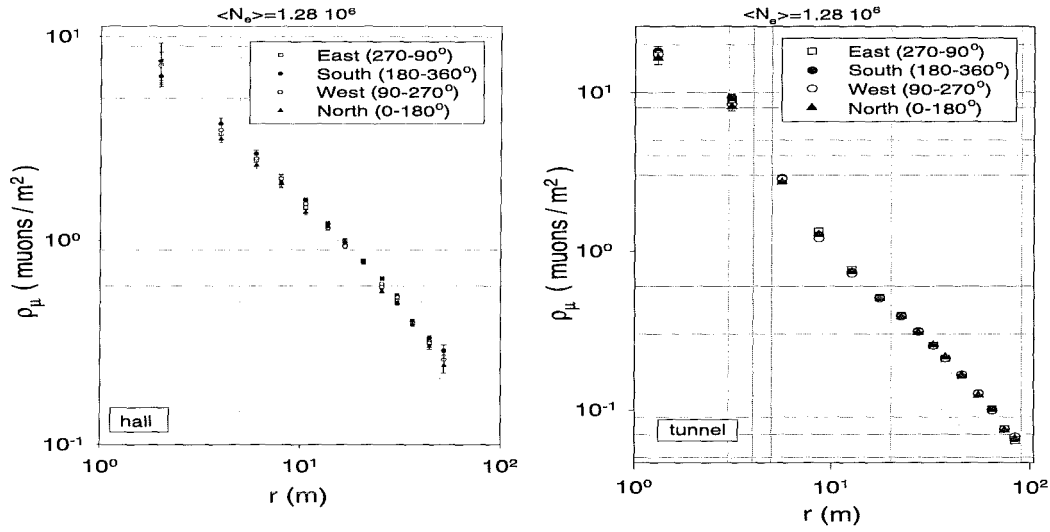


Fig. 3: Muon lateral distributions measured for different azimuthal angle ranges with the hall detectors (a) and the tunnel detectors (b).

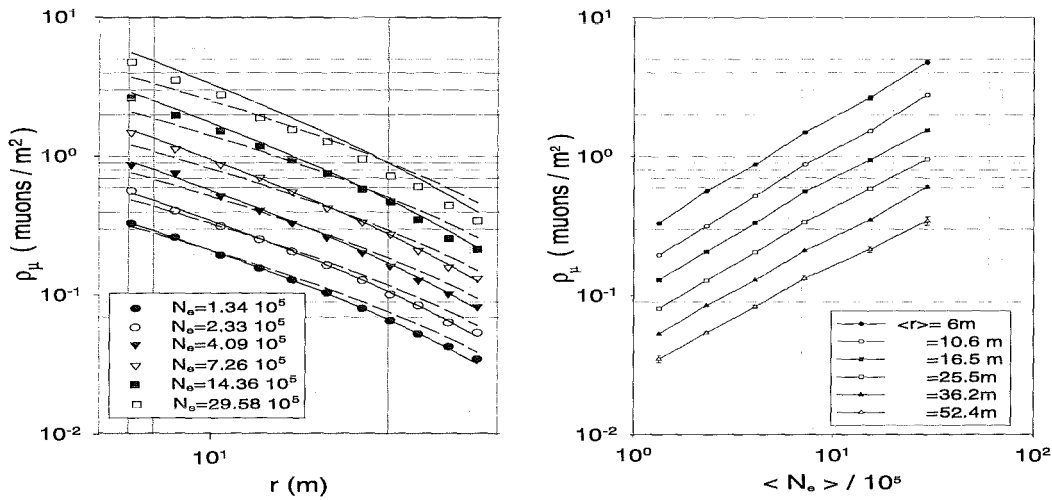


Fig. 4: Muon lateral distributions for different shower sizes (a). The dependence of muon density versus the shower size at different averaged radial distances (b).

Figure 4b shows the dependence of muon densities for different fixed distances from the shower centre ρ_μ versus the shower size N_e . Obviously $\rho_\mu(N_e)$, ($r_\mu = \text{const}$), exhibits a power law dependence with a power index different for each fixed distance.

The observed experimental lateral distribution is described by the empirical formula

$$\rho_\mu(r, N_e) = 1.164(N_e/10^5)r^{\alpha(N_e)}\exp(-r/80), \quad (1)$$

where $\alpha(N_e) = a_0 + a_1 \ln(N_e/10^5)$ and $a_0 = 0.8$, $a_1 = 0.0476$.

from such a parametrization of the muon lateral distribution for the total muon number N_μ has the following power dependence on N_e results

$$N_\mu = A \cdot N_e^{0.79}. \quad (2)$$

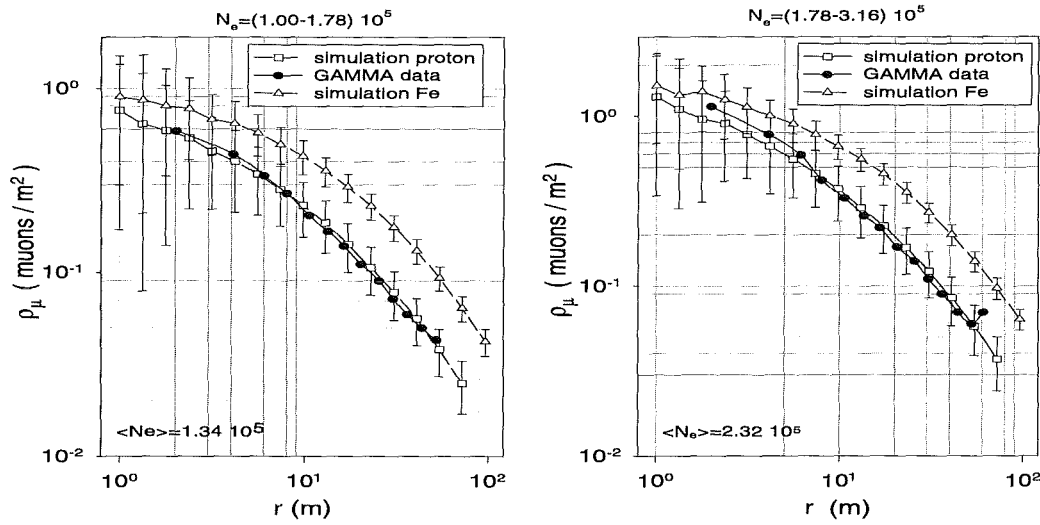


Fig. 5: Measured muon lateral distributions for $\langle N_e \rangle = 1.34 \cdot 10^5$ and $\langle N_e \rangle = 2.33 \cdot 10^5$.

Fig. 5 compares the experimental data with CORSIKA simulations [3].

Conclusions

From studies of the azimuthal dependence of the particle detection by the GAMMA array we infer that the results are not distorted by the installation geometry. The muon lateral distribution proves to be steeper with increasing N_e than the Tien Shan results. There is a power law dependence of the muon density on shower size at fixed distance from the shower centre. An empirical formula for the approximation of the muon lateral distribution is obtained and applied for the estimation of the total muon number.

References

1. S.A. Arzumanian et al., *Proc. 24th ICRC (Rome) 1995*, 1,482
2. S.F. Abdrashitov et al., *Proc. 17th ICRC (Paris) 1981*, 6, 156
3. D. Heck et al., *FZKA report 6019*, Forschungszentrum Karlsruhe, 1998

Measurements of the characteristics of the soft EAS component with the GAMMA array

A.P. Garyaka* for the ANI collaboration

Yerevan Physics Institute, Cosmic Ray Division, Armenia

The lateral distribution of the soft component of Extensive Air Showers (EAS), shower size spectra and the angular distribution of incidence has been measured with the GAMMA detector array on Mt. Aragats in Armenia. The results are compared with results of other experiments and model predictions.

Introduction

The investigation of Extensive Air Showers (EAS) at energies $10^{14} - 10^{17}$ eV provides important information with astrophysical and high-energy particle physics aspects. The extraction of the information invokes the solution of a quite complicated inversion problem, inferring the energy and nature of the primary particle from the appearance of the EAS at the observation level. In general there is a quest for experimental data of increased accuracy and improved data evaluation procedures. In this contribution experimental data for the soft EAS component, measured with the GAMMA detector array on Mt. Aragats (3250 m a.s.l.) in Armenia are presented. The detector layout is described elsewhere [1,2]. The presented data stem from 1600 h operation time. With increased statistical accuracy they would allow a consideration of the shower parameter distributions on event-by-event basis using advanced statistical methods of nonparametric analyses [3].

Experimentals

The surface part of the GAMMA detector array is intended to register charged component

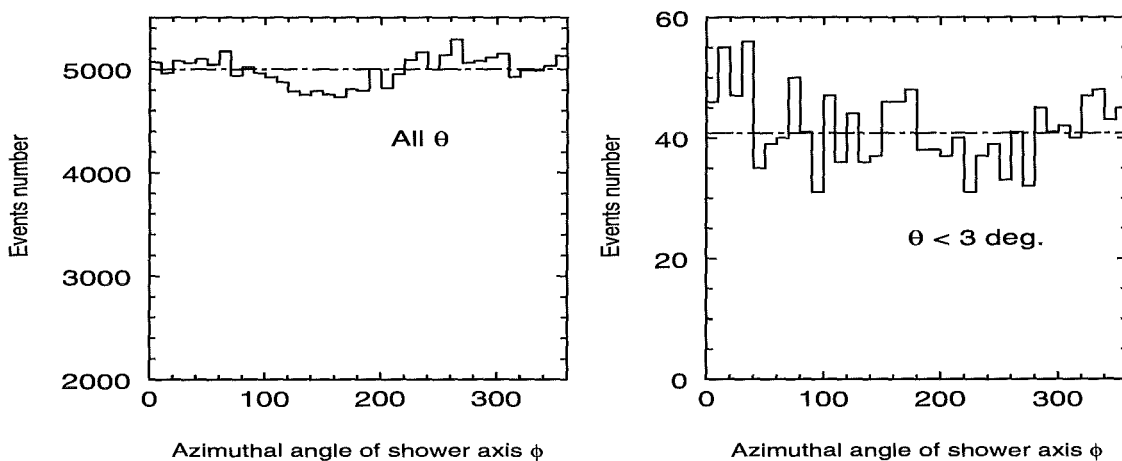


Fig. 1: Azimuth angle distribution of EAS incidence observed by the GAMMA array

*corresponding author: e-mail: alegari@jerewan1.yerphi.am

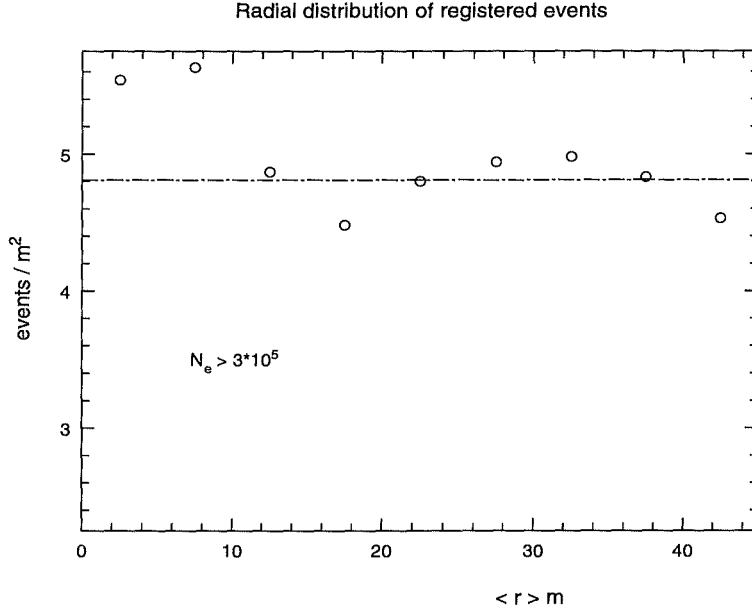


Fig. 2: Density dependence of registered EAS on the distance from the centre of the GAMMA array

of the EAS. It consist of 25 registration stations which are positioned on concentric circles of radii of 17, 28, 50 and 70m. Each detector station is equipped by 3 scintillation detectors with a timing channel in electronic readout device of one of detectors. The scintillation detectors with 1m^2 area are of the same type as those used in the Tien-Shan experiment. The detector control and readout are organised in a central station. The efficiency and response of the detector setup (dynamic range of single detector: $1\cdot 10^4$) have been carefully studied using simulated shower events and taking into account the geometry of the array. Unfortunately the used simulated EAS data have been calculated with a Monte - Carlo program, which did not produce the fluctuations realistically. Improved calculations with the code CORSIKA [4] and the detector simulation code GEANT [5] are in progress. Since the detector stations are distributed on the hilly region on the Mt.Aragats side, the actual altitudes of the stations vary within 18 m. This condition has to be taken into account in the shower reconstruction program. For the determination of a special shower parameter (see [6]) a cluster of 20 detectors is placed in a distance 135 m from the array centre. Analysis of the experimental data gives some notion on measurement uniformity on distance from array centre and azimuth angle. Fig.1 shows the distribution of the events registered by the GAMMA array vs. the azimuth angle of the shower axis for different conditions for the zenith angle Θ . There is no significant asymmetry in the distributions and the fluctuations have statistical origin. Fig.2 represents the dependence of the registered events number on $\langle r \rangle$ the distance from the array centre to EAS axis position. The uniformity is considered to be sufficient up to $\langle r \rangle = 40\text{m}$. In Fig.3 the zenith angle distribution $dN/d\cos(\theta)$ is shown. The solid curve corresponds to the fit of the zenith angle dependence of the EAS intensity by expression:

$$F(\cos(\theta)) = F(\theta = 0^\circ) \exp(-700(\sec\theta - 1)/L),$$

with the value of absorption length $L = 165 \text{ g/cm}^2$ in good agreement with Tien-Shan

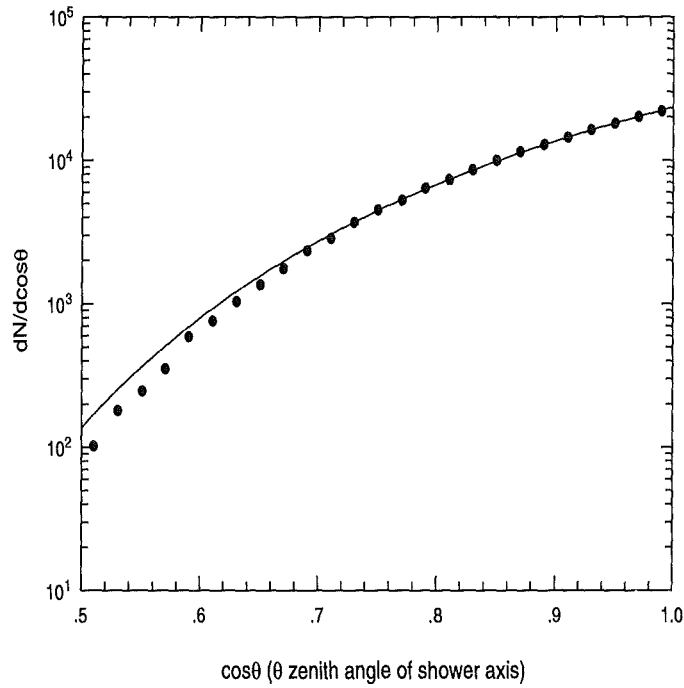


Fig. 3: *EAS zenith angle distribution*

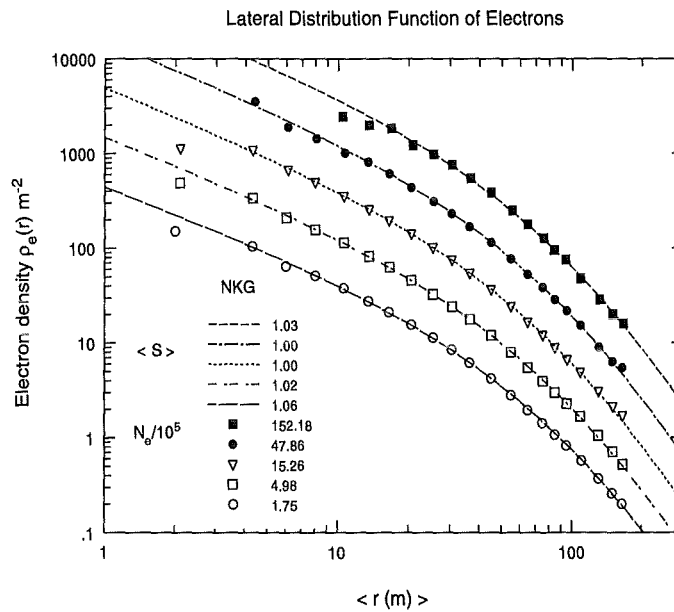


Fig. 4: *The measured lateral distributions of the EAS charged particle component for different shower sizes, fitted by the NKG function*

results [7]. In the following we restrict to observations with $\langle r \rangle < 40\text{m}$ and $\theta = 0^\circ - 30^\circ$.

Results

The following figures (Figs. 4-6) display the results of the lateral distributions of the charged particle EAS component, of the shower size spectrum and the mean age distribution. The NKG form proves to be an adequate description of the lateral distributions (Fig. 4). Compared to the Tien-Shan results [8] the measured distributions show

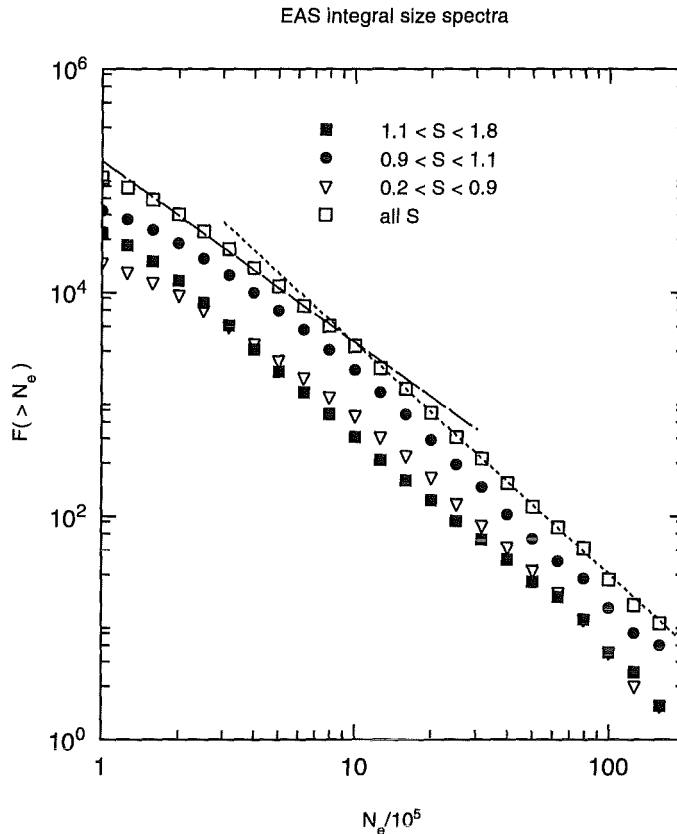


Fig. 5: EAS size spectra. The measured integral spectra of the EAS size for different mean age values

a less steeper slope, and the corresponding mean age values appear to increased by 0.1. The knee around $N_e \approx 10^6$ is evident in the size spectra, obviously more pronounced for "young" showers and smoother for "old" showers (Fig. 5). A possible explanation of this feature may be a changing mass composition, possibly with enriched heavy primaries in the sample of large ages, for which the knee should be shifted to higher primary energies. This speculation fits well to the preliminary results of the KASCADE experiment [9]. The dependence of the mean age from the shower displays for $N_e < 3 \cdot 10^6$ a behaviour expected for a constant mass composition and unchanged characteristics of the interaction (Fig. 6). The results for larger sizes suffer from statistical inaccuracies, whereby the increase around $N_e \approx 10^7$ need further confirmation.

In conclusion, the data accumulated in the current measurements with the GAMMA array are promising in view of an analysis of the primary energy spectrum and mass composition, combined with corresponding studies of the EAS muon component [10].

References

- [1] A.A. Arzumanian et al.: *Proc. 24th ICRC*, Rome (1995), **1**, 482
- [2] A.A. Chilingarian et al.: *Proc. 16th ECRS*, Alcalá de Henares (1998), to be published
- [3] A.A. Chilingarian: *Computer Physics Communications* (1989), **54**, 381
- [4] GEANT : CERN Program Library Long Writeup W5013, CERN (1993)
- [5] J.N. Capdevielle et al.: *KfK-Report 4498* (1992); D. Heck et al.: *FZKA-Report 6019* (1998)

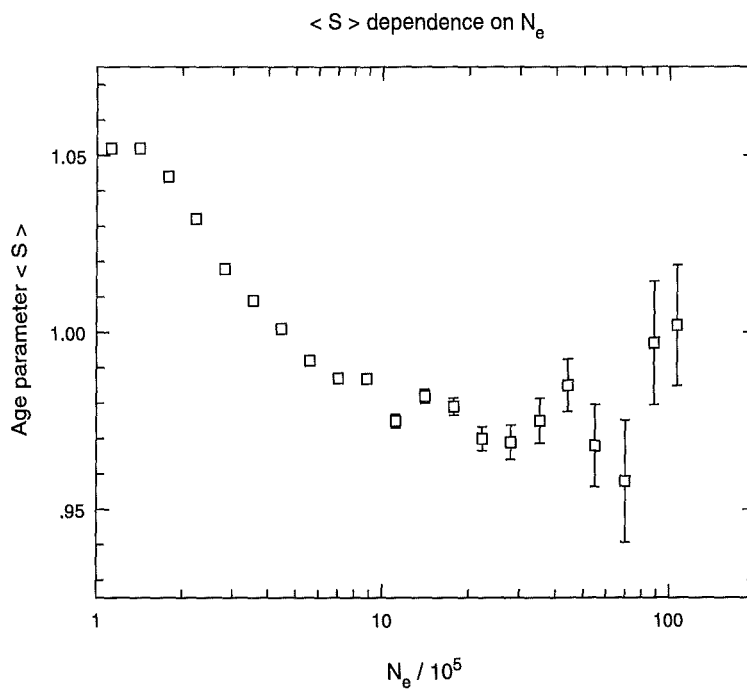
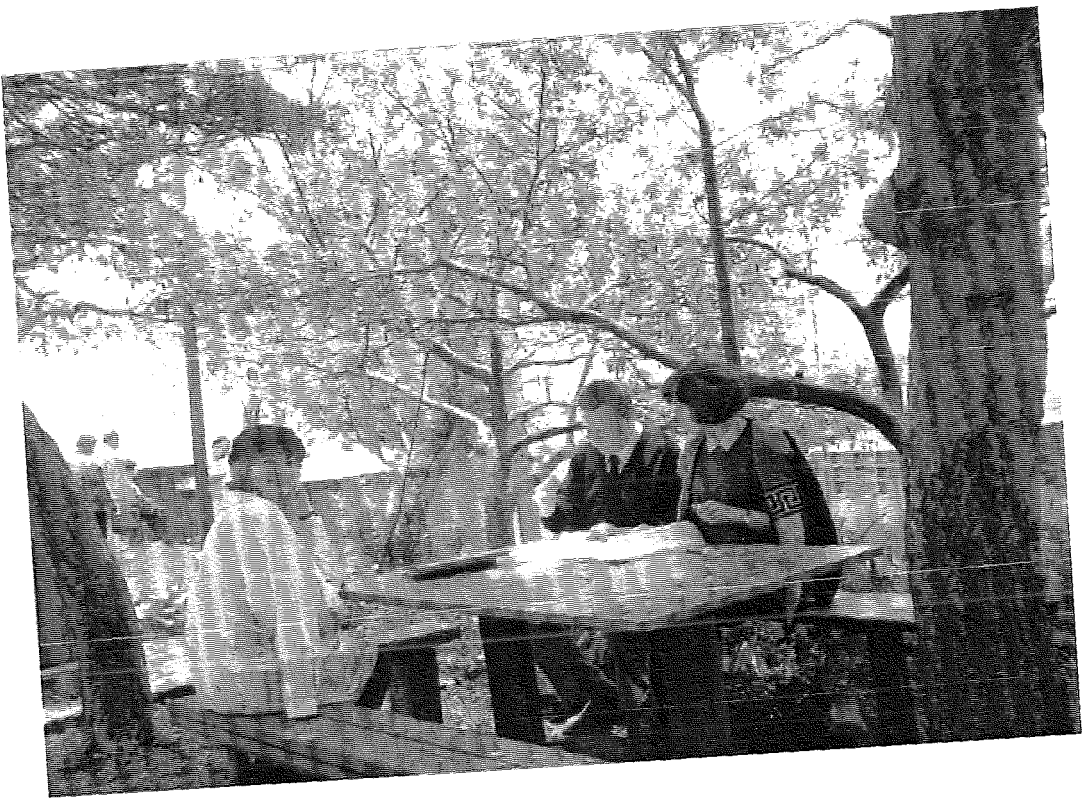


Fig. 6: The mean age $\langle S \rangle$ dependence on the shower size

- [6] M. Brankova et al.: ANI workshop (1998), these proceedings
- [7] S. Miyake et al.: *Proc. 16th ICRC*, Kyoto (1979), 13, 191
- [8] E.V. Danilova et al.: *Izv. RAN, Ser Fiz.*, (1994), **58**, 67
- [9] H. Rebel: ANI workshop (1998), these proceedings
- [10] A.A. Chilingarian et al.: ANI workshop (1998), these proceedings



Studies of the muon detector response of the GAMMA installation with the simulation program ARES

M.Z. Zazyan^{1*} for the ANI collaboration and A. Haungs²

¹*Yerevan Physics Institute, Cosmic Ray Division, Armenia*

²*Institut für Kernphysik, Forschungszentrum Karlsruhe, Germany*

The response of the underground plastic scintillator detector array of the GAMMA installation on Mt. Aragats, Armenia, to the extensive air shower muon component has been studied by the detector simulation program ARES. Particularly the amount of secondary particles produced in the absorber which fake the numbers of measured muons are taken into consideration. The dependence of the correlation of the number of true and faking secondaries from the shower core distance to the muon detectors is studied.

Introduction

One of the main aims of the measurements at the GAMMA experiment [1,2], located on Mt. Aragats (3200 m a.s.l.), Armenia, is the determination of the energy spectrum and of the mass composition of cosmic rays in the energy region of the so-called knee.

For the measurements of the extensive air shower (EAS) characteristics of the muon component a large underground array of plastic scintillation detectors has been put in operation. The underground array consists of two parts (see also [3,4]): 60 plastic scintillators (1m² area and 5cm thickness each) are placed in the underground hall below the ANI calorimeter building, and additional 90 detectors of the same type are installed in the so-called tunnel, where the absorber consists of concrete and ground only, with a lower energy threshold for traversing muons. The evaluation of the registered data in terms of EAS parameters requires a detailed study of the efficiency and response of the detectors.

In the present contribution a report is given about the first step in setting up a dedicated detector simulation program ARES (ARagats Event Simulation), illustrated by some particular response studies.

Methodical procedure

The ARES detector simulation program is based on the GEANT package [5] specified

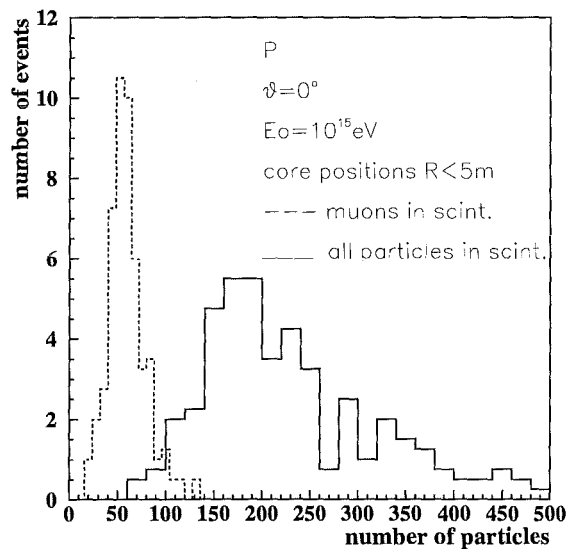


Fig. 1: Numbers of all hits and of registered muons per event.

*corresponding author: e-mail: mary@jerewan1.yerphi.am

by the actual layout of the GAMMA muon detector arrangements. The geometrically and materially setup of the absorber as well as the housing of the scintillators are taken into account. The present investigation uses the CORSIKA program [6] to simulate EAS for the observation level of Mt. Aragats. ARES tracks all particles and produced secondaries through the absorber and the detectors, including all relevant interactions of the particles with matter. In this way, for each shower the number of particles hitting the detectors and the deposited energy at each scintillator is received. There are contributions to the number of traversing muons by δ - electrons, particles created by pair production, or by small electromagnetic showers resulting from bremsstrahlung, cascading δ - electrons, or by secondary particles

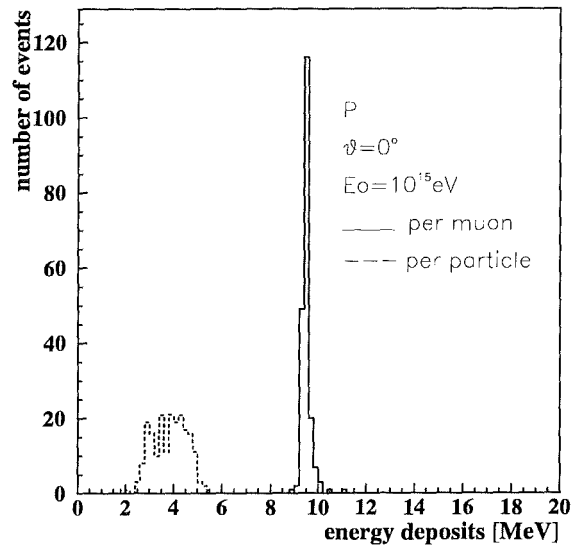


Fig. 2: Energy deposits of the registered muons and of the secondary particles in the scintillators.

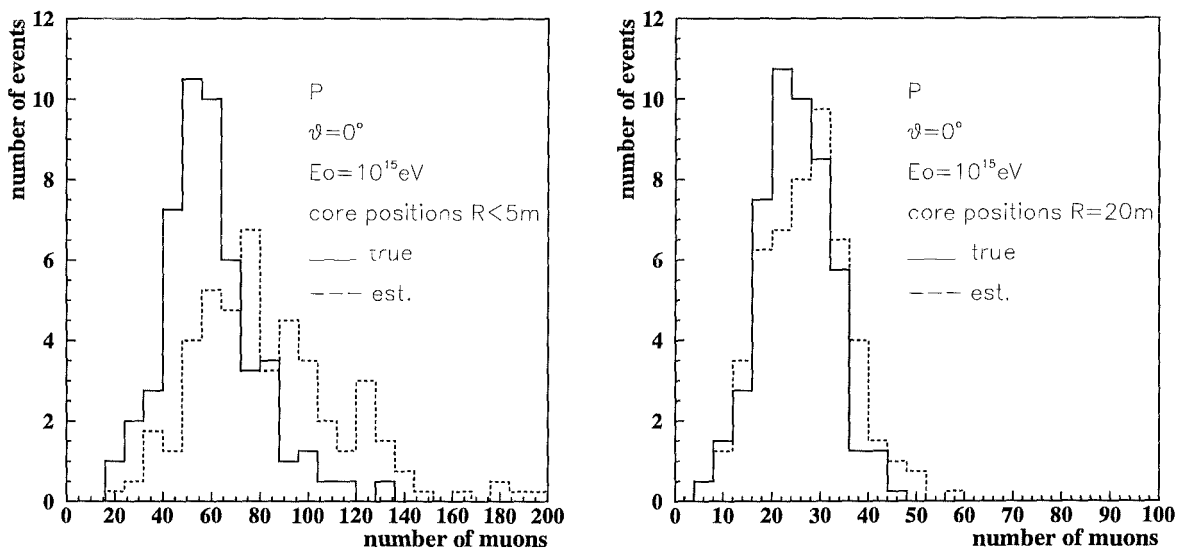


Fig. 3: True and estimated muon numbers in all scintillators for two different shower core positions.

of nuclear interactions of muons and even of the punch-through of EAS hadrons. Fig.1 shows the distributions of all hits (i.e. particles which have an energy deposit in one of the scintillators) per event (in all scintillators) and the number of "real" muons for air showers initiated by primary protons with $E_0 = 10^{15}$ eV, $\theta = 0^\circ$ and the core position near $x=0$, $y=0$ (= middle of the tunnel and hall border, see ref.[4]). To obtain the number of muons per scintillator in EAS measurements at the GAMMA experiment the deposited energy is divided by 9.5 MeV which is the theoretical mean energy deposit in 5 cm thick

scintillation material. The simulated distributions of the energy deposits of the muons and of the secondary particles are presented in fig.2. Muons show a narrow distribution with mean energy deposit of 9.5 MeV. So it is reasonable to obtain the number of muons registered by each detector by dividing the sum of deposited energy in the detector by a factor of 9.5 MeV. In the further investigations this number is called "estimated" muon number. This will be compared with the "true" muon number which is known due to the simulation procedure. To test the estimation procedure the true muon number distributions are compared with the estimated muon numbers for various core positions (fig.3). The two numbers are similar for core positions far from the scintillation detectors, while in showers close to the detectors the number of muons is overestimated.

Results

The mean muon number dependence on the shower core distance from the muon detector setup for both, estimated and true muons, is presented in fig.4 (the distances R varies along the x-coordinate axes). One can see that the muon number overestimation is about 40% for core distances near zero and 18% for $R=10$ m. For greater distances there is a good coincidence of estimated and true muon numbers. Thus, following this results the muon number in each scintillator can be estimated if the core position and the shower direction is known. But different primary energies and primary particles, as well as large intrinsic shower fluctuations are disturbing this approximative calculations. These results are the first approach to the problem and a full description of the GAMMA installation including the surface detectors in the ARES program for a more detailed analysis is needed.

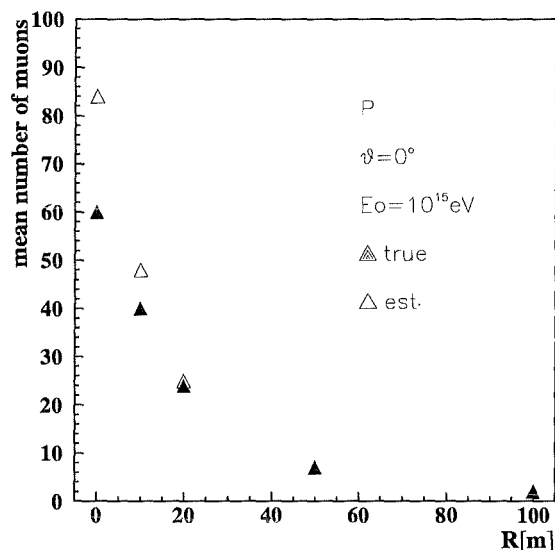


Fig. 4: True and estimated muon number for various core distances from center of the muon detector installation.

Acknowledgements

We would like to thank H. Rebel for the initiation and support of this work. We acknowledge the encouragement of A.A. Chilingarian and valuable discussions with R. Martirosov and A. Garyaka.

References

1. S.A. Arzumanyan et al., *Proc. 24th ICRC (Rome) (1995)* 1, 482
2. A.A. Chilingarian et al., *Proc. 16th ECRS (Alcala de Henares)*, to be published;
A.A. Chilingarian et al., *ANI Workshop 98*, these proceedings
3. H.J. Mathes et al., *ANI Workshop 98*, these proceedings
4. A.F. Badea et al., *ANI Workshop 98*, these proceedings
5. GEANT: *CERN Program Library Long Writeup W5013*, CERN (1993)
6. J.N. Capdevielle et al., *KfK-Report 4498 (1992)*; D. Heck et al., *FZK-Report 6019 (1998)*



Determination of the measurement accuracy of the GAMMA array

L.S. Haroyan*

Yerevan Physics Institute, Alikhanyan Br.2, Yerevan, Armenia

A new indirect method for the determination of the measurement errors in the GAMMA array has been worked out. The determination of the measurement errors of each detector is demonstrated to be better than 10% for number of EAS events more then 10^4 . The proposed method has been tested by Monte-Carlo simulations and experimental data, and it can be used for the callibration of the GAMMA array detectors.

Introduction

The determination of EAS parameters like N_e - shower size, s - shower age, x_0, y_0 - location of shower core is generally performed by minimization of a χ^2 function

$$\chi^2 = \sum_{k=1}^m \left(\frac{f(N_e, s, x_0, y_0, x_k, y_k) - \rho_k(x_k, y_k)}{\sigma_k} \right)^2 \quad (1)$$

where $\rho_k (k = 1, \dots, m)$ is the density of EAS charged component measured by k -th detector located at x_k, y_k coordinates, $f(N_e, s, x_0, y_0)$ is the adopted lateral distribution function, σ_k is the total measurement error for k -th detector. During the experiment the conditions of the detectors (scintillators) and electronic channels usually are changing and therefore it is necessary to rescale all values of measurement errors [1,2]. Moreover, because the measurement error can generally depend on measured number of charged particles in the detector [1-3] it is necessary to investigate these dependences often.

In this work we propose for the GAMMA array both a method for an operative determination of measurement errors and a method of investigation of correlations between measurement error and measured number of particles. The detail description of the GAMMA experiment is presented in [4].

Method

The method is based on a speciality of the GAMMA array (see [4]), where each registration station consists of 3 scintillation detectors. Each i -th ($i = 1, \dots, 3$) detector in the k -th registration station measures a particle density. The final density estimate for k -th station we propose to take in following form

$$\rho_k \approx \frac{n_1 + n_2 + n_3}{3S} \quad (2)$$

where n_i is observed number of EAS charged particles in the i -th detector, $S = 1 \text{ m}^2$ is area of each detector [4].

Using the random values of the differences (Δ) for a given registrating station

*e-mail: lilit@crd3.yerphi.am

$$\Delta_{1,2} = n_1 - n_2, \quad \Delta_{2,3} = n_2 - n_3, \quad \Delta_{3,1} = n_3 - n_1,$$

one can estimate $\sigma_{1,2}^2, \sigma_{2,3}^2, \sigma_{3,1}^2$ (the variances of $\Delta_{1,2}, \Delta_{2,3}, \Delta_{3,1}$) values for a given number (N) of EAS events. On the other hand, as long as the measurements are independent, we have

$$\sigma_{1,2}^2 = \sigma_1^2 + \sigma_2^2, \quad \sigma_{2,3}^2 = \sigma_2^2 + \sigma_3^2, \quad \sigma_{3,1}^2 = \sigma_3^2 + \sigma_1^2,$$

where $\sigma_i (i = 1, 2, 3)$ are unknown measurement errors of i -th detector. Solving this set of equations for a given ρ_k we can obtain the values of $\sigma_i^2(\rho_k)$ for each i -th detector.

For an investigation of the dependence of measurement errors on observed number of particles in a detector Poisson fluctuations of observed number of particles (n_i) have to be taken into account. Assuming a linear logarithmic dependence of measurement error on n_i in the form $\alpha_i \ln n_i$ [2], where the α_i are unknown parameters and the total relative error is approximated by the expression

$$\left(\frac{\sigma_i}{n_i}\right)^2 = \frac{1}{n_i} + (\alpha_i \ln n_i)^2, \quad (3)$$

The unknown value of α_i expressed by

$$\alpha_i^* = \sqrt{\frac{\sum_{j=1}^N (\ln n_{i,j})^2 \left(\sigma_i^2 - \frac{1}{n_{i,j}}\right)}{\sum_{j=1}^N (\ln n_{i,j})^4}} \quad (4)$$

is determined by a χ^2 minimisation procedure.

Results and conclusions

The proposed method has been tested by use of Monte-Carlo simulations. The basic results of the reconstruction of the measurement errors (σ_i/n) are presented in figs.1-3. The detection of EAS charged particles have been simulated using the Poisson fluctuations and the Gaussian measurement errors according to expression (3). The results of the simulations for different fixed average values of $n \equiv \langle n \rangle = 2, 5, 10, \dots, 5 \cdot 10^3$ are shown in fig.1 (symbols). The results of simulations of n_i using the power law spectrum of shower size (N_e) and the uniform distribution of shower core coordinates x_0, y_0 on the GAMMA array are presented in fig.2 (symbols). The measurement errors of detectors at each

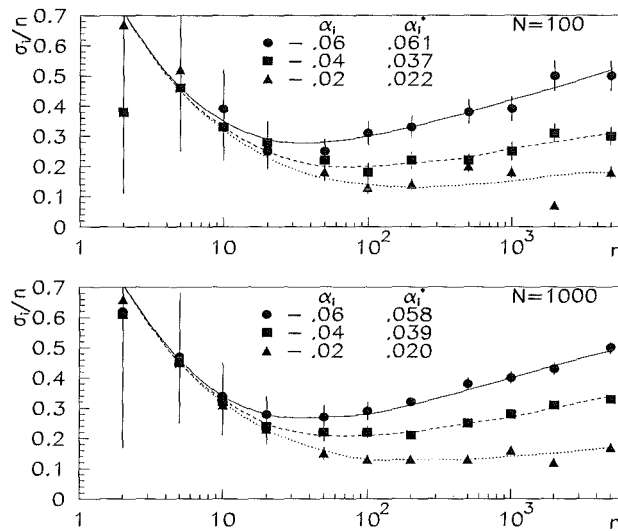


Fig. 1: Measurement error vs. number of charged particles in the detector. The dotted, dashed and solid lines correspond to α_i^* (4).

registration station correspond to $\alpha_i = 0.02; 0.04; 0.06$. The reconstructed values of α_i^* (4) and reconstructed variations (3) of the measurement errors for different numbers of detected particles are presented in figs.1,2 (solid, dash and dotted lines, respectively).

The number of simulated events (N) was equal 100 (upper fig.1) and 1000 (lower fig.1) for each given value of n . The total number of EAS events was equal to $5 \cdot 10^3$ (upper fig.2) and 10^4 (lower fig.2).

The accuracy of the α -parameter reconstruction is ca. 10% for $N \sim 10^4$ EAS events. For $n \leq 10$ the measurement errors could not be reconstructed due to very large Poisson fluctuations. Unfortunately, the steepness of the EAS size spectrum and the limited experimental sampling do not allow to investigate the $10^3 - 10^4$ range of n (see fig.2). The minimum necessary number of the detected EAS events for determination of

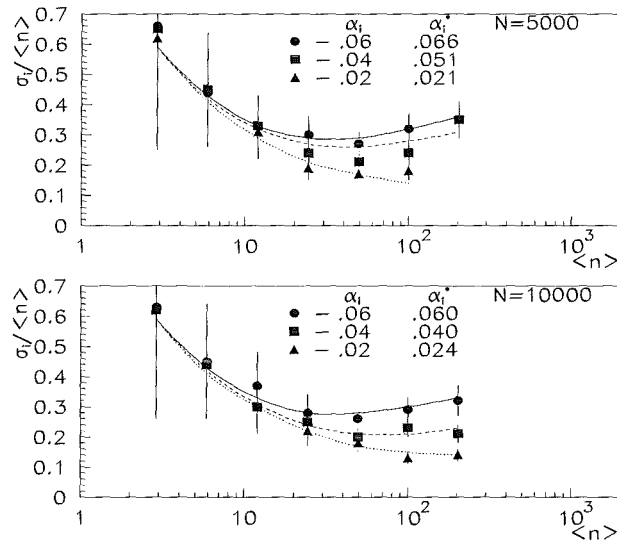


Fig. 2: Measurement error vs. number of charged particle simulated with the EAS size spectrum. The dotted, dashed and solid lines correspond to obtained α_i^* according to (4).

of measurement errors with accuracy better than 10% is approximately 10^4 for the GAMMA

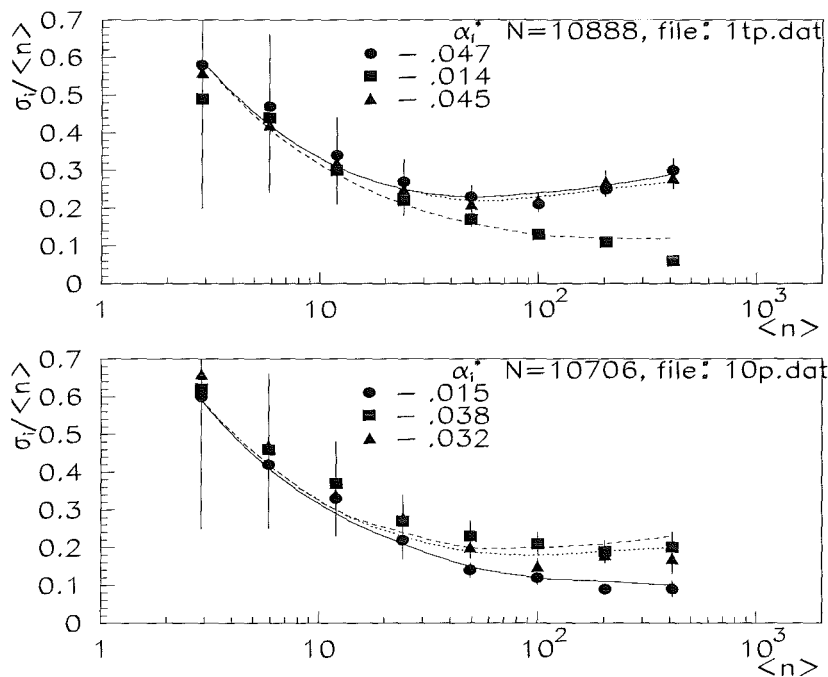


Fig. 3: Measurement error vs. number of charged particle in the GAMMA array detectors.

array. For $N_e \geq 10^5$ this number corresponds to one week of operation time of the GAMMA array.

The examples for the determination of the measurement errors from experimental data of GAMMA array are displayed in fig.3. then 10888 (upper fig.3) and 10706 (lower fig.3) observed EAS for 2 different registration stations are used. The results of simulations and experimental data analyses point out the high efficiency of the method of operative determination of measurement errors for the GAMMA array.

Acknowledgements

I am grateful to S. Ter-Antonyan for putting my attention to the problem and for his encouragement. I thank R. Martirosov and A. Garyaka for providing experimental data and for useful discussions.

References

1. V.C.Aseykin et al., *Preprint FIAN 31*, Moscow, 1987(in Russian)
2. S.V.Ter-Antonyan et al., *Proc. 24th ICRC* (Rome) 1995, **1**, 365;
V.V.Avakian et al., *Proc. 24th ICRC* (Rome) 1995, **1**, 348
3. T.Hara et al., *Proc. 18th ICRC* (Bangalore) 1983, **9**, 198
4. S.A.Arzumanian et al., *Proc. 24th ICRC* (Rome) 1995, **1**, 482

The measurement of the EAS charged particle component using a logarithmic ADC

G.G. Hovsepyan* for the ANI collaboration

Yerevan Physics Institute, Cosmic Ray Division, Armenia

For a nonlinear electronic system like a logarithmic ADC, it is impossible to derive an absolutely correct transformation. This can be a source of additional experimental errors. A hardware system is developed to obtain a priori information (the slope of background particles spectra) and to estimate the scale factor of transformation. Results of detector calibration and response simulation are presented.

Introduction

A common technique for Extensive Air Shower (EAS) detection is the sampling of the electron-photon component by a dense scintillator array. The number of particles incident on particular detector can approach 10^4 . Therefore logarithmic ADC's are usually used to transform the photo-multiplier (PM) signal in an amplitude range covering four orders of magnitude.

The logarithmic ADC amplitude - code transformation is described by

$$K = d \ln A + C \quad (1)$$

K is the registered code (output of ADC), d is the scale factor of ADC, A is the output signal of the photo-multiplier and C a calibration constant. If C is defined as a code of mean energy deposit corresponding to the incidence of the vertical single particle, then A is measured in units of particle number.

From (1) we can obtain

$$\frac{\Delta A}{A} = \frac{\Delta d}{d} \ln A \quad (2)$$

In order to achieve 10% accuracy in the upper ADC dynamic range, the scale factor has to be determined within 1% accuracy!

Estimation of the scale factor

A special system is used for the linearity control of the photomultiplier output and the

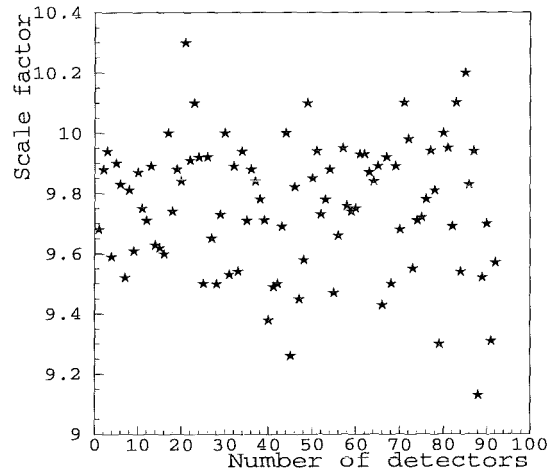


Fig. 1: The distribution of primary estimates of scale factor b_i^0 for all detectors of MAKET.

*e-mail:hgg@jerewan1.yerphi.am

ADC in a dynamic range of 10^4 and for primary estimation of the scale factor b_0 with accuracy, not worse than 10% (Fig. 1). For correction of scale factor primary estimate during installation running, such fundamental characteristic as background spectra slope measured by scintillation detector is used. Every 3 hours the installation recorded background for each of 92 detectors. The background spectrum is fitted and the power index β_i is used for scale factor correction. The background spectrum has the form

$$\frac{dF}{dA} = WA^{-\gamma}. \quad (3)$$

As the ADC is not an 'ideal' apparatus, the obtained estimate of scale factor $b^0 \neq d$ and the observed spectrum has to be unfolded

$$\frac{dF}{d\tilde{A}} = \left(\frac{dF}{dA}\right) \frac{dA}{d\tilde{A}}, \quad (4)$$

where $\tilde{A} = A \frac{d}{b^0}$ and

$$\frac{dF}{d\tilde{A}} = W \frac{b^0}{d} \tilde{A}^{-\left(\frac{b^0}{d}(\gamma-1)+1\right)}. \quad (5)$$

Using following notations

$$\tilde{W} = W \frac{b^0}{d} \quad (6)$$

$$\beta - 1 = \frac{b^0}{d} (\gamma - 1) \quad (7)$$

the observed spectrum takes the same functional form

$$\frac{dF}{d\tilde{A}} = \tilde{W} \tilde{A}^{-\beta}. \quad (8)$$

For all detectors with logarithmic ADCs which have different scale factors d_i and corresponding b_i^0 , we can estimate β_i and recalculate the estimate of scale factors b_i^1 for these ADCs using

$$b_i^1 = b_i^0 \frac{\gamma - 1}{\beta_i - 1}. \quad (9)$$

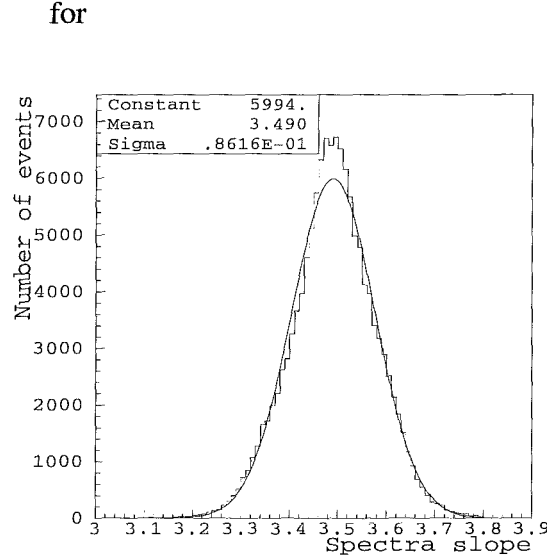


Fig. 2: The distribution of slopes β of the background particles spectra for all detectors of MAKET.

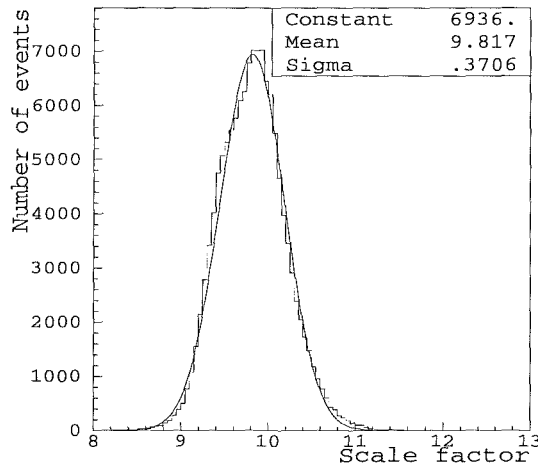


Fig. 3: The distribution of scale factors b_i^1 for all detectors of MAKET after recalculation.

For the estimate of background slope γ the median of variation of single slope estimates β_i is taken (Fig 2). The obtained value of $\gamma = 3.49$, is in good agreement with previously measured value [1].

This recalculation procedure takes place after each 3 hours of installation operation. Ca. 35000 background events were collected and used for the β_i calculation. If $\Delta\gamma \ll \Delta\beta$ then

$$\frac{\Delta b^1}{b^1} = \frac{\Delta\beta}{\beta - 1} \quad (10)$$

$$\frac{\Delta A}{A} = \frac{\Delta\beta}{\beta - 1} \ln A \quad (11)$$

The scale factors b_i^1 after recalculation (Fig.3) and the errors $\Delta\beta_i/(\beta_i - 1)$ (Fig.4) for all detectors of the MAKET installation are shown. The individual slopes (see Fig.5) are measured with 1 – 2% accuracy and therefore the ADC errors are proportional to

$$\sigma_{ADC} \sim (0.01 - 0.02) \ln A \quad (12)$$

All registered background spectra obtained in the years 1997-1998 were taken into account (Figs. 2 - 5).

Calibration and simulation results

For checking the obtained estimates a detector with two attached photo multipliers and ADC's was constructed. The readout system for both registration channels was the same as for all other detectors (EAS trigger, background registration, etc.). Measurements of the number of particles by two attached PM + ADC's provide the possibility to estimate the mean accuracy of the single detection channel. The variance of the average number of particles $A = 0.5(A_1 + A_2)$ equals to

$$\sigma_A^2 = 0.5(\sigma_{A1}^2 + \sigma_{A2}^2) \quad (13)$$

For each detecting channel

$$\sigma_{Ai}^2 = \sigma_{di}^2 + \sigma_{ci}^2 + \sigma_{ADCi}^2, \quad (14)$$

is written, where σ_{di} are the fluctuations due to light collection, PM quantum efficiency and amplifier fluctuation, σ_{ci} is the fluctuation due to

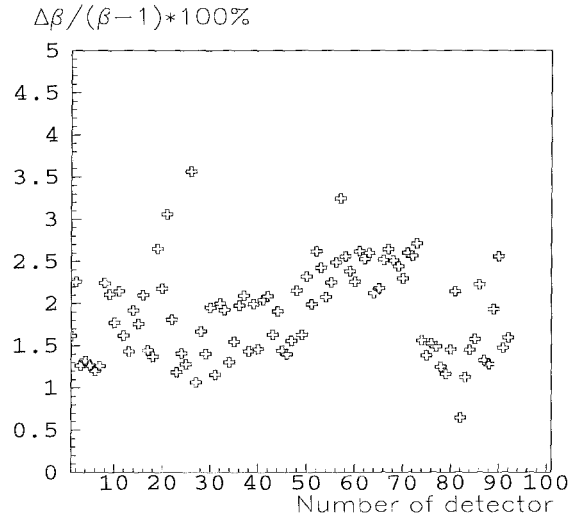


Fig. 4: The errors of mean slopes of the background particles spectra for all detectors of MAKET.

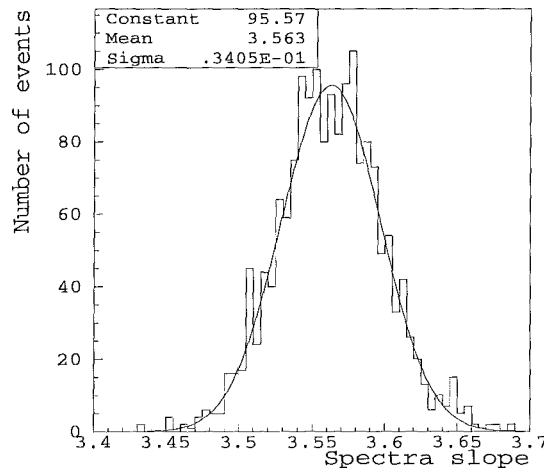


Fig. 5: The distribution of slopes β for one of the detectors of MAKET.

code discretisation and σ_{ADC_i} is the logarithmic ADC error ($\ln A$).

σ_{ADC} can be estimated from (11-12) for a particular detector. The mean square deviation (MSD) of the β distribution for the first channel of the test setup equals 2.3%, for the second 1.6%. Proceeding from the value of the ADC discretisation step ca. 0.1A we obtain $\sigma_c = (0.03 - 0.04)A$.

σ_d can be estimated by comparing a GEANT simulation [1] of detector response for single particles with the measured background distribution of charged particles.

Simulations were done for 1.5 mm Fe and 1.5 mm Al (the housing construction) and 5 cm plastic scintillators for a mixed flux (700 g/cm² atmosphere depth) of 30% electrons and 70% muons [2]. The primary energies of electrons have been fixed to 80 MeV and for muons 300 MeV. The angular distribution was assumed to be as $(\cos\theta)^{2.5}$ and $(\theta \leq 70^\circ)$. The simulated data of energy deposits E_{dep} in MeV were recalculated to ADC codes for comparing with experiment by:

$$K = d \ln(\phi) + C \quad (15)$$

$$\phi = \int f\left(\frac{E_{dep}}{E_1}\right) \Phi\left(A, \frac{E_{dep}}{E_1}\right) d\left(\frac{E_{dep}}{E_1}\right)$$

where E_1 is mean energy deposit of single charge particle in 5cm thick scintillator; $C = d \ln E_1 f\left(\frac{E_{dep}}{E_1}\right)$ energy deposit distribution in units of equivalence particles number;

$\Phi\left(A, \frac{E_{dep}}{E_1}\right) = \frac{1}{\sqrt{2\pi\sigma}} \exp\left(-0.5\left(\frac{A - \frac{E_{dep}}{E_1}}{\sigma}\right)^2\right)$ is the kernel of the Fredholm integral equation.

The tail of the experimental background distribution contains also contributions ($\sim 20\%$) of more than one particle. Therefore the comparison of measured and simulated distributions was made in code region of 1 : 8, corresponding to the single particle detection. In this case we can take the variance of the Gaussian distribution as estimate of the σ_d . The normalized simulated and experimental distributions coincide for a variance of ca. ~ 0.2 (Fig.6). Therefore the estimated mean detector error equals to:

Number of events/ N_{mod}

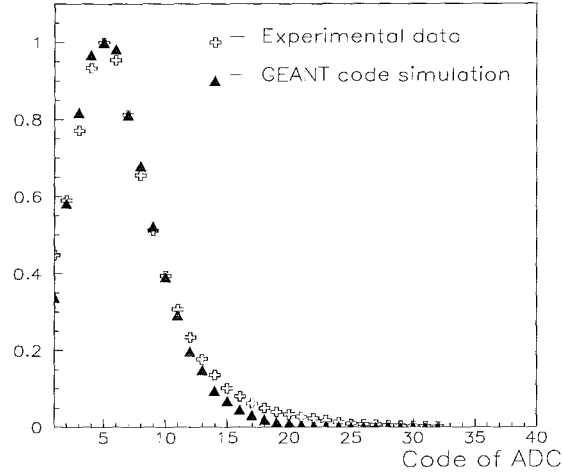


Fig. 6: The energy deposit distribution of the background particles

σ_A/A

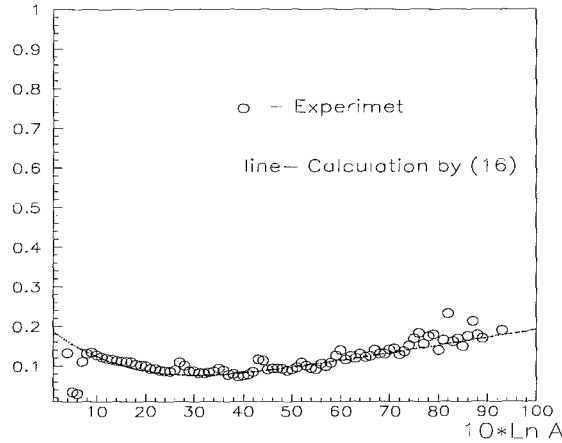


Fig. 7: The distribution of relative errors of examined channels

$$\sigma_A \sim A \sqrt{0.5 \left(\frac{0.26^2}{A} + 0.07^2 + (0.027 \ln A)^2 \right)} \quad (16)$$

In Fig.7 the obtained errors σ_A of the examined detector are shown with the estimates by eq. (16). The presented results agree with estimates of $\sigma_A \sim 20\%$ obtained earlier.

Conclusion

For all 92 MAKET scintillator detectors after implementing the correction procedure the scale factor errors are in the range of ca. $(0.01 \div 0.02) \ln A$.

The relative error of estimation of number of particles incident on $1m^2$, 5 cm thick scintillator are restricted by 20% in dynamic range of four orders of magnitude.

Acknowledgments

We would like to thank the colleagues from the KASCADE collaboration. Special thanks to Dr. A. Haungs for the great help in simulating the detector response.

References

1. GEANT: CERN Program Library Long Writeup W5013, CERN (1993)
2. O.C. Alkofer, P.K.F. Grieder *Physics Data. Cosmic Ray on Earth*, 25-1, Karlsruhe (1984) 5



EAS size spectrum for $1 \cdot 10^5 \leq N_e \leq 5 \cdot 10^7$ measured by the MAKET array

G.V. Gharagozyan* for the ANI collaboration

Yerevan Physics Institute, Cosmic Ray Division, Armenia.

The extensive air shower (EAS) size spectrum measured by the MAKET detector array, located on Mt. Aragats (3250 m a.s.l.) is presented. The EAS parameter reconstruction methods are discussed.

The MAKET installation

The MAKET installation (Fig. 1) consists of 100 plastic scintillation detectors with thickness of 5 cm. Twenty four of them with the area 0.1 m^2 are arranged in the central part and the others with the area 1 m^2 additionally in the center and on the periphery. The central part consists of 81 scintillation detectors and is arranged in a rectangle of $95 \times 63 \text{ m}^2$. At two peripheral points of a distance of 100 m and 70 m from the center of the installation there are 15 and 4 scintillation detectors, respectively. The signals from 92 detectors are included in the data analysis.

In order to estimate the zenith and azimuthal angles nineteen detectors (1 m^2) are equipped with timing readout measuring the EAS front appearance with an accuracy of ca. 5 ns.

The photomultipliers (PM-49) are placed in light-tight iron boxes. Logarithmic amplitude-digital converters (ADC) and constant fraction discriminators (CDF) are combined with the PM. The dynamic range of the registered particle number is $\sim 10^4$, corresponding to the code of the logarithmic ADCs from 0 to 100.

Three types of triggers are used:

1. A hardware trigger by 11 pre-selected trigger detectors with the conditions that at least 7 of them are firing with more than 3 particles.
2. A timing trigger by 19 timing detectors with (arranged symmetrically relatively to the center) the requirement that at least 9 are triggering. Four of them must work including the central detector in the geometrical center of the installation. The time delays are measured with respect to to the central detector.

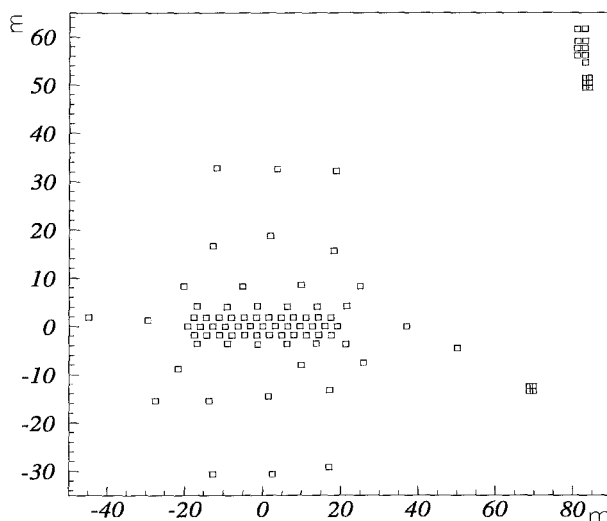


Fig. 1: Schematic view of the MAKET detector array.

*e-mail: gagik@crdlx4.yerphi.am

3. A software trigger derived from two groups of 8 symmetrically arranged detectors, with signals of at least one particle.

If the first two conditions are fulfilled together in interval of $20 \mu s$ the event is stored. If the third condition is fulfilled the event is transferred to the data base.

EAS parameter reconstruction

In the parallel with the main data acquisition system, the background events sampling is carried out for all array detectors. The sampling time is equal to $80 s$. For each detector the background distribution mode must be in the range of $5 \div 7$ codes.

In intervals of ca. 3 hours the collected background spectrum is stored as special file, and the slopes of differential spectrum with corresponding errors are determined and stored.

The conversion of the ADC code to the number of particles is done by

$$n_i = e^{-\frac{(k_i - k_i^0)(\beta_i - 1)}{b_i * (\gamma - 1)}}, \quad (1)$$

where k_i^0 is the mode of background spectrum, k_i is the ADC code, b^i is the estimate of scale factor, β_i is the slope of the background differential spectrum measured by i -th detector, γ is the estimate of the background spectra slope. For details see ref. [1].

For the determination of EAS parameters the lateral distribution function (LDF) is parametrised by the Nishimura-Kamata-Greisen (NKG) form and various modifications [2,3]:

$$\rho(R, N_e, s) = \frac{N_e}{R_m^2} \times 0.366 \times s^2 (2.07 - s)^{1.25} \left(\frac{R}{R_m}\right)^{s-2} \left(1 + \frac{R}{R_m}\right)^{s-4.5}, \quad (2)$$

where $R_m = 118 m$ is the Molière radius, N_e is the number of charged particles, s is the age parameter, R is the distance from EAS core. For $N_e < 10^7$ and $R < 100 m$ the contribution of the muon component is estimated to be smaller than 7% for depth $\simeq 700 g/cm^2$ [2]. Two independent programs of the reconstruction of EAS parameters using CERN χ^2 minimisation programs FUMILI and MINUIT were implemented.

The angular coordinates θ and ϕ were derived from timing information according to [4]. The uncertainties for θ and ϕ are less than 3° and 7° , respectively.

For the calibration we used Monte-Carlo simulations and reconstruct the EAS parameters. As long we assume that the response function of the detectors is known exactly, the EAS parameter reconstruction is believed to have an accuracy of 100% in the area $100 \times 80 m^2$. Taking into account the apparatus errors the following accuracies were obtained: $MSD(R) \simeq 2.25 m$, $rel.err.(N_e) \simeq 16\%$, $rel.err.(s) \simeq 6\%$ for the EAS with centre within of $40 \times 20 m^2$.

The experimental data stem from a running time of 5000 h in the period of June 1997 to July 1998, comprising ca. $3 \cdot 10^5$ events with $N_e > 10^5$.

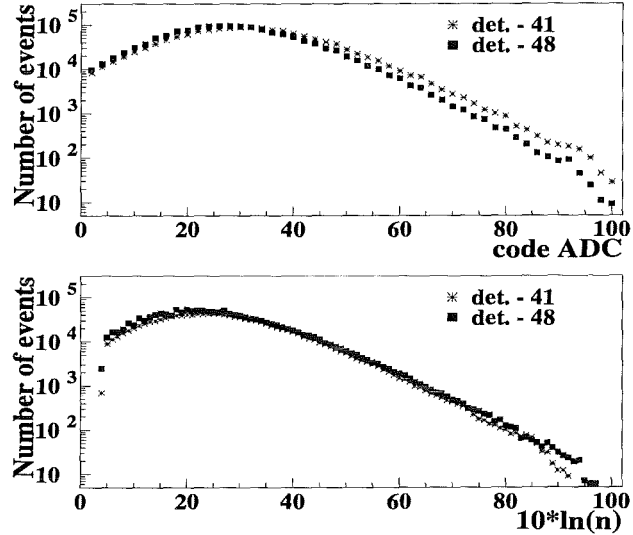


Fig. 2: Code spectrum (a) and n_i spectrum (b).

EAS size spectra

Fig. 2a shows the code spectrum for two detectors, symmetrically arranged around the center. The difference of the distributions is due to the individual ADC characteristics [1]. Fig. 2b displays the corresponding particle number spectra. Fig. 2 indicates the used calibration yields of the identical particles number spectra for symmetric (equivalent) detectors.

The data analysis excludes cases of detectors if

1. the dispersion σ is larger than 0.6 of k^0 -mode (the distribution of the energy deposits of the background);
2. $k^0 < 4$ or $k^0 > 8$;
3. $k_i > 90$ - ADC saturation condition;
4. $\beta_i < 3.35$ or $\beta_i > 3.65$, where β_i is the slope of the differential spectrum of the background.
5. the detector output corresponds to the maximal code for each registered EAS.

The relative error in each channel is due to Poisson fluctuations in addition to 12% from the discretisation of the code and $0.02 \ln(n_i)$ (ADC calibration errors) [1]. At the end of the dynamic range the last two contributions do not exceed 20%.

The total particle number of the observed EAS is calculated by

$$\ln(N_e) = \frac{\sum \left(\frac{\ln(n_i/f_i^t)}{\sigma_i^2} \right)}{\sum \left(\frac{1}{\sigma_i^2} \right)}, \quad (3)$$

where n_i is the measured particle number in i -th detector, f_i^t the particle number in the i -th detector expected by the NKG form, σ_i the mean square errors.

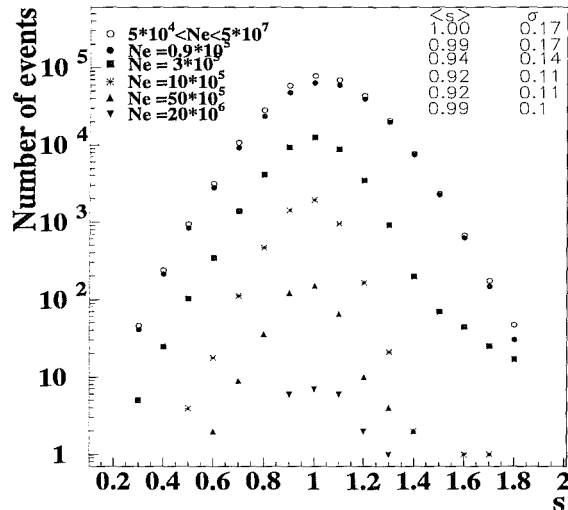


Fig. 3: Distribution of the age parameter for different N_e .

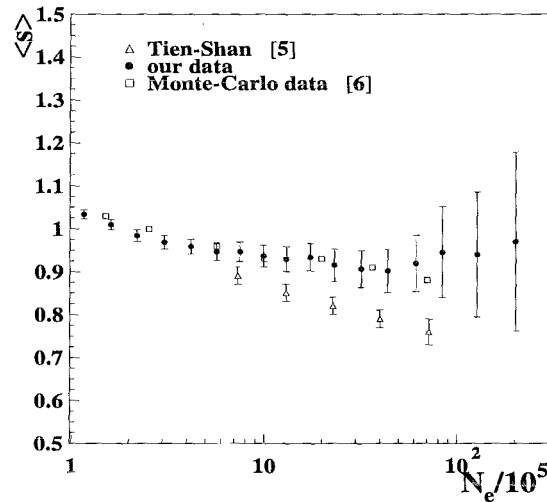


Fig. 4: Distribution of mean age vs. N_e .

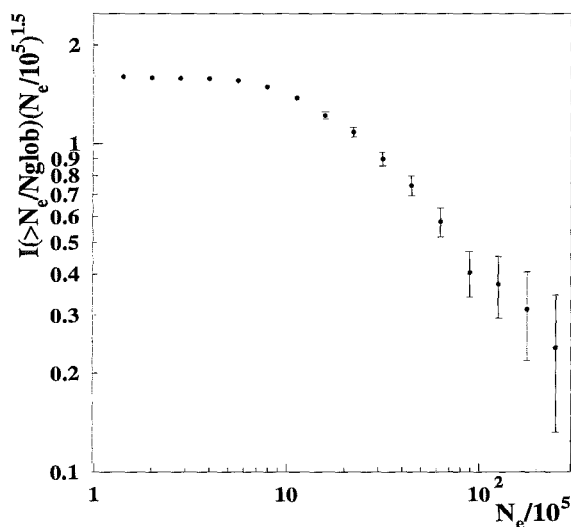


Fig. 5: The integral EAS size spectrum.

The analysis showed that both reconstruction procedures for the EAS parameters lead to identical results.

In present analysis the experimental data are selected with the following coordinates of EAS centers: $|x| < 20$ m, $|y| < 10$ m, and $1 \times 10^5 \leq N_e \leq 5 \times 10^7$. The number of events equals to ca. 3×10^5 . The mean age of these events $\langle s \rangle = 0.98$ with $\sigma = 0.17$. In Fig. 3 the age parameter (s) distributions for 5 logarithmically equal intervals of N_e with mean N_e , $\langle s \rangle$ and $\sigma(s)$ are shown. In Fig. 4 the EAS size distributions in interval $0.2 < s < 1.8$ are presented.

With increasing N_e the mean age ($\langle s \rangle$) seems to decrease up to $N_e = 10^6$; then it remains nearly constant up to $N_e = 10^7$. Additionally the Tien-Shan data

[5] and the results of a Monte-Carlo calculation on basis of the QGS model are displayed [6]. In Fig. 5 the integral EAS size spectrum in the interval $N_e = 1 \times 10^5 - 5 \times 10^7$, (multiplied by $N_e^{1.5}$) is shown. The quantity $N_{glob} = \frac{N_{tot}}{1 - \cos(42^\circ)}$, with N_{tot} the selected number of events. The "knee" appears at $N_e = (1.08 \pm 0.8)10^6$, the slope of the spectrum before the "knee" is $\gamma_1 = -1.48 \pm 0.01$, and after the "knee" $\gamma_2 = -1.91 \pm 0.02$. In Fig 6 the differential spectrum of N_e is shown with the scale factor $N_e^{2.5}$ on the ordinate.

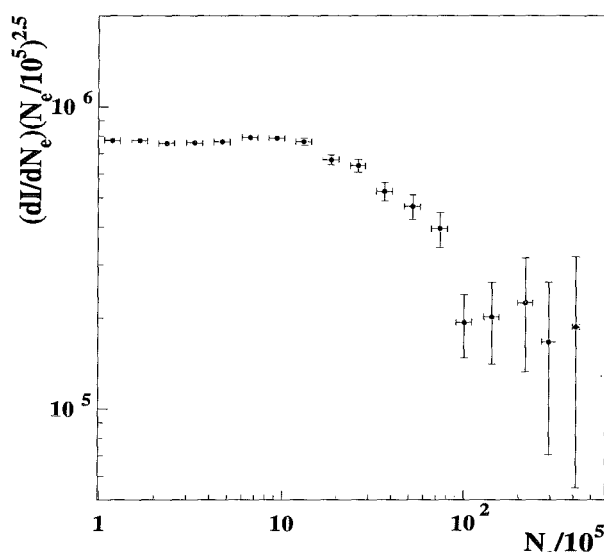


Fig. 6: The differential EAS size spectrum.

References

1. G.G. Hovsepyan, *ANI 98 workshop*, these proceedings
2. K. Greisen, *Progress in Cosmic Ray Physics* **3**, North Holland Publ. (1956);
K. Kamata, J.Nishimura, *Progr. Theoret. Phys., Suppl.* **6** (1958) 93
3. V.S. Aseykin et al., *Lebedev Institute Proceeding*, **109** (1979) 3 (in Russian)
4. V.V. Avakyan et al., *Journal of Nuclear Physics* **55** (1993) 174 (in Russian)
5. R.A. Antonov et al., *Proc. 24th ICRC*, (Rome) **2** (1995) 776
6. S.V. Ter-Antonian et al., *Proc. 24th ICRC*, (Rome) **1** (1995) 365

Investigation of the integral EAS size spectra in the knee region

S. H. Sokhoyan* for the ANI Collaboration

Yerevan Physics Institute, Cosmic Ray Division, Armenia

Results of measurements of the integral N_e -spectra above $\log(N_e) = 5$, from data accumulated with the MAKET detector installation (Mt. Aragats, Armenia at 700 g/cm^2) in the period of 1997- 1998 ($\sim 10^6$ events) are presented. The method of determining the position and shape of the knee is illustrated by the data. The spectral indices below and above the knee are determined, and the dependence of the shape of the knee region on different zenith angles of EAS incidence is studied and compared with other experiments.

Introduction

The origin of the so-called knee in the size spectrum of extensive air showers (EAS) is one of the most interesting topics of current cosmic ray investigations. Though the existence of this peculiarity of the spectrum is known since long time [1] and is a matter of a common consensus [2,3], the details of the knee region have not yet explored with sufficient accuracy. Contradictory results about the location of the knee and spectral shape of the knee region, dependent on the atmospheric height of the observation level and on the zenith angles of EAS incidence need a clarification by use of more detailed methods of the analyses. While Danilova et al. [4] do not observe a dependence of the knee position on the zenith angle, other investigations, like the KASCADE experiment at sea level [5] or the EAS TOP [6] measurements on mountain altitude (810 g/cm^2), infer an approximately linear displacement with the zenith angle.

Traditionally EAS size spectra $I(N_e)$ around the knee are approximated by

$$\log I(N_e) = \gamma * \log(N_e) + \text{const} \quad (1)$$

with two different spectral indices below and above the knee, defining the knee position as intersection of the two lines in logarithmic presentation. However, a more specific characterization of the shape of the knee region on basis of recent experimental results requires a more detailed description [7].

In the present contribution we communicate integral EAS size spectra measured with the MAKET detector array for a threshold of $N_e > 5 \times 10^4$. Using these results a method for the analysis of the spectral shape of the knee region is discussed and illustrated. The results are compared with recent studies of the KASCADE [5] and EAS TOP [6] collaborations.

Basic procedures

For a detailed description of the knee phenomena it is necessary to estimate the boundaries of this region and to parametrise the slope by an approximation function. The concept of finite and dividing differences is used to solve this problem. This concept is often used for the interpolation of continuous functions by n-power polynoms [8]

*e-mail: serg@crd6.yerphi.am

$$y \approx \varphi(x) = a_0x^n + a_1x^{n-1} + a_2x^{n-2} + \dots + a_n. \quad (2)$$

Let $x_k = x_0 + kh$, where k is an integer, $h > 0$, $y_k = y(x_k)$.

The first order finite difference(FD) of function in point x_k is the magnitude

$$\Delta y_k = y(x_{k+1}) - y(x_k) = y_{k+1} - y_k \quad (3)$$

The second order FD of function in point x_k is the magnitude

$$\Delta^2 y_k = \Delta y_{k+1} - \Delta y_k \quad (4)$$

Generally, n-order FD of function in point x_k determined by recurrence formula

$$\Delta^n y_k = \Delta^{n-1} y_{k+1} - \Delta^{n-1} y_k, \quad (5)$$

where $n \geq 1$, $\Delta^0 y_k = y_k$.

The first order dividing differences(DD) of function are magnitudes defined by

$$\bar{\Delta} y_0(x_0, x_1) = \frac{y_1 - y_0}{x_1 - x_0}; \quad \bar{\Delta} y_1(x_1, x_2) = \frac{y_2 - y_1}{x_2 - x_1}; \quad \bar{\Delta} y_2(x_2, x_3) = \frac{y_3 - y_2}{x_3 - x_2} \dots \quad (6)$$

Evidently,

$$\bar{\Delta} y_0(x_0, x_1) = \frac{y_0}{x_0 - x_1} + \frac{y_1}{x_1 - x_0} \quad (7)$$

Generally, n- order dividing DD of function is magnitude defined by recurrence formula

$$\bar{\Delta}^n y(x_0, x_1, \dots, x_n) = \frac{\bar{\Delta}^{n-1} y(x_1, x_2, \dots, x_n) - \bar{\Delta}^{n-1} y(x_0, x_1, \dots, x_{n-1})}{(x_n - x_0)} \quad (8)$$

where y_0, y_1, \dots, y_n are the node values of a function. In case of constant binning steps ($h = \text{const}$) this magnitude is determined by recurrence formula

$$\bar{\Delta}^n y_0(x_0, x_1, \dots, x_n) = \frac{\Delta^n y_0}{n!h^n}, \quad (9)$$

where $\Delta^n y_0$ are FD-values.

The properties of DD were used for a determination of the boundaries by fitting the knee range before approximating EAS spectra by χ^2 minimisation. That is: DD for n-order polynom takes constant value, independent from choice of the nodes (x_0, x_1, \dots, x_n) . DD of higher orders are equal zero.

If the linear behavior of spectrum in the regions below and above knee is generally accepted, then the usage of DD values will help to find not only the orders of polynom, but also to define the boundaries within which DD constancy is found.

The search of the knee region boundaries was done in the following sequence.

DD are calculated for the each pair (x_k, x_{k+1}) of neighboring points of the first five points of spectrum and for these values the standard deviation and average value are calculated.

Evidently, that value $\langle \bar{\Delta} y(x_k, x_{k+1}) \rangle \approx \gamma_1 \approx -1.5$ is the index of spectrum in region below knee.

If in the subsequent process of increasing of x_i points the violation of the first order DD constancy occurs (the criterium of constancy is $\bar{\Delta} y(x_k, x_{k+1}) \in \langle \bar{\Delta} y \rangle \pm 3\sigma$), then the last executed point is declared as the first point of the knee region. The first four orders DD calculations are carried out in wide region of spectra points, enclosing the searched knee region. The results demonstrate the constancy of the third order DD. It is violated only in linear regions of spectrum.

Therefore iteratively increasing of the executed spectra points a constancy of value $\bar{\Delta}^3 y(x_k, x_{k+1})$ is traced. The spread in values within $\langle \bar{\Delta}^3 y \rangle \pm 3\sigma$ is accepted.

In the region above knee only a linear fit procedure is performed. Only the spectrum points with number of events $n_k > 100$ are included in straight line fitting procedure.

It is necessary to note, that in procedure of searching of three spectra regions the overlap is allowed. Evidently, that accuracies of determination of the region boundaries essentially are depended on width of binning intervals. The found values of the spectrum regions boundaries include the knee region and have to be checked. Later at spectrum approximation procedure (shown below) this values will be determined with higher accuracy.

Lets denote: $N_e^{(1)}, N_e^{(2)}, N_e^{(3)}, N_e^{(4)}$ -the found boundaries of three regions of spectrum, n_i - number of events in i -th interval with $N_e > N_e(i)$, n_{tot} -total number of events.

The approximation function is

$$\log\left(\frac{n_i}{n_{tot}}\right) = \begin{cases} b_1 + \gamma_1 \log(N_e) & \log(N_e^{(1)}) \leq \log(N_e) \leq \log(N_e^{(2)}) \\ a[b - \log(N_e)]^3 + c & \log(N_e^{(2)}) < \log(N_e) < \log(N_e^{(3)}) \\ b_2 + \gamma_2 \log(N_e) & \log(N_e^{(3)}) \leq \log(N_e) \leq \log(N_e^{(4)}) \end{cases} \quad (10)$$

The cubic function was used for the spectrum approximation for KASCADE experiment [5].

The conditions of continuity of approximation function and its derivatives results in the four equation system with five unknown parameters $(a, b, c, N_e^{(1)}, N_e^{(2)})$

$$\begin{cases} -3a(b - \log(N_e^{(1)}))^2 & = \gamma_1 \\ -3a(b - \log(N_e^{(2)}))^2 & = \gamma_2 \\ a[b - \log(N_e^{(1)})]^3 + c & = \gamma_1 \log(N_e^{(1)}) + b_1 \\ a[b - \log(N_e^{(2)})]^3 + c & = \gamma_2 \log(N_e^{(2)}) + b_2 \end{cases} \quad (11)$$

From this equations one can obtain

$$b = \frac{\log(N_e^{(1)}) - \alpha \log(N_e^{(2)})}{1 - \alpha}$$

$$a = -\frac{\gamma_1}{3(b - \log(N_e^{(1)}))^2}$$

$$c = \gamma_1 \log(N_e^{(1)}) + b_1 - a[b - \log(N_e^{(1)})]^3$$

$$\log(N_e^{(1)}) = \frac{\log(N_e^{(2)})(d_1 + d_2 - \gamma_2) + b_1 - b_2}{d_1 + d_2 - \gamma_1}$$

Where

$$\alpha = \sqrt{\frac{\gamma_1}{\gamma_2}}$$

$$d_1 = -\frac{\gamma_1 \alpha}{3(1 - \alpha)}$$

$$d_2 = \frac{\gamma_2}{3(1 - \alpha)}$$

The value $N_e^{(2)}$ is taken as free parameter of approximation function in the knee region.

Then the spectrum approximation was achieved in following steps. First of all the linear regions of spectrum are approximated within found boundaries and the parameters $\gamma_1, b_1, \gamma_2, b_2$ of both lines are determined.

Then the approximation of knee region by the cubic function (10) is done. The free parameter of the fit is a right boundary of knee region ($N_e^{(2)}$). The rest parameters of approximation function a, b, c and left boundary of knee region $N_e^{(1)}$ are analytically tractable values.

Thus not only parameters (a, b, c) of approximation function are determined, but additionally the knee region boundaries get defined more exactly.

Results

For studies of the zenith angle dependence, the size spectra are accumulated in different angular bins so that the atmospheric thickness increases by a constant amount ($\approx 70 \text{gcm}^{-2}$).

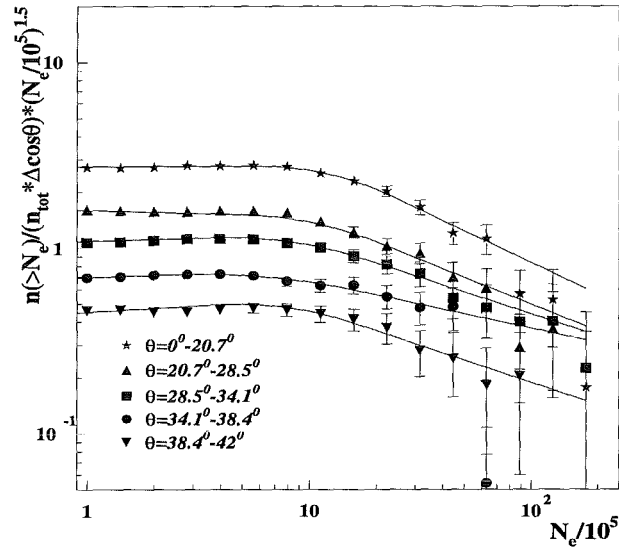


Fig. 1: Integral spectra for different zenith angles (MAKET, 1997-1998 data).

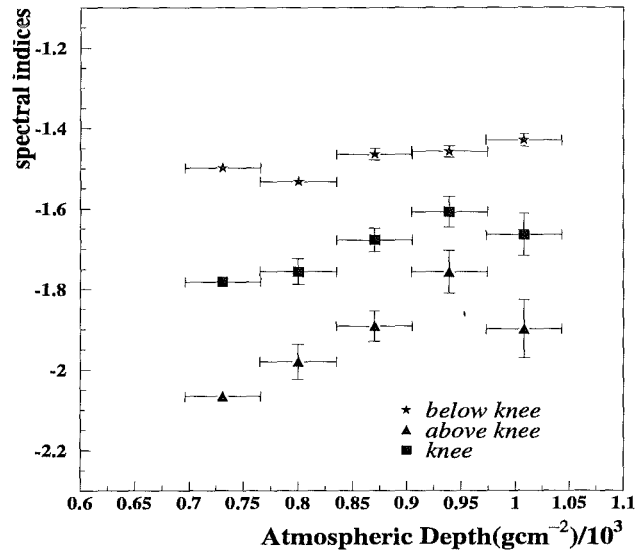


Fig. 2: Spectral indices of the size spectra vs. the atmospheric depth of the observation (MAKET data).

The integral flux of air showers as function of the shower size N_e and its approximation are shown in Fig. 1. The flux is multiplied by a factor $N_e^{1.5}$, emphasizing the change in slope between $N_e = 10^5$ and $N_e = 10^6$.

It is seen rather from Fig. 1, that suggested approximation function describes well the experimental spectra. It is evident that the knee region is displaced to the left with zenith angle increase.

The knee position considered to be equal to the first spectrum moment (center of weight) in the knee region

$$\log N_e^{(knee)} = \frac{\sum_{i=1}^k (\log(N_e^{(i)}) \log \frac{n_i}{n_{tot}})}{\sum_{i=1}^k \log(\frac{n_i}{n_{tot}})}$$

The weighted average values of indices are $\gamma_1 = -1.48 \pm 0.006^{(stat)}$ below, $\gamma_2 = -1.914 \pm 0.02^{(stat)}$ above the knee and $\gamma_3 = -1.7 \pm 0.01^{(stat)}$ in the knee point. Fig. 2 gives the spectral indices for the electron size spectra below knee, in knee point and above the knee. The spectral index in the knee is the first derivative of approximation function in this point. While the authors of [5] note that the spectra become steeper with increasing depth, our data do not confirm this observation. On the contrary, our result find that they become more gently sloping.

Fig. 3 shows the knee position as function of the relative depth of the atmosphere in comparison with KASCADE and EAS TOP experiments results. The shower sizes at knee position become smaller with larger zenith angles and exponentially decrease with the atmosphere depth.

References

1. G.V. Kulikov and G.B. Khristiansen, Sov. Phys. JETP **35** (1959) 441;
S.N.Vernov, G.B.Khristiansen: Proc. 10th ICRC (Calgary) **5** (1967) 345
2. G. Clark et al., Phys. Rev. **122** (1961) 637
3. S.I. Nikolsky, Proc. ICRS (Tokyo) (1984) 507
4. E.V. Danilova et al., Izv. RAN, Ser. Fiz. **58** (1994) 67

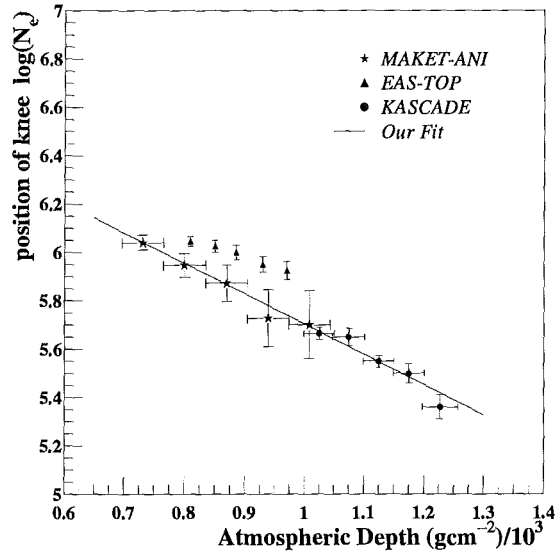


Fig. 3: Knee position as function of atmospheric depth.

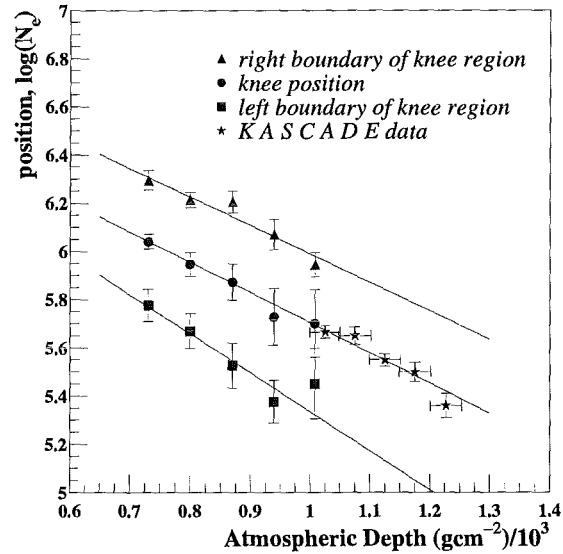


Fig. 4: Knee region boundaries and position of knee as function of atmospheric depth.

5. H.O. Klages for the KASCADE Collaboration: Proc. 25th ICRC (Durban) **6** (1997) 141;
R. Glasstetter for the KASCADE Collaboration: Proc. 25th ICRC (Durban) **6** (1997) 157
6. G. Navarra for the EAS TOP Collaboration: Proc. 25th ICRC (Durban) **6** (1997) 37
7. A.D. Erlykin and A.W. Wolfendale, *Astropart. Phys.* **7** (1997) 203
8. E. Volkov, *Numerical methods*, Nauka, Moscow 1982, p.48 (in Russian)

Expected cosmic ray background flux at Aragats level

S.V. Ter-Antonyan^{1*} and R.S. Ter-Antonyan²

¹*Yerevan Physics Institute, Alikhanyan Br.2, 375036 Yerevan, Armenia*

²*Moscow Institute of Physics and Technology, MFTI-8, Pervomaiskaia str. 141700 Dolgoprudny, Moscow region, Russia*

Calculations of the cosmic ray background spectra for γ, e, μ, p, n particles and (e^+e^-) pairs generated by γ -quanta in scintillators of ANI installation (mountain Aragats, 3200 m a.s.l., Armenia) are presented. The results of the calculations have been compared with corresponding world data. On the basis of the expected background fluxes the results of the calibration of an energy deposit - analog-to-digital converter (ADC) code for the Maket-ANI and GAMMA setups are obtained.

Introduction

The cosmic ray background flux is used in Maket-ANI [1] and GAMMA [2] experiments for both the PM high voltage control and the determination of the energy deposit of a minimum ionizing particle in scintillators. In the both cases the single particle spectrum directly connected with the energy deposits of the single background particles in the scintillators is measured. In this connection, it is essential to calculate precisely the expected energy spectra and the composition of the cosmic ray background on the observation level (mountain Aragats, 700 g/cm²). Moreover, the expected background flux on the observation level is of interest from the point of view of dependences on magnitudes of a solar modulation and a geomagnetic rigidity.

In this paper the method and results of the calculation of the energy spectra and the zenith angular distribution for γ, e, μ, p, n in the MeV energy region are presented. On the basis of the calculated cosmic ray fluxes the results of the calibration of the single particle energy deposit in the scintillator and the ADC code are also presented.

Calculation of the expected cosmic ray background flux

Calculations are carried out according to the expression

$$\frac{\partial I_{\zeta}(E_{\zeta})}{\partial E_{\zeta}} = \sum_A \int_{E_g(A)}^{\infty} \frac{\partial \mathfrak{S}_0(E_0, A)}{\partial E_0} \frac{\partial \Omega_{\zeta}(E_0, A, E_{\zeta})}{\partial E_{\zeta}} dE_0 \quad (1)$$

where $\partial \mathfrak{S}_0(E_0, A)/\partial E_0$ - are the energy spectra of the primary nuclei of mass A (A=1, 4, 16, 28, 56),

*corresponding author: e-mail: samvel@jerewan1.yerphi.am

$$\frac{\partial \Omega_{\zeta}(E_0, A, E_{\zeta})}{\partial E_{\zeta}} = \int \int \frac{\partial \omega_{\zeta}(E_0, A, E_{\zeta}, \theta)}{\partial E_{\zeta}} d \cos \theta d \varphi, \quad (2)$$

$\partial \omega_{\zeta}(E_0, A, E_{\zeta}, \theta) / \partial E_{\zeta}$ - is the differential energy spectrum (surviving function) for the $\zeta \equiv \gamma, e, \mu, p, n$ particle at observation level, generated by the primary nucleus of energy E_0 , mass A , zenith and azimuthal angles θ, φ . The values of Ω functions are calculated by the CORSIKA560-EGS-QGSJET code [3,4] taking into account a fragmentation of primary nuclei. The superposition model is applied in the simulation processes up to 80 GeV/nucleon. The zenith and azimuthal angles are simulated in the range of $(0 - 70^{\circ})$ and $(0 - 360^{\circ})$ correspondingly.

The primary energy spectrum $\frac{\partial \mathfrak{S}_0(E_0, A)}{\partial E_0}$ has a form $\Phi_0(A)(E_0 + E_{SM})^{-2.7}$, where $E_{SM} = 1.5$ GeV is a solar modulation term. We have got this approximation from the BESS balloon borne experiment [5] and approximations [6]. The geomagnetic rigidity ($P = 7.5$ GV) for the Aragats location determines the lower limit $E_g(A)$ of integral (1). In this case $E_g(p) = 7.5$ GeV and $E_g(A > 1) = A \cdot 4$ GeV.

The results of calculations of the background differential energy spectra and the corresponding calculations and experimental data [7-10] are presented in Fig.1. The integral fluxes

$$I_{\zeta}(> E_{\zeta}) = \int_{E_{\zeta}} \frac{\partial I_{\zeta}(E)}{\partial E} dE \quad (3)$$

are shown in Fig.2 in units of $(m^{-2}sec^{-1})$. The spectrum of the energy deposit of (e^+e^-) pairs by $\gamma \rightarrow e^+e^-$ processes in a 5 cm thickness plastic scintillators is also presented in Fig.1,2

The corresponding approximations (see Fig.1) of the vertical differential energy spectra for γ, e and μ fluxes have the following forms:

$$E_{\gamma} \frac{\partial I_{\gamma}}{\partial E_{\gamma}} = (320 \pm 5)(E_{\gamma} + 50 \pm .5)^{1.6 \pm .01}, \quad (4)$$

$$E_e \frac{\partial I_e}{\partial E_e} = (2095 \pm 70)(E_e + 225 \pm 5)^{1.9 \pm .03}, \quad (5)$$

$$E_{\mu} \frac{\partial I_{\mu}}{\partial E_{\mu}} = \frac{E_{\mu}}{1000} (.2 \pm .002) \left(1 + \frac{E_{\mu}}{1680 \pm 20}\right)^{-2.5 \pm .02}, \quad (6)$$

where $E_{e,\mu}$ are the kinetic energies in MeV of e, μ particles correspondingly.

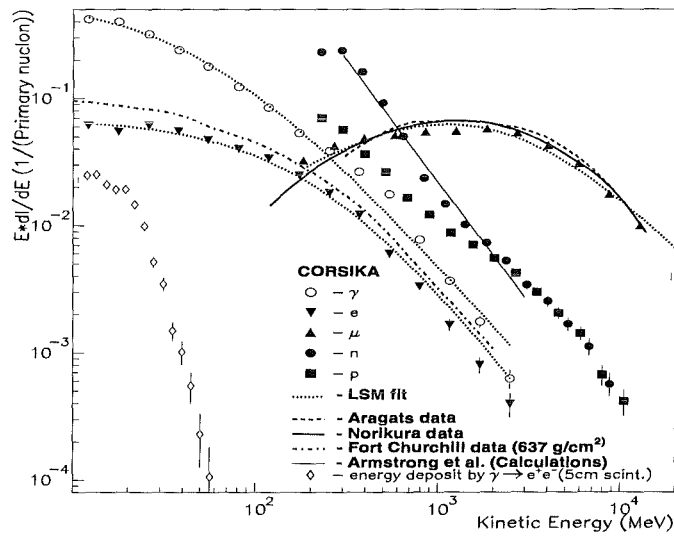


Fig. 1: *Differential energy spectra of cosmic ray in the MeV region.*

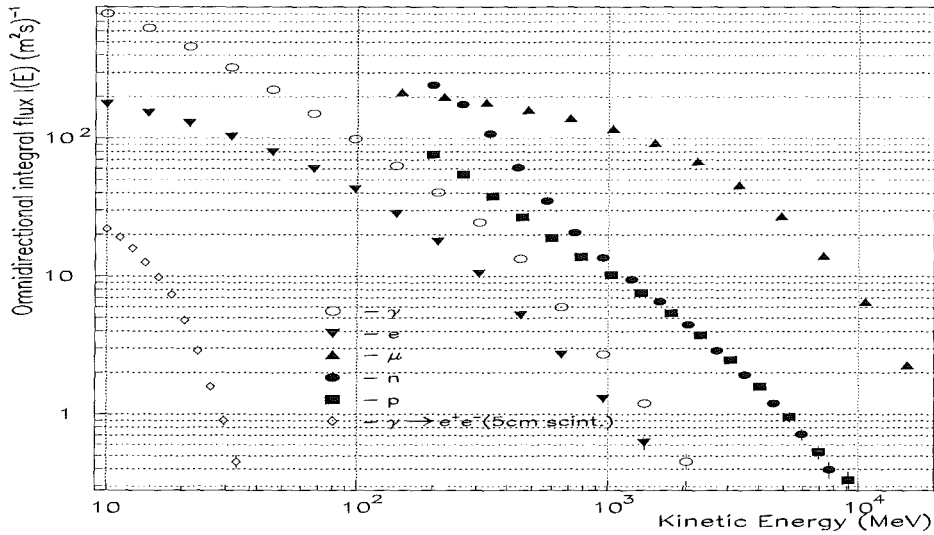


Fig. 2: Omni-directional integral energy spectra of cosmic ray particles.

The differential zenith angle distribution for different secondary energy thresholds (MeV) and for different particles are presented in Fig.3. The zenith angle distribution can be approximately described by the expression

$$\frac{\partial I(\theta)}{\partial \cos \theta} = \frac{\partial I(\theta=0)}{\partial \cos \theta} \cos^\rho \theta, \quad (7)$$

where the power index ρ depends on a background particle type. The contributions of different particles in the total integral flux and the values of $\rho(\zeta)$ at energy and zenith angular thresholds E_{min} and $\theta_{max} = 70^\circ$ are presented in the table.

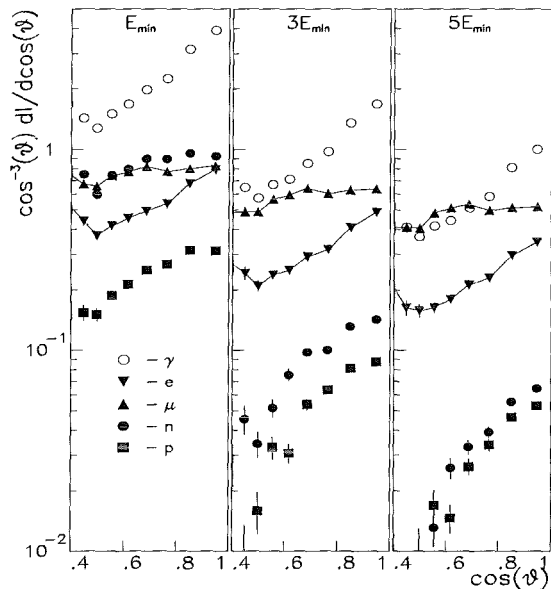


Fig. 3: Zenith angle distribution of cosmic ray for different energy thresholds.

ζ	$E_{min}(MeV)$	$I(m^{-2}sec^{-1})$	$\rho(\zeta)$
γ	10	800	$4 \pm .3$
e	10	178	$3.3 \pm .4$
μ	150	215	$2 \pm .3$
p	200	76	$3.3 \pm .5$
n	200	230	$3.2 \pm .5$
$e^+e^-(\gamma)$	10	22	$(4 \pm .3)$
$\sum Ich$		491	

Calibration of the energy deposit - ADC code for single charged particles

Key assumptions: It is assumed that the energy deposit $\frac{\partial E}{\partial x}$ in a scintillation detector is connected with scintillation light yield (I_{ph}) by the following transformation [11]

$$\frac{\partial E}{\partial x} \simeq \delta_{Sc} I_{ph}, \quad (8)$$

where I_{ph} is the total number of light photons deposited in scintillator, $\delta_{Sc} \simeq (100 - 200)$ eV/photon is the light transformation efficiency of scintillator. The further transformation of light photons to the photomultiplier's output voltage (U) has the form $I_{ph} \simeq \delta U^\eta$, where η is the power index of the transformation depending on a PM type. Repeating this transformation for n charged particles we obtain the following expression

$$[n] = \frac{\left(\frac{\partial E}{\partial x}\right)_n}{\left(\frac{\partial E}{\partial x}\right)_1} = \left(\frac{U_n}{U_1}\right)^\eta. \quad (9)$$

And taking into account the logarithmic ADC transformation in the form $k = [d \ln U]$, where k , an integer, is the ADC code and d is a scale factor, we connect the energy deposit and the ADC code which corresponds to n charged particles passing through the scintillator by the following expression

$$\ln \left(\frac{\partial E}{\partial x}\right)_n = \beta k + \alpha, \quad (10)$$

where α and β are parameters that depend on $d, \eta, \left(\frac{\partial E}{\partial x}\right)_1, k_1$. Using the expression (10) we can determine the α and β parameters by fitting the measured single particle spectrum $N_m(k)$ with the corresponding theoretical distribution $N_t(k)$.

Method of calculations and the results

Using the expected cosmic ray background fluxes at Aragats level for different particles we can present the expected differential ADC code spectrum $N_t(k)$ in the following form

$$N_t(k) = \sum_j \Delta_{k,j}(\epsilon_k, \epsilon_{k+1}), \quad \epsilon_k \equiv \left(-\frac{dE}{dx}\right)_k \simeq \exp(\alpha + \beta k) \quad (11)$$

where k are the ADC codes corresponding to the single particle energy deposits ($k = 1 \dots 10$), α and β are the unknown parameters, $\Delta_{k,j}$ are the contributions of different particles ($j \equiv \mu, e, \gamma$) in a summary energy deposit. The general expression for the $\Delta_{k,j}$ that takes into account pair production processes by γ and bremsstrahlung of electrons in scintillators and metallic casings, can be presented as the following integrals

$$\Delta_{k,j} = \int_{\epsilon_k}^{\epsilon_{k+1}} \int_1^{\cos \theta_m} \int F_j(E_{min}, \theta, \epsilon) \cos^{p_j+1}(\theta) d \cos \theta d \epsilon d \varphi \quad (12)$$

where,

$$F_{j \equiv \mu, e} = \int_{E_m - \epsilon_{Fe}}^{\infty} \frac{\partial I_j}{\partial E_j} f(E_j, \epsilon, t / \cos \theta) d E_j, \quad (13)$$

$$F_\gamma = \int_{E_m}^{\infty} \frac{\partial I_\gamma}{\partial E_\gamma} \Phi(E_\gamma, \theta, t, \varepsilon) dE_\gamma, \quad \Phi = \Phi_1 + \Phi_2, \quad (14)$$

$$\Phi_1 = \left(1 - e^{-\frac{x_{Fe}}{\lambda_{Fe}}}\right) f\left(\left(E_\gamma - \frac{\varepsilon_{Fe}}{2}\right), \varepsilon, \frac{t}{\cos\theta}\right), \quad (15)$$

$$\Phi_2 = e^{-\frac{x_{Fe}}{\lambda_{Fe}}} \int_0^{\frac{t}{\cos\theta}} \frac{1}{\lambda_{Sc}} e^{-\frac{x}{\lambda_{Sc}}} f\left(E_\gamma, \varepsilon, \left(\frac{t}{\cos\theta} - x\right)\right) dx, \quad (16)$$

$f(E_j, \varepsilon, t/\cos\theta) = \frac{1}{\xi} \varphi(\omega)$ is the Landau distribution with parameters

$$\omega = \frac{\varepsilon - \varepsilon_p}{\xi} - 0.225, \quad \text{end } \xi = \frac{t}{\cos\theta} \cdot D \cdot 0.1536 \cdot \frac{Z}{A} \cdot \frac{1}{\beta^2}$$

In the presented expressions θ, φ are the zenith and azimuthal angles of j -th particles, ε_p is the likelihood energy deposit in scintillator, $\lambda_{Fe, Sc}$ are the pair production interaction lengths in the casing and scintillator materials, x_{Fe} is the thickness of the iron casing, ε_{Fe} is the average energy deposit in the iron, t is the thickness of scintillator, $\frac{\partial I_j}{\partial E_j}$ are the differential energy spectra of j -particles, ρ_j are the power indexes of the zenith angle distributions, and E_{min} is the minimum energy of j -particles. The zenith angle distributions and the differential energy spectra of j -background particles are presented in a previous section (expressions 4-7).

The α and β unknown parameters (expressions 10,11) can be obtained for each scintillator on the basis of a $\chi^2(N_t, N_m)$ minimization for the expected single particle spectrum $N_t(k)$ from expression (11) and the corresponding measured spectrum $N_m(k)$. This calculations are performed for Maket-ANI and GAMMA experiments. The basic results of the calculations for 4 scintillators from each experiment are illustrated in Fig.4. The lines correspond with the expected single particle spectrum from expressions (11-16), the dots are experimental data. The good agreements in the (1-10) ADC code measurement range which responsible for the single particle

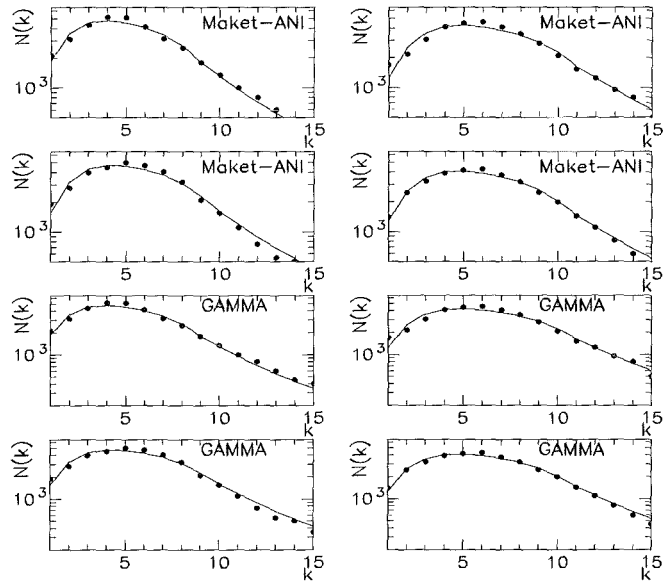


Fig. 4: Measured single particle spectra $N_m(k)$ (symbols) and expected spectra $N_t(k)$ (lines).

spectrum, point out on a correctness of the energy deposit - ADC code transformation is shown in Fig.5 (lines) for MAKET-ANI and GAMMA arrays (8 scintillators from each

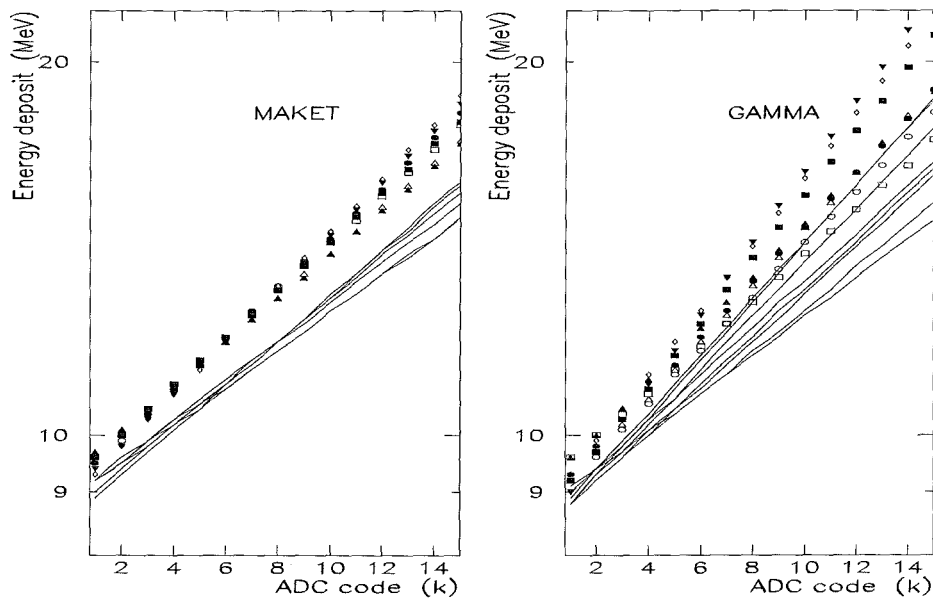


Fig. 5: Energy deposit vs. code ADC for the MAKET and GAMMA experiments.

experiment). The symbols in Fig.5 describe the results of the calculation where the monoenergetic muon flux ($E_\mu = 300$ MeV) is the only flux used as a background cosmic ray spectra. The discrepancies of lines in Fig.5 are the consequences of distinctions in ADC technical parameters such as a scale factor d (expression 10) for different detectors.

It is seen, that the contribution of the e component is significant and the minimum detectable energy deposit in both Maket-ANI and GAMMA arrays is equal to 9 MeV. Moreover, from Fig. 5 we can check the ADC for each array. The discrepancy of the energy deposit - ADC code transformation lines for the Maket-ANI array is lower than for the GAMMA array.

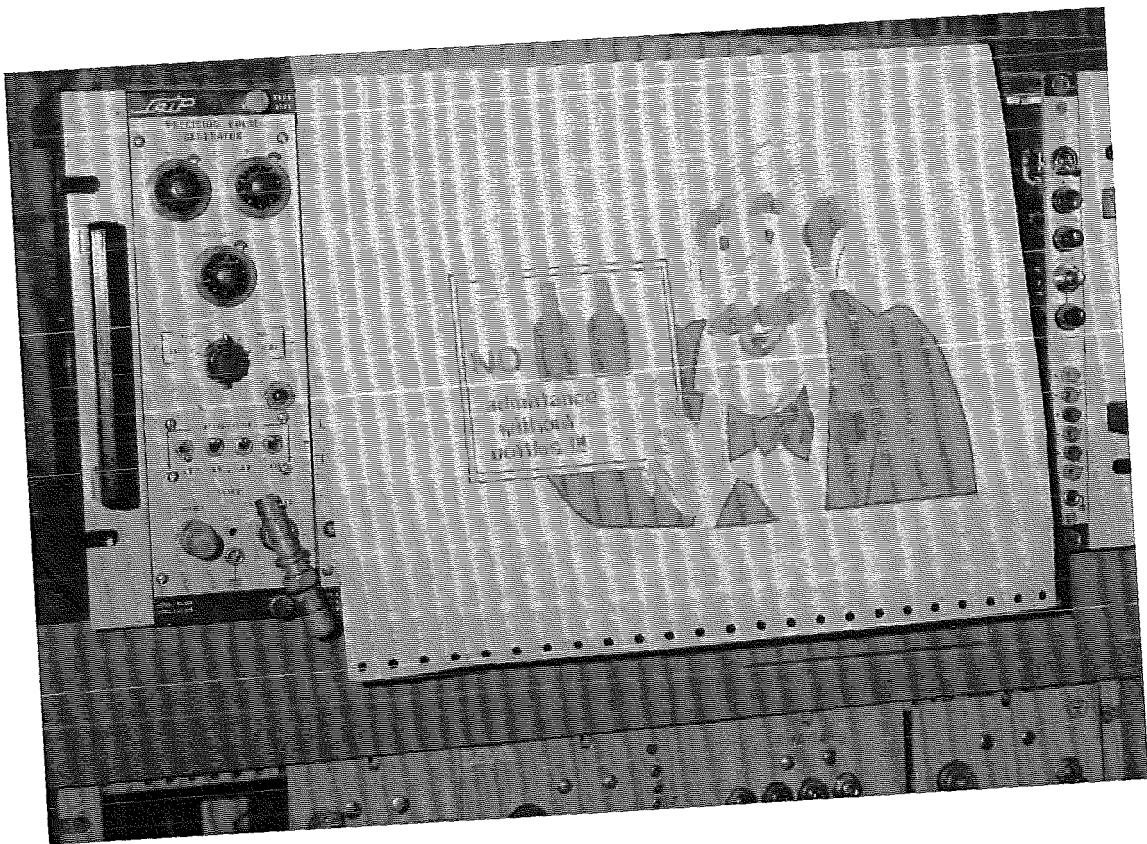
Acknowledgements

We are grateful to A.A. Chilingaryan for putting our attention to the problem, and we thank H. Rebel, J. Knapp and D. Heck of Forschungszentrum Karlsruhe for providing the CORSIKA code. We would like to thank the ISTC A116 grant for the support of the investigations.

References

1. S.V. Ter-Antonian et al., *Proc. 24th ICRC*, (Rome) 1995, **1**, 365
2. S.A. Arzumanyan et al., *Proc. 24th ICRC* (Rome) 1995, **1**, 482
3. J. Knapp et al., *Proc. 24th ICRC* (Rome) 1995, **1**, 403
4. D. Heck et al., *Report FZKA 6019*, Forschungszentrum Karlsruhe 1998
5. B. Wiebel-Sooth et al., *Proc. 24th ICRC* (Rome) 1995, **2**, 656
6. E.S. Seo et al., *Proc. 24th ICRC* (Rome) 1995, **2**, 648
7. N.M. Kocharian et al., *Soviet Phys. JETP* 1956, **3**, 350
8. J. Brooke et al., *J. Phys. Soc. Japan*, suppl. **17** suppl. A-III, 1962, 311

9. R.R. Daniel and S.A. Stephens, *Rev. Geoph. and Space Phys.* **12** (1974), 233
10. T.W. Armstrong et al., *J. Geophys. Res.* 1973,**78**, 2715
11. E. Segre, *Experimental nuclear physics* New York-London, 1953 **1**, 273



The α parameter is model independent

M. Brankova¹, R.M. Martirosov², N.M. Nikolskaya³, V. Pavlyuchenko³,
J. Procureur^{4*}, J.N. Stamenov¹

¹*Institute for Nuclear Research and Nuclear Energy, Sofia, Bulgaria*

²*Yerevan Physics Institute, Cosmic Ray Division, Armenia*

³*P.N.Lebedev Institute, Moscow, Russia*

⁴*Centre d'Etudes Nucleaires de Bordeaux-Gradignan, France*

A bias in analyses of experimental data of EAS observations is the classification by fixed shower sizes. It is well known that showers of such classes originate from primaries with different masses and different primary energies. For the GAMMA experiment (Mt. Aragats 3250m a.s.l.) we have defined an adequate parameter α for a selection along the primary energy. In the present work, we show that this α parameter is nearly model independent. The result is based on simulations using three different simulation codes, SMI (Bordeaux, France), GENEAS (P.N.Lebedev, Institute-Moscow, Russia) and CORSIKA (Karlsruhe, Germany) using different fragmentation modes of the hadronic interactions.

Introduction

The main purpose of EAS experiments is a determination of the energy and the mass composition of the cosmic projectiles generating extensive air showers (EAS). Though the goal is clear, an approach for a correct answer is rather complicated. Important reasons are the current standard procedures in use to extract physical information from the experimental data, e.g. a shower selection by fixed values of the showersize. It is known that fixed sizes of showers generated by primaries of different masses correspond to different primary energies. Therefore the determination of the primary mass composition from fixed size bins is not a very promising way.

Selection of showers with fixed energies

A new parameter allowing a selection by fixed energies has been proposed by J.Procureur and J.N.Stamenov some years ago for high-mountain altitude experiments [1]. For the altitude of the Tien Shan experiment, this parameter is chosen by

$$\alpha(70) = 70^2 \rho_e(70) / f_{NKG}(10, S_{6-70})$$

where $\rho_e(70)$ is the lateral density of the electromagnetic component measured at 70m from the shower centre, f_{NKG} is the well known Nishimura-Kamata-Greisen function with S_{6-70} the local age determined from densities measured at 6m and 70m from the core. Fig.1 shows that $\alpha(r)$, estimated at 120m from the shower centre, depends on the primary energy, but is practically independent from the mass. Actually in the Tien Shan experiment there were no detectors placed at 120m distance from the core. Therefore the EAS selection has been approximated for fixed values of $\alpha(r)$ measured, at 70m distance where detectors were

*corresponding author: e-mail: jproc@cenbg.in2p3.fr

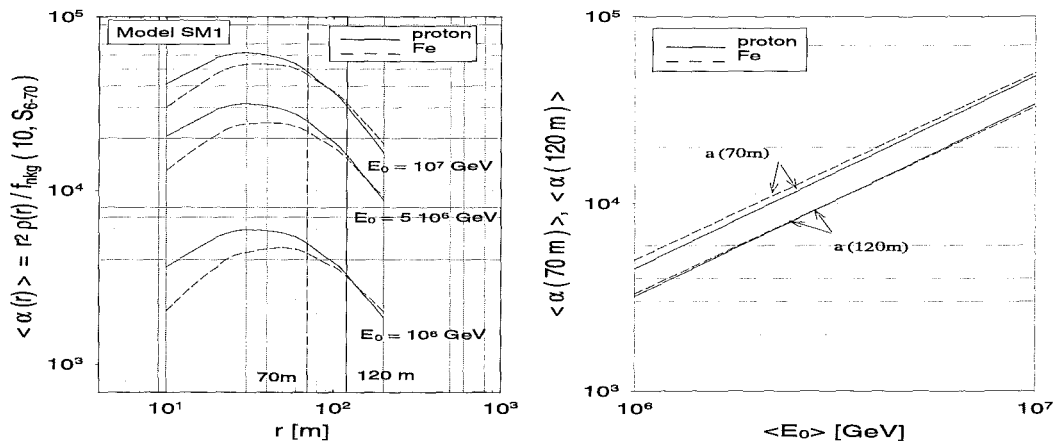


Fig. 1: The selection parameter $\alpha(70)$ versus the distance from the shower centre simulated by the SM1 code (a) and the dependence of $\alpha(70)$ and $\alpha(120)$ on the primary energy E_0 (b).

placed. As fig. 1b indicates $\alpha(70)$ exhibits obviously some dependence of the mass, while it is less significant for $\alpha(120)$. But the mass dependence is weak (as shown in fig. 2 for the SM1 calculations). Nevertheless the question how different interaction models may lead to different calibrations is still open.

Model dependence of the $\alpha(70)$ parameter

In order to test the influence of different models used in different simulation codes, we considered the following models:

1. The SM1 Model [2],
2. The GENEAS code developed by V. Pavlyuchenko and N.M.Nikolskaya, but still unpublished,
3. CORSIKA, in version 4.50 [3].

All these Monte-Carlo programs applied for the development of the muon and hadron components, use an analytic approach for the electromagnetic component (at least optionally). In fact, the main differences originate from the description of the nuclei-air interactions.

Figs. 3 and 4 display results for the dependence of α from the distance of the shower core and from the primary energy, resulting from calculations with different Monte-Carlo simulation codes.

Improvement of the α parameter definition using CORSIKA

Following the CORSIKA results, the crossing point appears to be located at $r = 200\text{m}$. Such a large value of r implies experimental difficulties due to small partial densities.

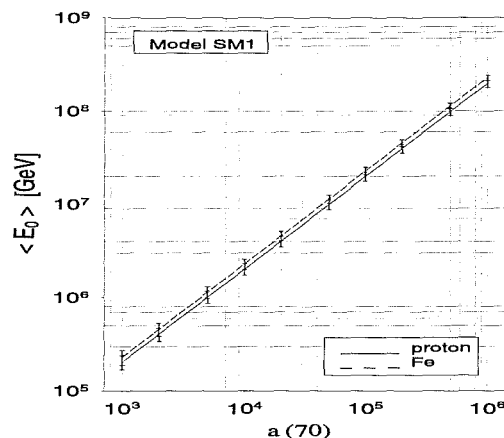


Fig. 2: Dependence of primary energy on $\alpha(70)$ calculated on basis of the SM1 model [2].

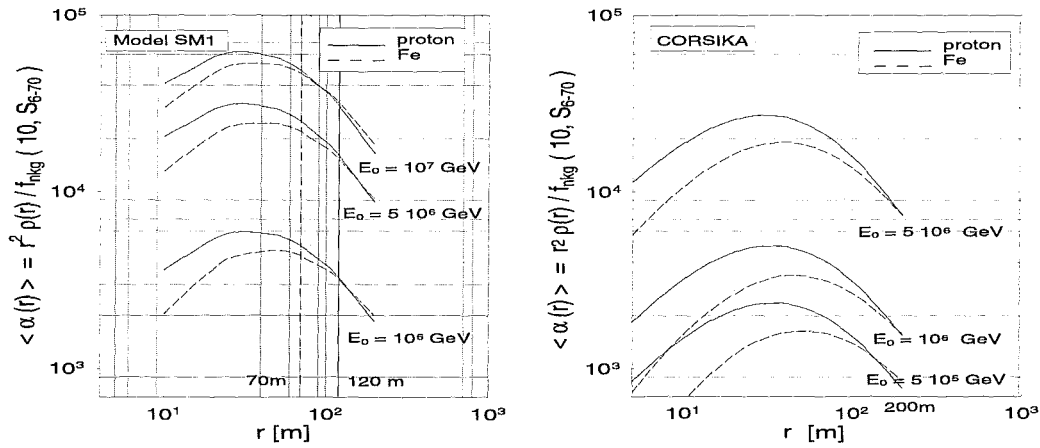


Fig. 3: The selection parameter $\alpha(70)$ versus the distance from the shower centre based on calculations with different Monte-Carlo codes: SM1 (a) and CORSIKA (b).

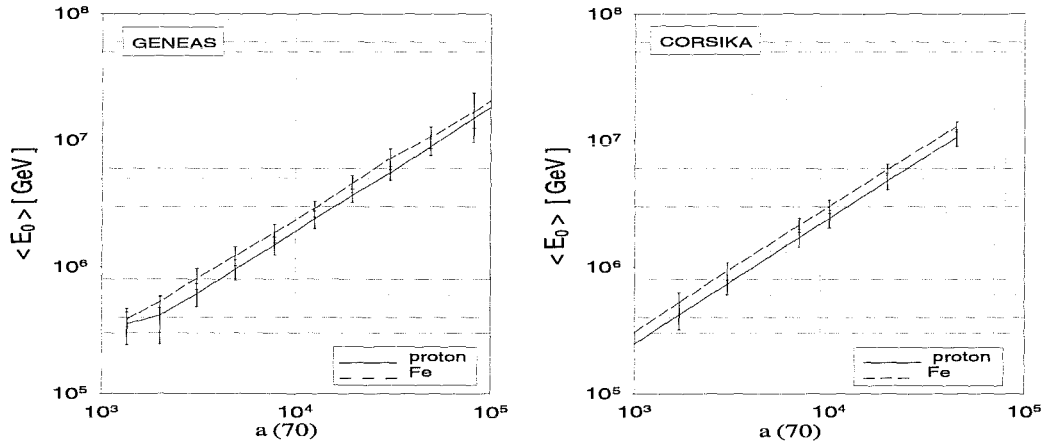


Fig. 4: The dependence of the primary energy on $\alpha(70)$ by different Monte-Carlo codes: GENEAS (a) and CORSIKA (b).

Therefore we try to redefine the α parameter

$$\alpha(r) = r^2 \rho_e(r) / f_{NKG}(3, S_{25-135}).$$

which shifts the crossing point to 135m (fig. 5a). This distance is particularly favorable for the GAMMA experiment on Mt. Aragats (a schematic layout is shown in fig. 5b), which aims at a determination of the mass composition around the 'knee'. These detectors (20m^2) are placed at 135m from the centre of the array, which enable to determine the lateral density $\rho_e(135)$. As indicated in fig. 6 the determination of the primary energy for showers selected with fixed values of $\alpha(135)$ is nearly mass independent. We note that the detector response has been taken into account for these calculations.

Conclusion

This study shows a new definition of the parameter $\alpha(135)$ as selection criterium for EAS observation, since the CORSIKA simulation prove that this parameter is an energy indica-

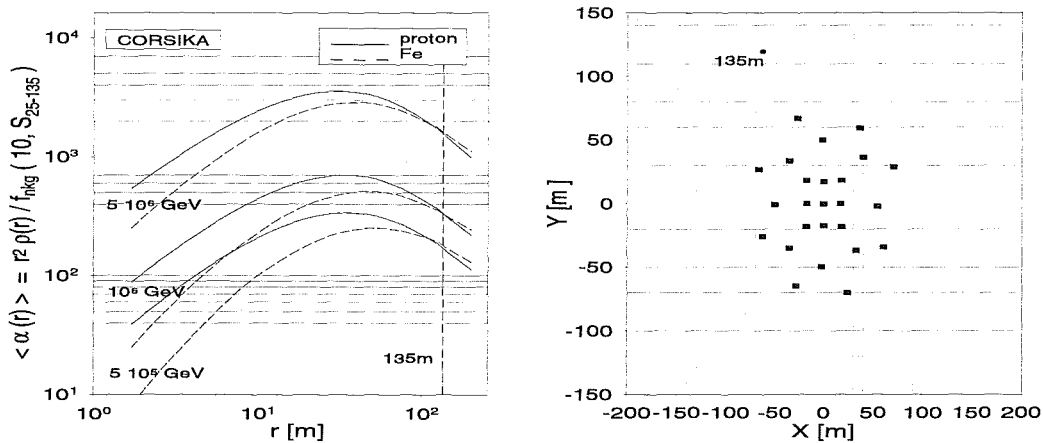


Fig. 5: (a) The selection parameter $\alpha(135)$ versus the distance from the shower centre from simulations with the CORSIKA code. (b) The surface part of the GAMMA installation.

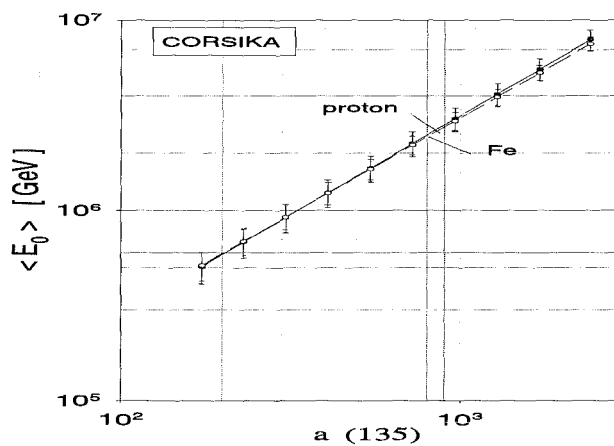


Fig. 6: The dependence of the primary energy on $\alpha(135)$ from simulations with the CORSIKA code.

tor, nearly independent from the primary mass for the observation level of the GAMMA experiment. The model dependence seems to be weak, though the different locations of the crossing points (see fig. 3) by different kinds of simulations need further clarification.

References

1. J.Procureur and J.N.Stamenov, *Nucl. Phys. B* 39A (1995) 242
2. J.Procureur and J.N.Stamenov, *J. Phys. G* 16 (1990) 317
3. J.N.Capdevielle et al, *Kernforschungszentrum Karlsruhe, KFK Report 4998* (1992);
D. Heck et al, *Forschungszentrum Karlsruhe, FZKA Report 6019* (1998)

Studying a new possibility of EAS selection

L.G.Melkumyan* for the ANI collaboration

Yerevan Physics Institute, Cosmic Ray Division, Armenia.

A new shower selection parameter has been studied using the experimental data from MAKET installation, located on Aragats research station (3250 m a.s.l.). The peripheral detector station 15 m² located at 120 m from geometrical center of installation was used for precise measurement of electron-photon density and determination of EAS selection parameter.

Introduction

Extensive air showers (EAS) provide basic information about mass composition and energy spectrum of primary cosmic rays in energy region above 10³ TeV. The appearance and consequently the efficiencies for the selection of EAS with fixed electron number N_e or muon number N_μ are different for EAS initiated by primaries of different masses A . This is due a different longitudinal development of the air showers in the atmosphere . Comparing the N_e and N_μ development obtained by using the superposition model [1,2] or applying a fragmentation hypothesis [3-5] and considering the steeply falling-off energy spectrum for all A , it gets obvious that EAS selected along fixed electron sizes originate dominantly from primary protons or light nuclei. On the contrary, in events selected with constant muon size N_μ , heavy primaries tend to get dominant.

The current methods for investigations of the energy spectrum and the mass composition of the primary cosmic radiation in the ultra high-energy region are mainly based on the experimental study of the N_e and muon N_μ spectra and on the analysis of the corresponding fluctuations. However, even for observation on mountain level (600-700 gcm⁻²), with reduced fluctuations, the conventional selection procedures imply a considerable bias for the primary spectrum and mass composition determination. One origin of the bias is the above mentioned dependence of the shower registration efficiency on the atomic number of the primary particle [2,5], when classifying along N_e or N_μ .

Thus merely the so-called observed mass composition can be inferred [5], and the true mass composition of the primary cosmic rays for a given energy needs an estimate of the primary energy using a not well defined correspondence between shower size and primary energy, e.g. which is in turn mass dependent. These features involve a bias in the determination of the mass composition or energy spectrum of the primary flux. Both types of mass compositions (observed and true) appear to be different [5], and their correspondence is largely model dependent.

In order to relieve such difficulties a new EAS selection parameter $\alpha_e(r)$ has been introduced by Procureur J. and Stamenov J. N.[6] defined as

$$\alpha_e(r_1) = \frac{r_1^2 \rho_e(r_1)}{F_{NKG}(r_2, s_{loc})} \quad (1)$$

*e-mail: laura@crdx4.yerphi.am

where $\rho(r_1)$ is density of the lateral electron distribution at the distance r_1 from the shower axis, $F_{NKG}(r_2, s_{loc})$ is the Nishimura-Kamata-Greisen function calculated for the distance r_2 from shower axis and for local age s_{loc} . With local age s_{loc} we denote an age parameter derived in certain radial interval of the lateral distribution.

The choice of r_1 , r_2 and s_{loc} is dependent from the actual observation level and from the existing detector displacements of the EAS array. It has been shown, that for the arrangement at altitude of the Aragats Cosmic Ray station a useful specification of the α parameter is

$$\alpha_e(120m) = \frac{120^2 \rho_e(120m)}{F_{NKG}(10m, s_{6-70})} \quad (2)$$

where local age s is derived from the $\rho_e(6m)$ and $\rho_e(70m)$. Indeed, model calculations [7] carried out on the basis of SM1 model show [8-10] that the α_e parameter at the distance 120 m is a good energy estimator and is nearly independent from the primary mass in a wide energy range of $5 \cdot 10^5 - 10^7$ GeV. This feature is a simple consequence of the peculiarity of the NKG function, which shows a strong dependence of $\rho_e(r)$ in the central part of the shower on the age parameter and therefore on the mass of the particle.

Results

We present preliminary results of the investigation of the α_e parameter applied to the data of the MAKET experiment on Mt. Aragats.

$$s = \frac{\ln \left(\frac{\rho_i}{\rho_j} * \left(\frac{r_i}{r_j} \right)^{2.18} * \left(\frac{r_i+r_m}{r_j+r_m} \right)^{4.5} \right)}{\ln \left(\frac{r_i}{r_j} * \frac{r_i+r_m}{r_j+r_m} \right)} \quad (3)$$

The determination of the α parameter contains following research steps: Us-

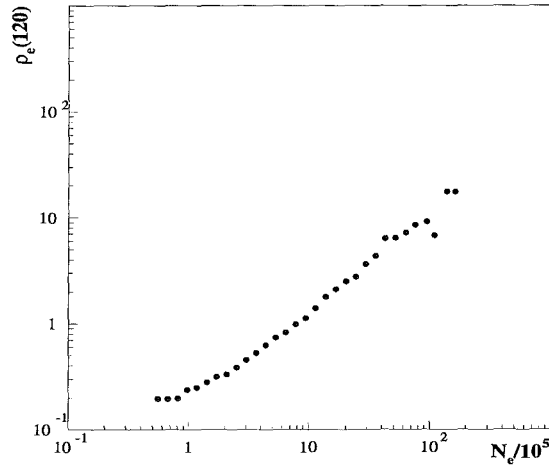


Fig. 1: Dependence of the average density $\langle \rho_e(120) \rangle$ on the EAS size N_e

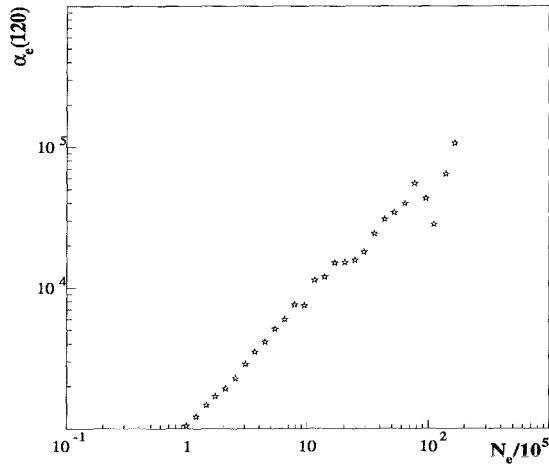


Fig. 2: Dependence of the parameter $\alpha_e(120)$ on the EAS size N_e

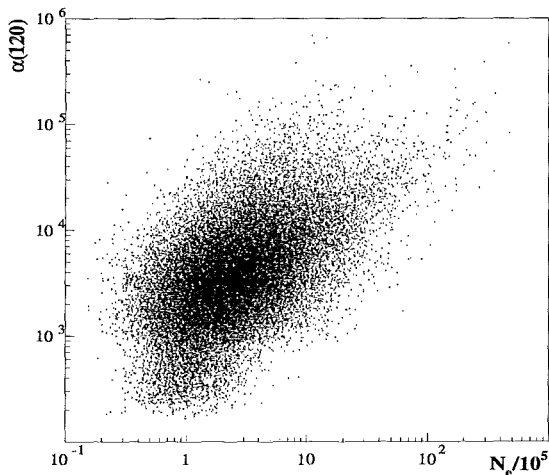


Fig. 3: $\alpha_e(120) - N_e$ correlation

ing the detector response of MAKET experiment we select the showers with axes on the distances of 110-130 m from the peripheral point, where 15 m^2 scintillation detectors are located and build data base of the appropriate data, i.e. EAS for which $\rho_e(120m)$ could be determined.

We obtain the average lateral density $\langle \rho_e(120m) \rangle$ for the showers with size $N_e \geq 5 \cdot 10^4$. The dependence of these densities on the shower size is shown on fig. 1.

Using these density distributions and applying the expression (1) we find the values of the α_e parameter for the selected showers. The local age s is calculated by means of the densities $\rho_e(10 \pm 5m)$ and $\rho_e(70 \pm 5m)$ as:

where r_m is the Molière unit (118m at Aragats). The Nishimura -Kamata-Greisen function [11] is calculated at the distance 10 m from the shower axis with the obtained local age as

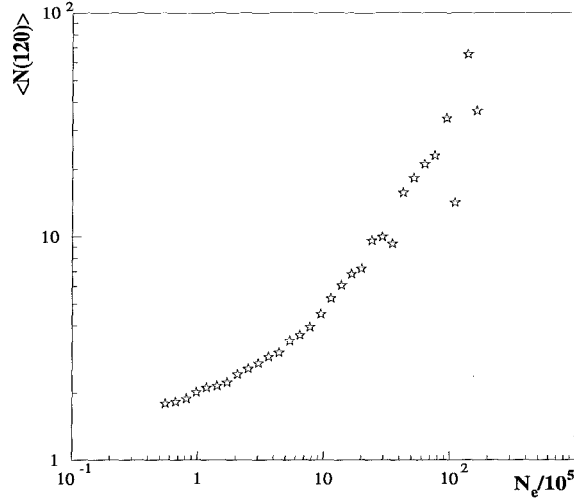


Fig. 4: Dependence of $\langle N(120) \rangle$ on the EAS size N_e

$$F_{NKG}(10m, s_{10-70}) = 0.366 * s^2 (2.07 - s)^{1.25} \left(\frac{10}{r_m} \right)^{s-2} \left(1 + \frac{10}{r_m} \right)^{s-4.5}. \quad (4)$$

The dependences of the electron size on the selection parameters $\alpha_e(120m)$ are depicted on fig. 2. The same investigation had been done for Gamma experiment on Mt. Aragats [12]. In fig. 3 the correlation of $\alpha_e(120m)$ and the shower size is plotted, reflecting rather big fluctuations of shower parameters.

It is also of interest to consider the experimental dependence of the mean number of charged particles for a circular area of 10 m radius at the distance 120 m from shower centre ($\langle N(120) \rangle$) on the EAS size (fig. 4).

The $\langle N(120) \rangle / N_e$ ratio dependence on the showers size is displayed in fig.5.

There is a knee positioned at $N_e \sim 10^6$.

The same procedure for the distance

$R = 50$ m exhibits a less pronounced knee in the $\langle N(50) \rangle / N_e$ ratio.

The detailed calculations of experimental data along with comparisons with relevant sim-

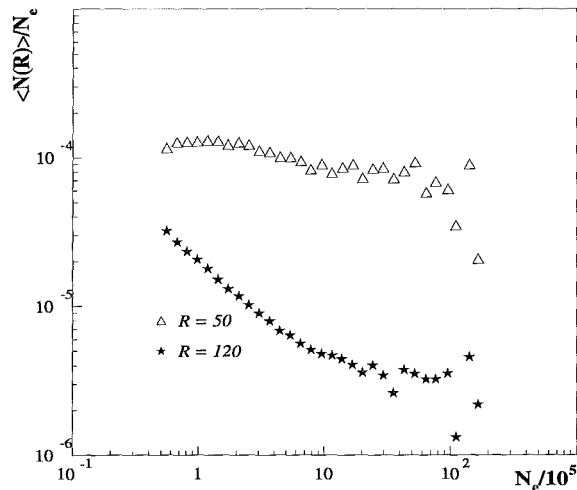


Fig. 5: The $\langle N(120) \rangle / N_e$ ratio vs the EAS size N_e

ulations are in progress for a more firm conclusion on the EAS classification possibility.

References

1. J.Engel et al., *Phys. D* **46** (1992) 5013
2. G.B.Khristiansen, G.V. Kulikov, U.A.Fomin, *Cosmic Rays of Super-high Energies*, Thiemig Verlag, Munich (1979)
3. S.N.Boziev, A.V.Voevodsky, A.E.Chudakov, *JETP LETT.* **50** (1989) 1
4. S.N.Boziev, A.V.Voevodsky, A.E.Chudakov, *J.Nucl. Res.* **630** (1989) 1
5. E.Chatelet, T.V.Danilova, A.D.Erlykin, V.P.Pavluchenko, J.Procureur, *J. Phys.G. Nucl.Phys.* **17** (1991) 1427
6. J.Procureur and J.N.Stamenov, *Nucl Phys. B.* **39A** (1995) 242
7. E.Chatelet, J.Procureur, J.N.Stamenov, *J. Phys.G.* **17** (1991) 93
8. E.Chatelet, J.Procureur, J.N.Stamenov, *J. Phys.G.* **18** (1992) 951
9. E.Chatelet, J.Procureur, J.N.Stamenov, *J. Phys.G.* **16** (1990) 317
10. I.N.Kirov, N.M.Nikolskaya, J.Procureur, J.N.Stamenov, *J. Phys.G.Nucl.Part.Phys.* **20** (1994) 1515
11. K.Greisen, *Handbuch der Physik*, XLVII/2 (1967) 1
12. A.A.Chilingarian et al., *Nuclear Physics B. (Proc.Suppl.)* **52B** (1997) 198

Correlation features of muon arrival time and angle-of-incidence distributions from EAS simulations at sea level and high mountain altitude

A.F.Badea¹, I.M.Brancus¹, M.Duma¹, A.Haungs², H.J.Mathes², H.Rebel², B.Vulpescu¹, A.A.Chilingarian³

¹National Institute of Physics and Nuclear Engineering – Horia Hulubei, Bucharest, Romania

²Forschungszentrum Karlsruhe, Institut für Kernphysik, Germany

³Yerevan Physics Institute, Yerevan, Armenia

Using the simulation code CORSIKA correlations of muon arrival time distributions and angle-of-incidence are studied for extended air showers developed at different atmospheric depth, corresponding to the sea level (KASCADE experiment) and at 3200 m on the mountain Aragats (ANI station). The temporal dispersion of the EAS muon component depends on the mass and the energy of the primary having characteristic features for different radial distances from the shower core and for different N_e and N_μ sizes. Special attention is given to multi-correlations in observations at different radial distances from the shower core, so-called "radial correlations" which provide additional information for the discrimination of different EAS primaries.

Introduction

The temporal structure of the muon component of Extended Air Showers (EAS) is of great interest for a detailed understanding of the EAS features, since the muon arrival time distributions map the longitudinal EAS development via the time-of-flight of muons produced in large atmospheric heights and show effects for mass discrimination of the EAS primaries [1, 2, 3]. The relative muon arrival times τ_μ at a radial distance R_μ refer to a defined zero-time, usually [1, 3] the arrival time τ_0 of the shower core:

$$\Delta\tau_{mean} = \tau_\mu - \tau_0 \quad (1)$$

$$\Delta\tau_1 = \tau_\mu^1 - \tau_0 \quad (2)$$

$\Delta\tau_{mean}$ and τ_μ^1 being the mean value and the arrival time of the foremost

muon, respectively. Introducing the travel distance l_μ of the muon from the origin, a simple triangulation procedure, as can be seen from the fig. 1, gives the relation between the production height of the muon and its travel time or its angle-of-incidence. Fig.

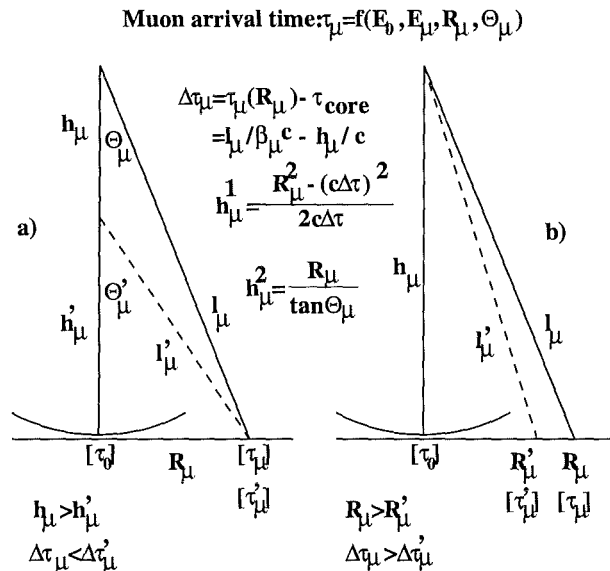


Fig. 1: Geometric description of the muon travel from the its production height to the place R_μ of detection.

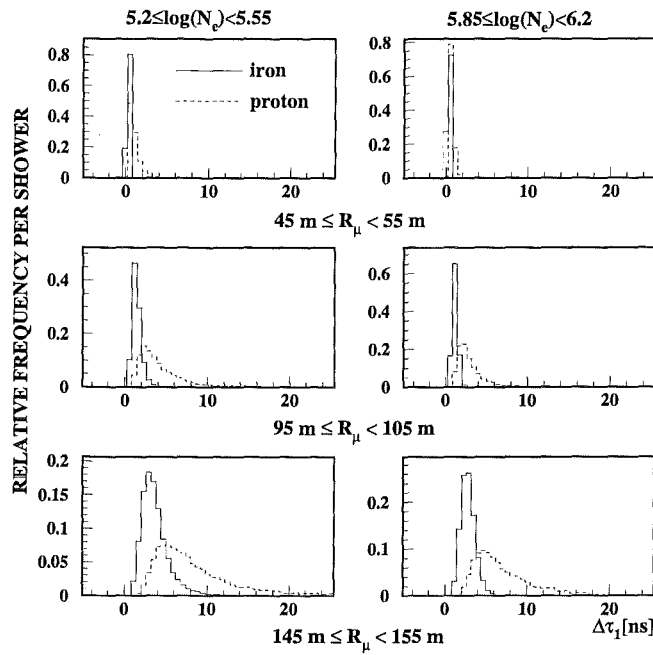


Fig. 2: Distributions of the relative arrival times of the foremost muons originating from proton and iron induced EAS observed for different shower sizes and radial distances from the shower center.

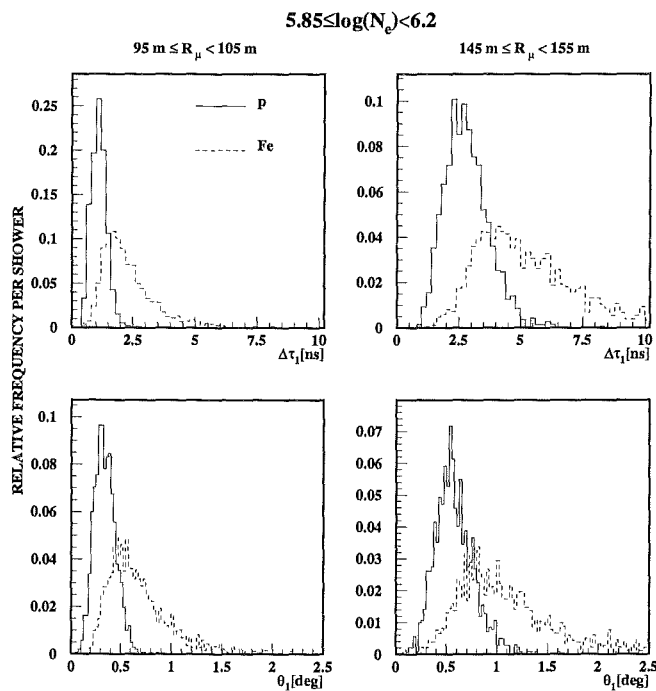


Fig. 3: Distributions of the relative arrival times and angle-of-incidence of the foremost muons originating from proton and iron induced EAS observed for different radial distances from the shower center.

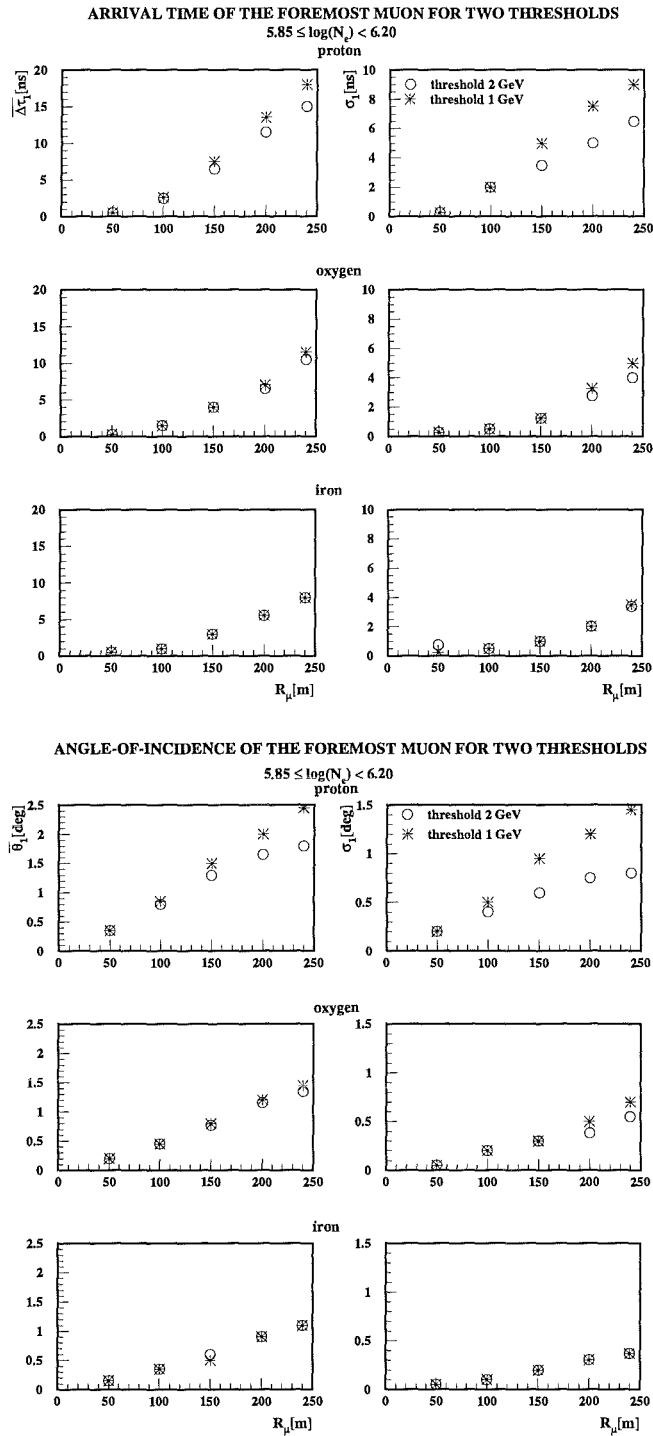


Fig. 4: The radial dependence of the mean of the arrival time and angle-of-incidence distributions for the foremost muons for two different energy thresholds of the detected muons from EAS initiated by proton, oxygen and iron primaries.

1a presents the case of muons produced at *different* heights and registered at the same distance from the shower core. Here a smaller travel time (relative to the core arrival)

results. Fig. 1b shows the case of muons produced at the same height but registered at *different* distances from the shower core. Guided by this basic feature and looking for discrimination signature for the mass of the primaries the dependence of muon arrival time distributions on various shower observables has been studied: from the distance from the shower center R_μ , the shower size N_e and muon shower content N_μ [4]. The relative arrival time distributions are characterized by the mean values, $\Delta\tau_{mean}$, by the median, $\Delta\tau_{median}$, or by the arrival of the foremost muon, $\Delta\tau_1$, which show different features on the distributions. All three kinds of distributions have been obtained by simulating the EAS time development.

EAS simulation data at the sea level: KASCADE

EAS induced showers for proton, oxygen and iron primaries have been simulated with CORSIKA code [5] developed in context of KASCADE [6] experiment. Nine values of the primary energy E_0 in equidistant steps of the $\log E_0$ between 10^{14} eV and 10^{16} eV and grouped in nine groups of the shower size have been studied.

Taking into account only vertical showers (zenith angle $\theta = 0^\circ$), the results are obtained for a hypothetical array of detectors of $10 \cdot 10$ m² area each, positioned within 10m broad radial bins in various distances from the shower center. The analyses have been done for 2 energy thresholds of the detected muons $E_\mu \geq 1$ GeV and $E_\mu \geq 2$ GeV [4, 7]. Following previous work [2], we have analysed the dependence of muon arrival time distributions on the radial distance R_μ from the shower center and on the shower size N_e (which is related to the energy of the primary), but this time we are focussed to find the correlations in different time distributions as significant for the mass of the cosmic ray primaries. Figs. 2 and 3 show general features of muon

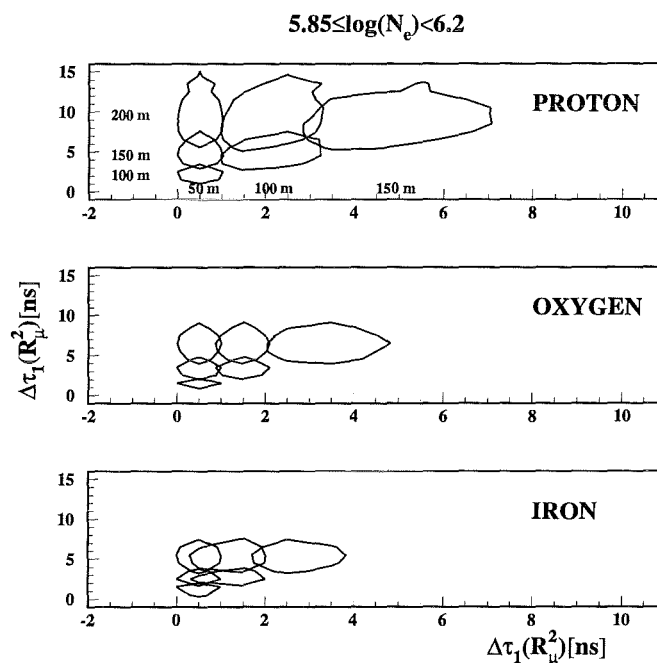


Fig. 5: The correlations of the arrival times of the foremost muons observed at different radial distances for proton, oxygen and iron induced EAS; the contours display the half maximum of the distributions.

arrival time and angle-of-incidence distributions for EAS initiated by proton and iron primaries at different radial distances from the shower core and different shower sizes: for the same primary the distributions becomes broader at larger radial distances and the distributions becomes narrower with increasing mass of the primary. Fig. 4 presents the dependence of the mean values of the muon arrival time and angle-of-incidence distributions and their standard deviations on the radial distance from the shower core, what is called the *muon shower profile* or the *disc thickness*. Increasing the energy threshold, the discrimination between different primaries becomes less pronounced. In previous studies

[2] it was shown that the correlations of muon arrival time distributions with the muon multiplicity N_μ enhance the separation quality between showers produced by different primaries. We extend this aspect with a special focus to observations correlated at different distances from the shower core. Fig. 5 shows the correlations of muon arrival times of proton, oxygen and iron induced showers observed at different distances from the shower core, emphasizing the strong dependence of the correlation on $R_\mu^1 - R_\mu^2$ combination. Fig. 6 presents the correlations between the muon arrival times of proton and iron induced EAS at two radial distances from the shower core indicating a pronounced dependence on the mass of the primary cosmic particle inducing EAS. Applying non-

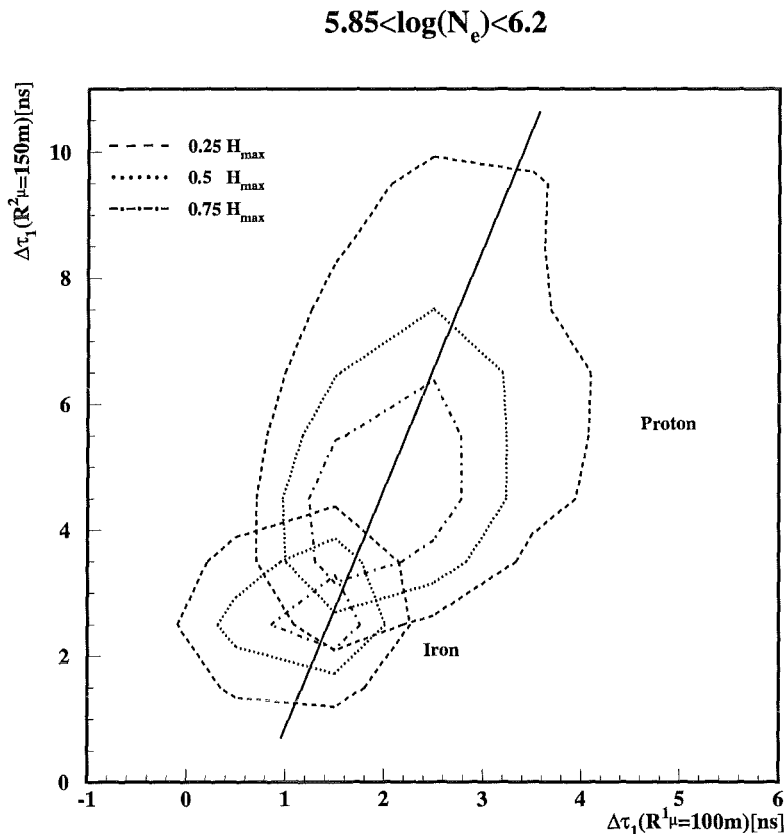


Fig. 6: The correlation of the arrival times of the foremost muons of proton and iron induced EAS observed with two detectors placed at 100 m and 150 m distance from the shower center. The straight line connects the maxima, and the distributions projected on the axis can be disentangled anticipating the shape of the different contributions.

parametric statistical analysis techniques, the overlap of multidimensional distributions and misclassification can be estimated [8]. Tab. 1 evaluates for $\log N_e = 5.85 - 6.20$ the trends of the classification and misclassification for various observation modes which correlate muon arrival time (and analogously angle-of-incidence) distributions of different radial distances.

It results:

- The observation of time-angle correlation at the same radial distance from the shower core (Time-Tracking Complementarity principle [9, 10]) does not improve the mass discrimination inferred from the arrival time and angle-of-incidence distributions separately.
- The chance of misclassification and the Bayes error decrease with increasing shower

Table 1: Reconstruction of a 7:1:3-p:O:Fe control sample of events induced by EAS in the N_e range: $5.85 \leq \log N_e \leq 6.20$, using different sets of variables.

Mode	p	O	Fe
$\Delta\tau_1(150m)$	4.68	3.31	3.23
$\Delta\tau_1(150m) - \theta_1(150m)$	4.49	3.33	3.12
$\Delta\tau_1(50m) - \Delta\tau_1(150m)$	5.74	2.37	2.88
$\Delta\tau_1(50m) - \Delta\tau_1(150m) - age$	5.75	2.18	3.07

size and the distance R_μ and is corroborated by adding some adequate other observables, like the shower age.

EAS simulation data at high altitude: ANI station at 3250 m on the Mt. Aragats

Using the CORSIKA code for EAS simulations with the observation level of 3250 m a.s.l, corresponding to the ANI experiment, simulations have been performed for proton and iron initiated EAS with different primary energies and vertical incidence. The results of these simulations (fig. 7) show that the EAS shower parameter combination $\log N_\mu^{tr} + 0.688 \cdot \log N_e$ turns out to be a good energy estimator of the primary energy, approximately independent from the primary mass. The quantity N_μ^{tr} is defined as the muon content of the lateral distribution between 25-140 m with $E_\mu \geq 4$ GeV [11].

The ANI EAS array consists of two subarrays: MAKET installation and GAMMA installation. The muon detection system is installed underground below the GAMMA installation (see fig. 8) consisting of 150 scintillator counters of $1 m^2$ area. It is important to stress that due to the sufficient large area a partition of the whole system (D30) in 3 subsystems of detecting muons D33 (40 plates), D32 (50 plates) and D31 (60 plates) could be introduced. This partition enables to study different correlations. Two cases for the position of the shower core have been considered: in a zone from the GAMMA installation (fig. 9a) and in an area comparable with the size of the MAKET installation (fig. 9b). The results are similar in both cases, so in the following we refer only to shower core positions with respect to the GAMMA installation.

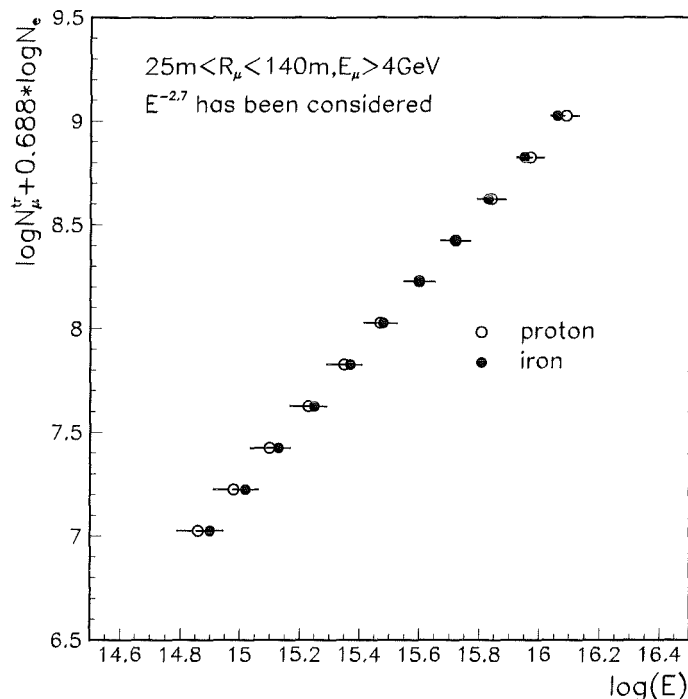
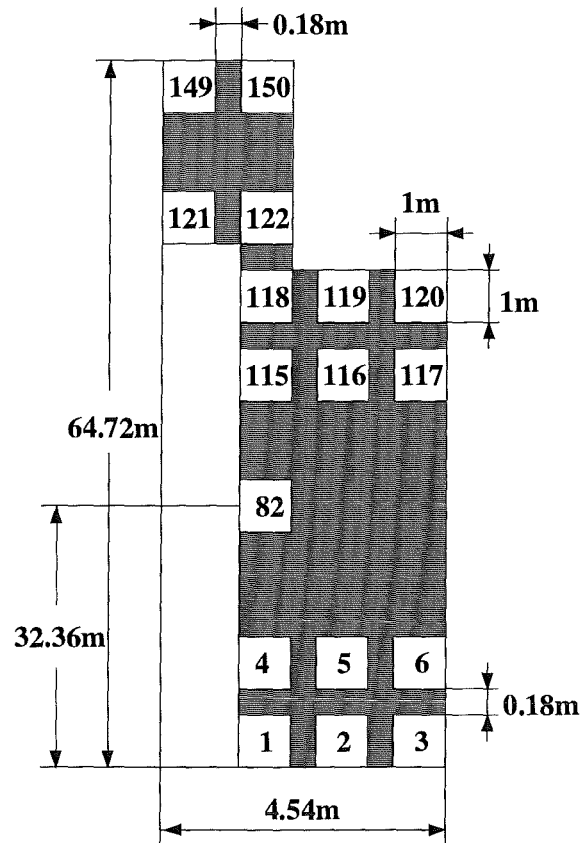


Fig. 7: The energy estimator for ANI experiment level: $\log N_\mu^{tr} + 0.688 \cdot \log N_e$ as function of primary incident energy for proton and iron induced air showers.

The results are similar in both cases, so in the following we refer only to shower core positions with respect to the GAMMA installation.



- plate 82 → reference plate
- subdetector D33 (plates 111-150)
 - subdetector D32 (plates 61-110)
 - subdetector D31 (plates 1-60)
 - all detector D30 (plates 1-150)

Fig. 8: Geometric view on the muon detection system.

The following conditions have been taken into account in the EAS simulations:

- due to the location of the tunnel there are in fact different energy thresholds for different partitions of the detectors [12]. For simplification we use 3.5 GeV ,
- the muon multiplicity which trigger one valid event is 2 for each subdetector, leading to a muon multiplicity > 6 for the whole detector, D30,
- the detector resolution has not taken into account. Figs. 10 and 11 give the probabilities for detecting muons produced from proton and iron initiated showers in the detector D30 and in the subdetectors D31, D32 and D33 for 2 energies of the primary cosmic ray particles. Figs. 12 and 13 show the relative arrival time distributions for the foremost muons produced from proton and iron initiated showers corresponding to the four different surfaces of detection D30, D31, D32, and D33. Figs. 14 and 15 show in two-dimensional plots the correlations between the number of muons detected in different partitions of the detection system, resulting a better discrimination between the showers produced by proton or iron than in the case of single distributions. Figs 16 and 17 present two-dimensional view of the correlations between the arrival time of the foremost muons of proton and iron initiated showers detected in different partitions of the detection system, corresponding to

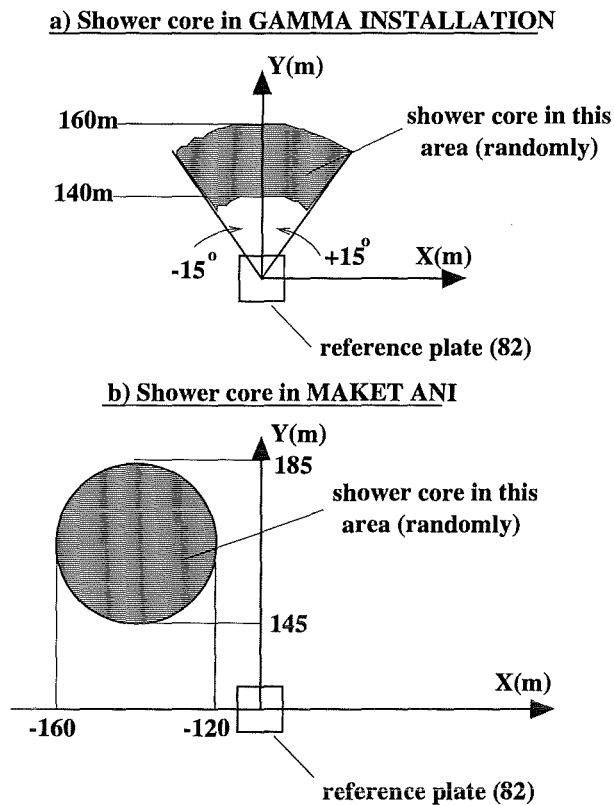


Fig. 9: Sketch of the shower core localization.

different radial distances from the shower core.

We have to add a remark concerning the explanation of the originally coloured figs. 14-17. Contour lines and borders between "coloured" areas are the isoprobability lines at 0.75, 0.50, 0.25 from the maximum probability in the histogram, respectively (see fig. 6).

The one-dimensional and two-dimensional distributions can be used for a nonparametric statistical analysis.

Concluding remarks

From the present analysis of muon arrival time observations at sea level and at high mountain altitude we conclude:

- The arrival time and angle-of incidence distributions show similar trends: they exhibit smaller values of the average arrival times and angles-of-incidence and smaller fluctuations with increasing mass of the primaries.
- The discrimination features are more pronounced by the distributions of the foremost arriving muons rather by the median or mean values of the distributions.
- The EAS muon profiles obtained for different primaries with different thresholds of the detected muons at the sea level (of 1 GeV and 2 GeV, respectively), indicate with increased threshold energy a decreasing discrimination of different primaries. This is corroborated by the observation that the simulations for the ANI situation ($E_\mu \geq 3.5$ GeV) show reduced discrimination power of the muon arrival time distributions.
- Introducing "radial correlations" as correlated observations of the arrival time (angle-of-incidence) distributions at *different* distances from the shower core, an improved mass discrimination is obtained, compared to the case of the strong correlation of muon arrival time and angle-of-incidence at the *same* radial distance.

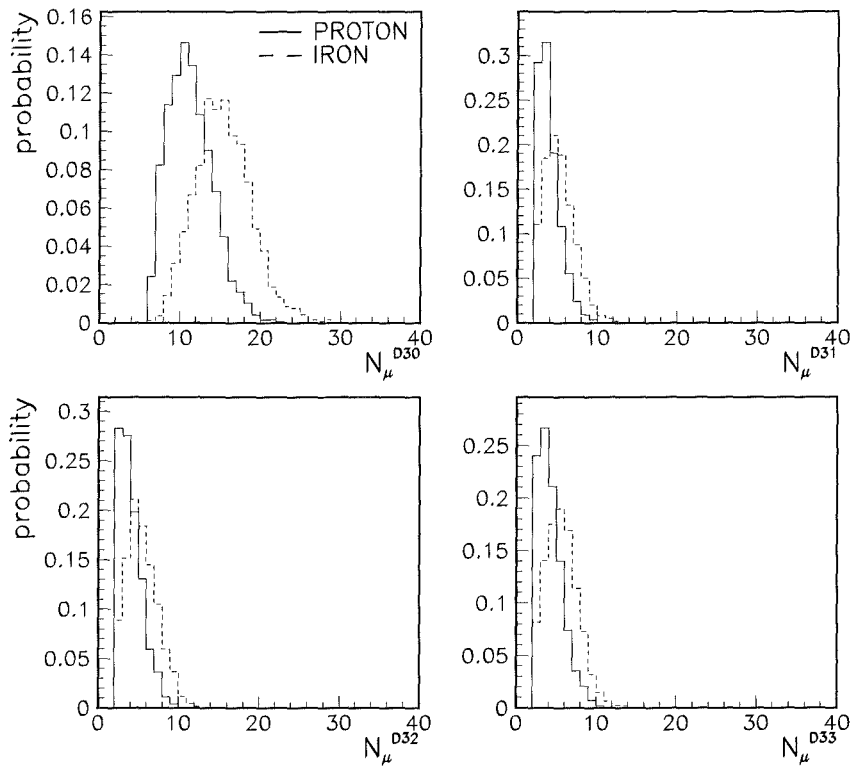


Fig. 10: Probabilities for number of muons registered in the complete detector (D30) and in 3 subdetectors (D31, D32, D33). Primary energy: $E_0 = 5.62 \cdot 10^{15}$ eV.

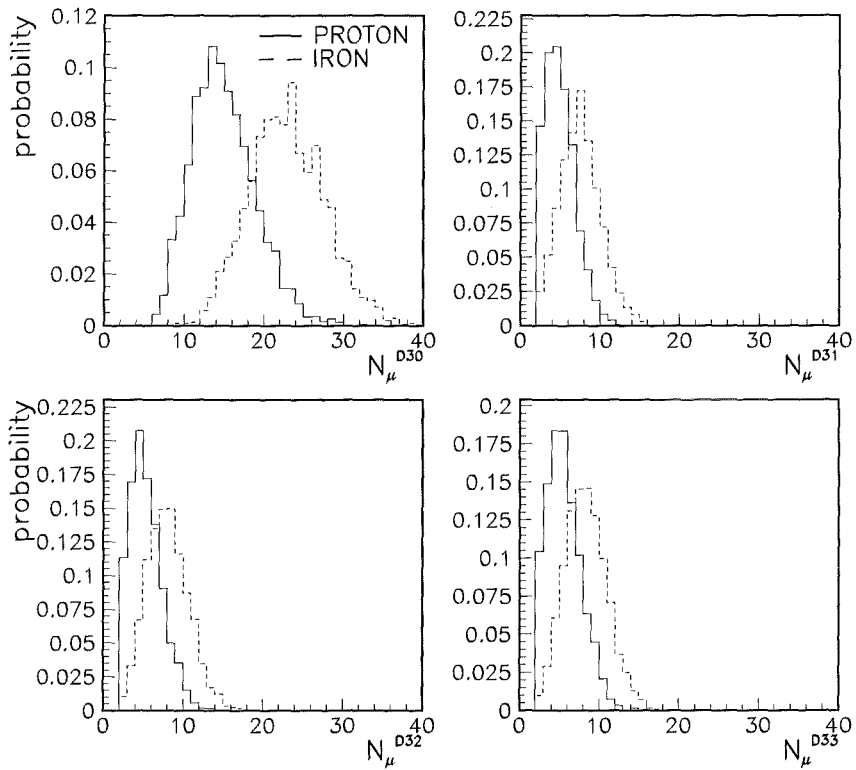


Fig. 11: The same as fig. 10 for the primary energy: $E_0 = 1.00 \cdot 10^{16}$ eV.

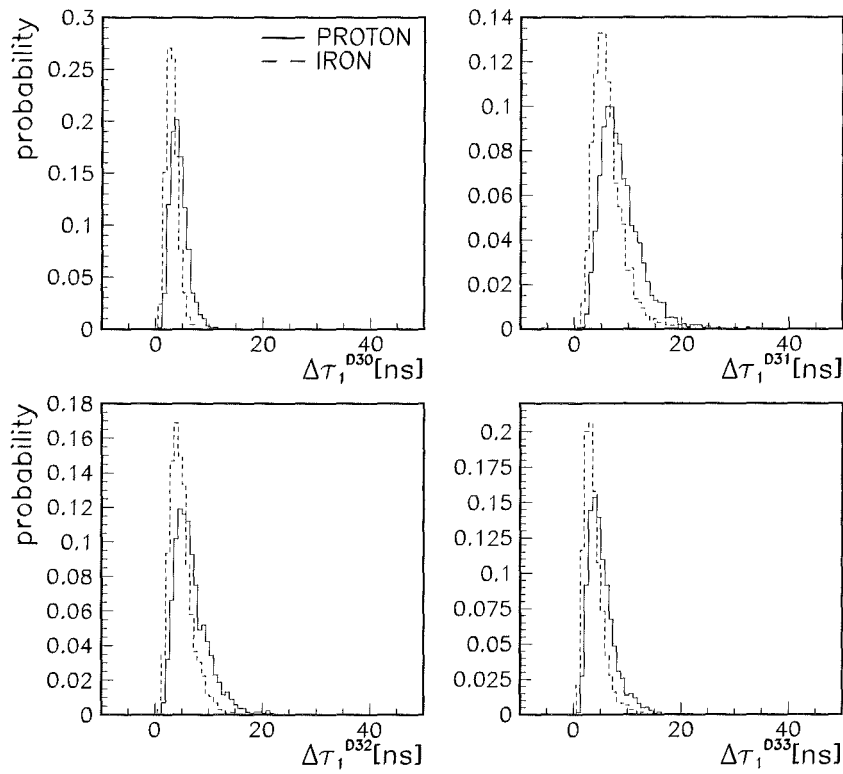


Fig. 12: *Relative arrival time distributions of the foremost muon relative to the arrival of the core in detector (D30) and subdetectors (D31, D32, D33). Primary energy: $E_0 = 5.62 \cdot 10^{15}$ eV.*

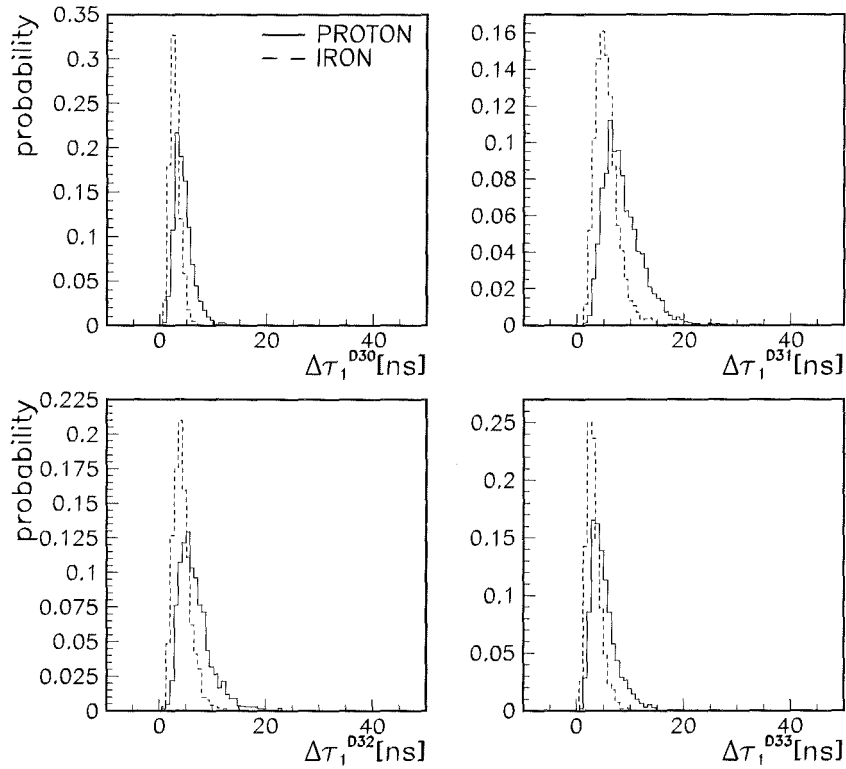


Fig. 13: *The same as fig. 12 for the primary energy: $E_0 = 1.00 \cdot 10^{16}$ eV.*

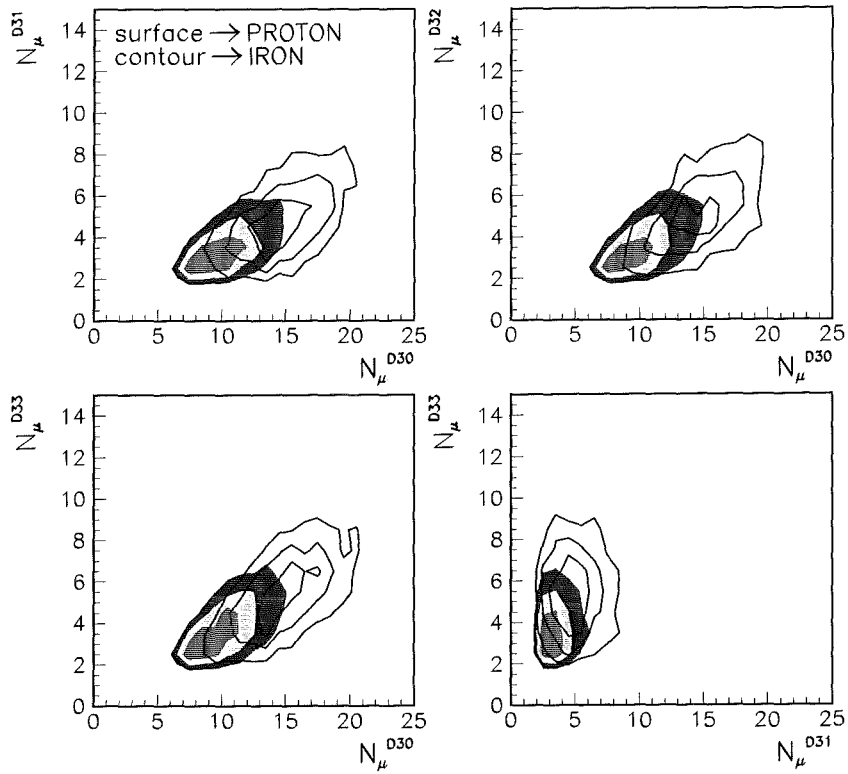


Fig. 14: 2-dimensional distributions for number of muons detected in different detector combinations: D31-D30, D32-D30, D33-D30, D33-D31. Primary energy: $E_0 = 5.62 \cdot 10^{15}$ eV.

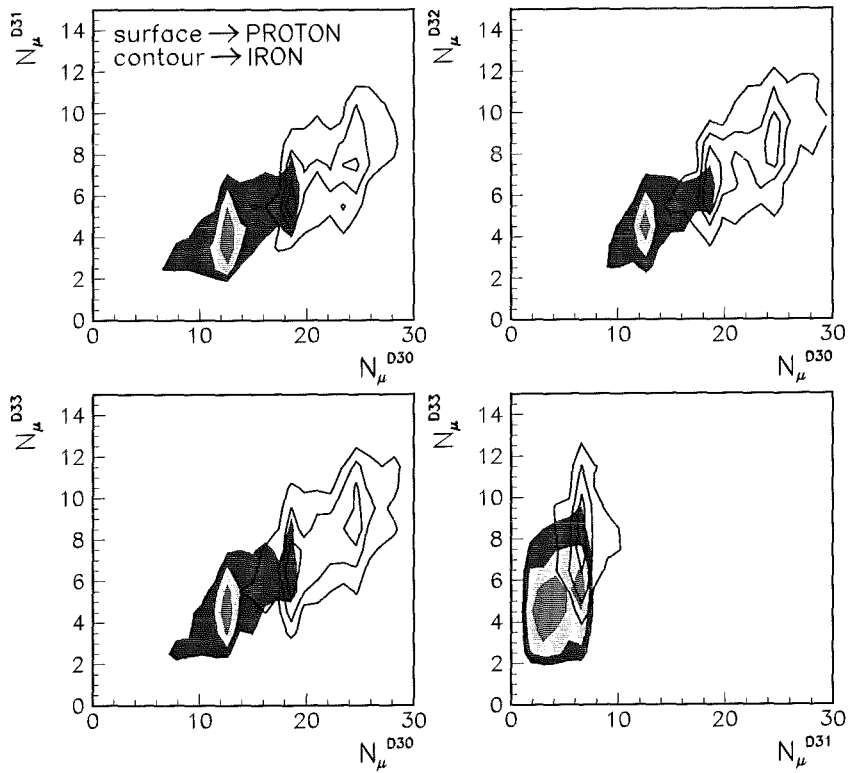


Fig. 15: The same as fig. 14 for the primary energy: $E_0 = 1.00 \cdot 10^{16}$ eV.

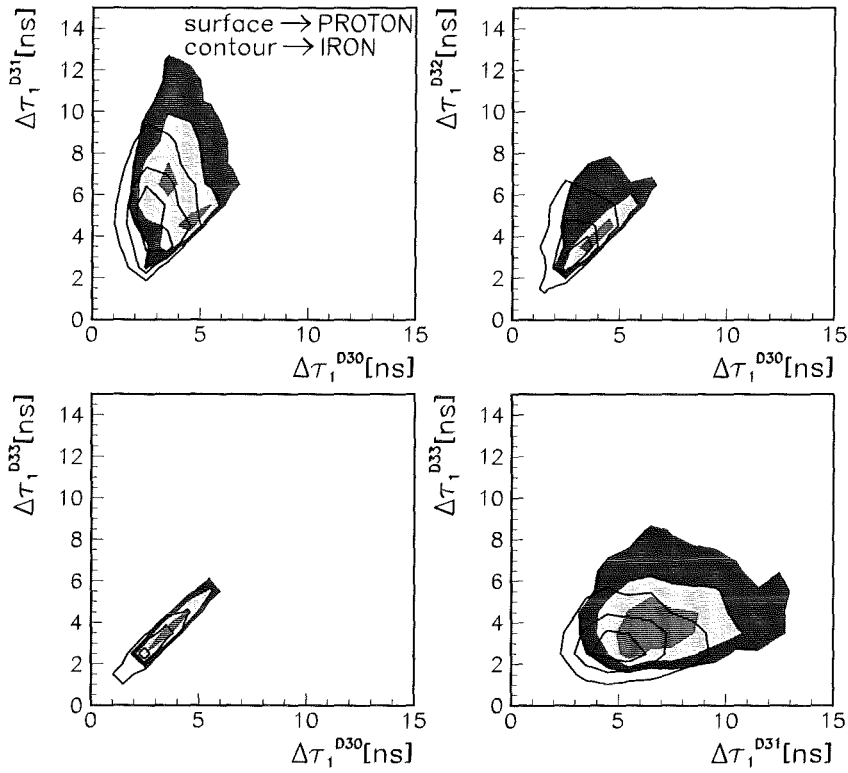


Fig. 16: 2-dimensional distributions for relative arrival time $\Delta\tau_1$ of the foremost muons in 4 different combinations: D31-D30, D32-D30, D33-D30, D33-D31. Primary energy: $E_0 = 5.62 \cdot 10^{15} \text{ eV}$.

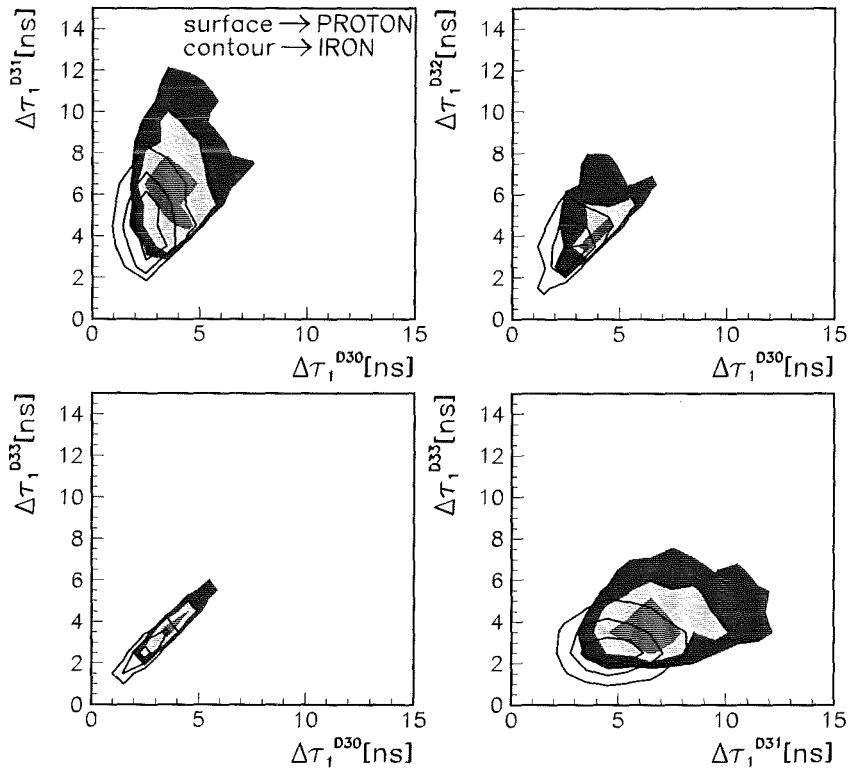


Fig. 17: The same as fig. 16 for the primary energy: $E_0 = 1.00 \cdot 10^{16} \text{ eV}$.

- Applying nonparametric statistical analysis techniques the classification in different classes of primaries is improved by choosing an adequate set of observables for mass discrimination, like the arrival time distributions considered at different radial distances from the shower core and the shower age.

Acknowledgements

We acknowledge the support of IPNE Bucharest, of Forschungszentrum Karlsruhe and of Yerevan Physics Institute to bring together the expertise of the authors. We thank for various communications of G.Hopsevan and M.Zazyan. Some authors (I.M.Brancus, H.J.Mathes, H.Rebel) remember with pleasure the hospitality of the Armenian colleagues.

References

- [1] J.Linsley et al.: Phys.Rev.92 (1961)485
- [2] T.V.Danilova et al.: Journ.Phys.G:Nucl.Part.Phys. 20 (1995)961
- [3] H.Rebel et al.: Journ.Phys.G:Nucl.Part.Phys.21 (1995)451
- [4] I.M.Brancus et al.: Astropart.Phys.7 (1997) 343
- [5] J.N.Capdevielle et al.: Report KfK 4998 (1992);
D.Heck et al.: Report FZKA 6019 (1998)
- [6] H.O.Klages for the KASCADE collaboration: Nucl.Phys.B (Proc.Suppl) 52 (1997) 92
- [7] I.M.Brancus et al.: Report FZKA 5835 (1996)
- [8] A.A.Chilingarian: Comp.Phys.Comm.54 (1989) 381;
A.A.Chilingarian and G.Z.Zazyan: Nuovo Cim.14 (1991) 355
- [9] G.Agnetta et al.: Astropart.Phys.6 (1997) 301
- [10] M.Ambrosio et al.: Astropart.Phys.7 (1997) 329
- [11] A.F.Badea and H.Rebel: ANI Note (10.06.1998)
- [12] M.Zazyan: ANI workshop (1998), these proceedings



Extension of the GAMMA muon underground detectors for studies of the longitudinal air shower development

H.-J. Mathes^{1*}, H.J. Gils¹, H. Rebel¹, A.F. Badea², H. Bozdog², I.M. Brancus², M. Petcu², A.A. Chilingarian³, G. Hovsepian³, V. Ivanov³ and R. Martirosov³ for the ANI-TIME collaboration

¹*Institut für Kernphysik, Forschungszentrum Karlsruhe, Germany*

²*National Institute for Physics and Nuclear Engineering, Bucharest, Romania*

³*Yerevan Physics Institute, Cosmic Ray Division, Armenia*

The lateral and longitudinal profiles of the EAS development differ for different primaries due to differences of interaction lengths, transverse momenta, multiplicity and energy distributions of the secondaries, produced in the cascading interactions in the atmosphere. The features are reflected by the relative arrival time and angle-of-incidence distributions of the penetrating muon component, observed in a sufficiently large distance from the shower center.

In view of a possible extension of the GAMMA muon underground installation on the Mt. Aragats Cosmic Ray Observatory ANI Monte-Carlo simulation studies of muon arrival times for the ANI altitude (3250 m a.s.l.) have been performed. Various configurations of the muon detectors underground with respect to the location of the core identifier (located at surface) are considered and some features related to the detector efficiency are regarded. The effects of different primaries (p, Fe) to the observation parameters, describing the time distributions are analyzed. The results lead to an analysis of the present experimental configuration and of the necessary modifications and extensions, the needed instrumentation for the readout and to considerations on the EAS induced background of the muon detection.

Introduction

Extracting information about the longitudinal air shower development from observations of EAS lateral particle distributions is rather difficult to do. This is mainly due to the fact that the particles arriving at ground level originate from a superposition of many subshowers generated at different interaction heights.

However, muons of sufficient high energy have a very low interaction probability with the molecules of the atmosphere thus having the possibility to resemble cascade features at the point of the particle generation. Especially high energetic muons carry valuable information about the first interactions within the hadronic cascade.

The differences in the height of the first interaction together with varying muon energies is reflected in the arrival times of the particles at observation level. But the major effect on the arrival times comes from the path lengths of particles arriving at the detector, as is shown in Fig. 1a.

Looking on the behaviours of proton and iron nuclei in the atmosphere and the resulting particle cascades some conclusions can be drawn about the features of the resulting

*corresponding author; e-mail: mathes@ik3.fzk.de

arrival time. On average, due to the smaller interaction length of iron primaries, their cascades will develop earlier at higher altitudes in the atmosphere. This together with the lower longitudinal momentum of resulting secondaries as compared with proton induced showers of same primary energy, lead therefore to a higher probability for muons to have longer path lengths (see also ref. [1]).

On observation level muons from proton induced showers thus have broader arrival time distributions shifted to slightly higher average values with respect to the arrival time of the shower front (see Fig. 1b).

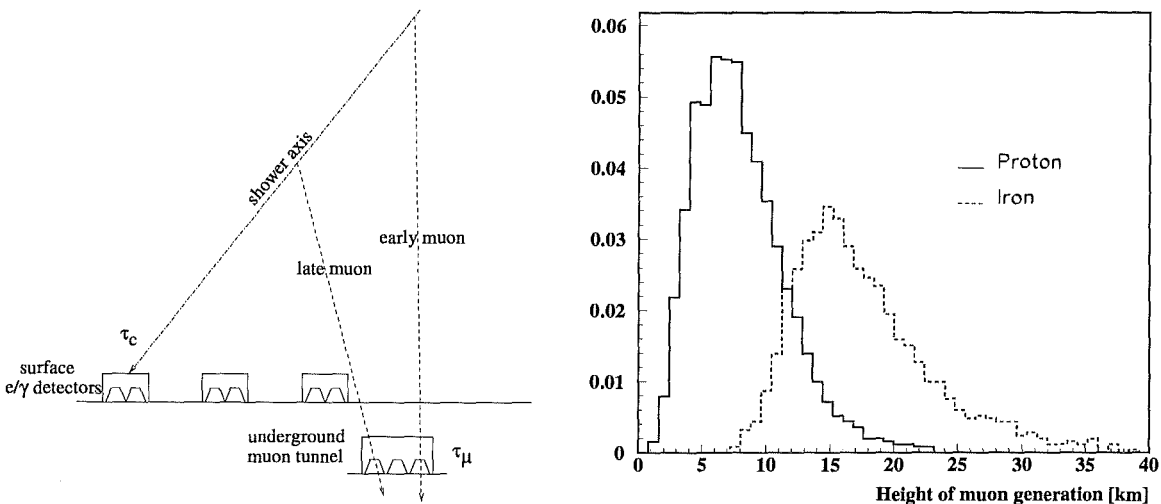


Fig. 1: Explanation of the muons arrival time dispersion due to geometrical path length differences (left). Production height of the foremost muons for Fe and p showers (right).

Muon Arrival Times in the ANI Experiment

A large number of MC simulations was carried out and must be further done to understand the characteristics of the events with respect to future timing studies.

For the purpose of simplification our first set of MC studies takes only the arrangement and the time resolution of the detectors into account. We use air showers simulated with the air shower simulation program CORSIKA [2] (version 4.60 with NKG, GHEISHA and VENUS option selected) for proton and iron primaries at fixed energies between $1 \cdot 10^{15}$ eV and $1 \cdot 10^{16}$ eV.

These simulations assume that the muon underground setup with its 150 detectors of 1 m^2 each is fully instrumented with appropriate timing electronics of reasonably good resolution. For this experiment the GAMMA installation and the MAKET installation are considered as possible trigger sources for the muon detectors. This leads therefore to a range of possible core distances of 100 ... 120 m for showers triggered from the GAMMA installation and of 190 ... 230 m for the MAKET installation respectively.

The detector subsequently registers the first muons at their specific place and on an event-by-event basis mean and median of the arrival times of all fired detectors are calculated. Finally we obtain the τ_{med} and τ_{mean} distributions for different primaries, energies and core distances.

From the MC program CORSIKA the particles are delivered together with their absolute arrival time with respect to the first interaction of the primary particle in the atmosphere.

In the analysis the arrival time of a hypothetical shower front, normally the arrival time of a spherical light front at the muon detection place is calculated.

A real experiment on the other hand has a lot of sources of errors which can make the determination of the exact time of the shower front arrival difficult or even impossible. That means, that the inaccuracy introduced by the method of measuring and/or determining this quantity can dissolve the features of the muons arrival times completely.

A second set of MC studies still going on are steps towards a more realistic view on the behaviour of the detectors and the surrounding materials. Using CORSIKA data together with CERNs GEANT detector simulation package [3], [4] the detectors response due to muons, electrons and other EAS particles have to be investigated. But not only particles belonging to the EAS itself are a source of additional signals. Muons can even produce further particles in the material forming walls and ceiling of the tunnel. Depending on the muons energy δ -electrons and radiative processes are a source for the so called faked muon signal in the scintillator detectors.

The percentage of events containing faked muon signals of course vary as function of primary particle, primary energy, core distance and zenith angle. Measuring the muon size of a shower will therefore result in higher muon numbers thus requiring a correction. Additionally, further faked timing signals will distort the resulting timing distributions.

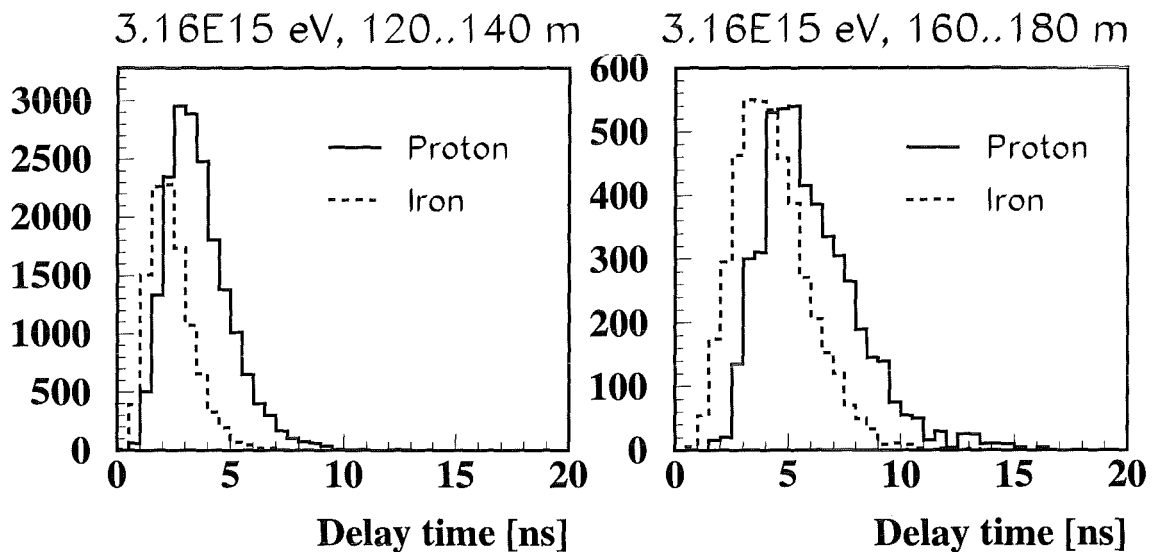


Fig. 2: Example of arrival times distributions of the first muon (τ_{μ}^1) with respect to the shower front (τ_C) obtained from the simulation at $E_0 = 3.16 \times 10^{15} \text{ eV}$: radius range 120...140 m radius range (left), 160...180 m (right)

Assuming the geometrical factor of the strongest influence on the muons path lengths it is obvious that the effects have to become smaller at higher altitudes as compared to sea-level observations.

The results from our first simulation studies therefore show clearly that the possibility to separate proton induced showers from iron induced showers is not very high. Only the τ_{μ}^1 distributions allow to distinguish between the primaries (Fig. 2), but the τ_{med} and τ_{mean} distributions are nearly identical (Fig. 3) for all considered primaries.

Nevertheless, comparing theoretical predictions obtained from simulations with experimental results could be a desirable aim to extend the present installation. Furthermore

comparing results obtained at mountain altitude with such from sea-level observations, as for example from the KASCADE experiment [5], is a further interesting perspective. A very important feature of the GAMMA muon underground installation is its large area together with its long base line (approx. 65 m). This gives for the first time the opportunity to study arrival time features at different core distances simultaneously, i.e. for the same event, and to correlate the obtained quantities with each other.

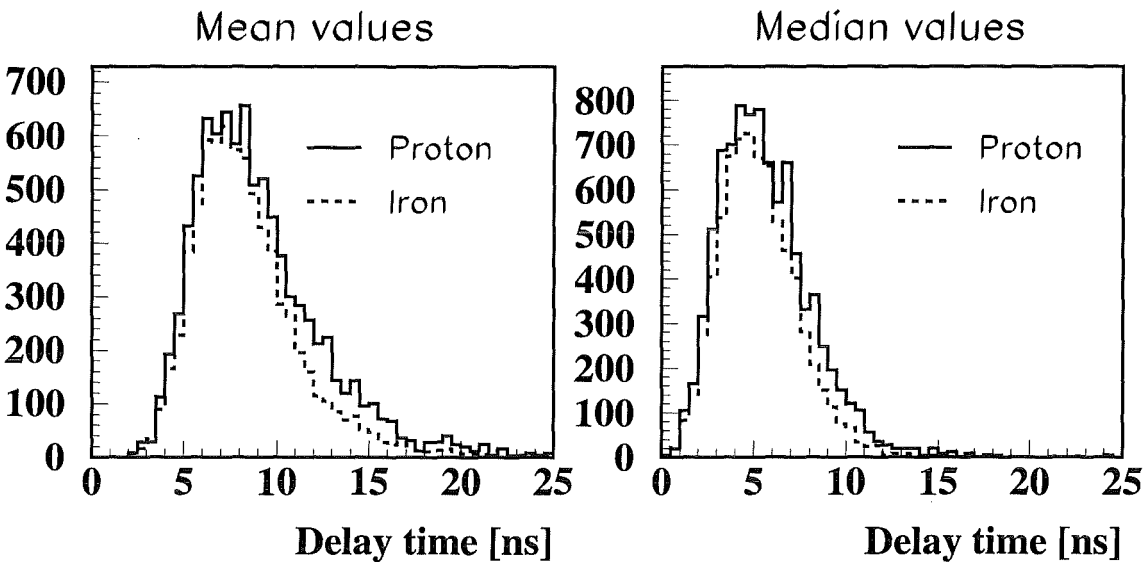


Fig. 3: Example for the obtained τ_{mean} and τ_{med} distributions.

The Proposed Timing Experiment

A rough sketch of the detector scheme used in the ANI experiment for the underground muon detectors is shown in Fig. 4. Currently the signal readout is done via Russian FEU-49 photomultipliers with a rise time of about 30 ns. The attached electronics is basically designed for the purpose of pulse height measurements so the overall timing resolution is approx. 4 ns. The present timing resolution is the Gaussian sum of the effects from the scintillator, the geometrical shape of the detector and of the electronic together with the currently used TDC modules (5 ns digitalization steps).

In 1997 Dr. G. Hovsepien carried out a number of tests with different phototubes and different detector layouts to study more detailed the effects [6]. In that setup the scintillator had only a size of $30 \times 30 \text{ cm}^2$. The obtained time resolutions are $\sigma_{opt} = 1.7 \text{ ns}$ for FEU-30 and FEU-130 phototubes and $\sigma_{opt} = 1.5 \text{ ns}$ for EMI 9902 phototubes.

Now the influence of the final detector geometry ($100 \times 100 \text{ cm}^2$) is estimated as follows: Due to different path lengths in the light cone above the scintillator plate a difference of 1.4 ns between shortest and longest light path is calculated. Investigated through a simple MC simulation this results in a time resolution of $\sigma_D = 0.4 \text{ ns}$.

Summarizing this results the required timing resolution of better than 2 ns seems to be achievable. In any case tests with the final detector geometry are very important to be carried out soon.

Fig. 5 shows a block diagram of the proposed timing experiment. Only a possible first phase, where only 32 detectors are equipped with timing channels, is shown. The trigger is assumed to come either from one of the two EAS experiments at the ANI site or from a

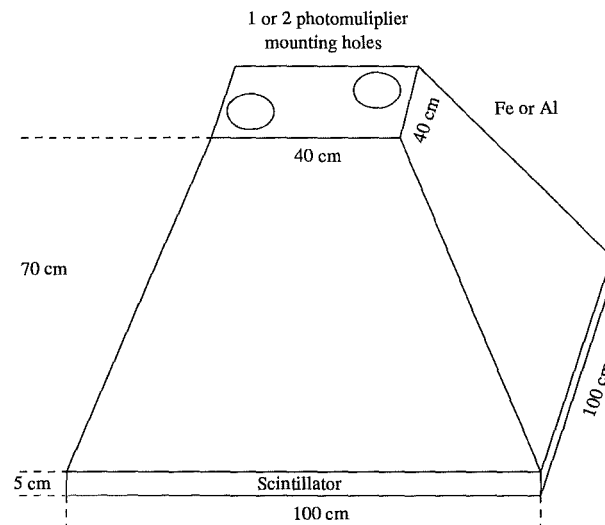


Fig. 4: Sketch of the detector layout used for the ANI muon underground installation. The real setup consists of detector boxes with 1 or 2 mounting holes for PMTs respectively.

majority logic fed by the logic signals of the muon detectors. These parts will be discussed later and are not shown here.

As was mentioned earlier at the discussion of the MC studies the GAMMA EAS installation as well as the MAKET installation could act as trigger source for this experiment. These two configurations will select showers in different radial distances. For later explained reasons it is necessary to understand the muon timing experiment not as an independent experiment. For calibration purposes the readout of the ADCs measuring the signal heights is needed. Using the MAKET experiment as trigger source seems a bit doubtful that this could be achieved. Estimating the rate of useful events with at least 2 muons in the detector (full instrumentation assumed) it comes out that above $5 \cdot 10^{15}$ eV we can expect only 4 events per day.

Additionally a majority logic can be used as a local trigger source. This trigger source could be very useful especially with respect to the calibration needs.

At present the readout of the GAMMA and the MAKET experiment is done separately. With the new timing experiment a third independent experiment, studying EAS observables, will run on Aragats. As the analysis of the simulation data has shown, an assignment of the muon timing events to the GAMMA or MAKET events is absolutely necessary. Only with this additional information the registered events can be classified in different N_μ , N_e or radius bins. To solve this problem a few ways can be offered:

- The use of clock modules in each experiment like it is done in the KASCADE experiment [7]. These modules are read out together with each event and give the time (in 200 ns resolution) of each event. Afterwards the data of different experiments can be merged using this information. These modules have to be provided with central clock signals and once with a central time information at acquisition start.
- The use of scaler modules in each experiment. All scalars are incremented with the trigger signals but only one trigger source is allowed.
- A master-slave operation scheme of the experiments. This means that none of the

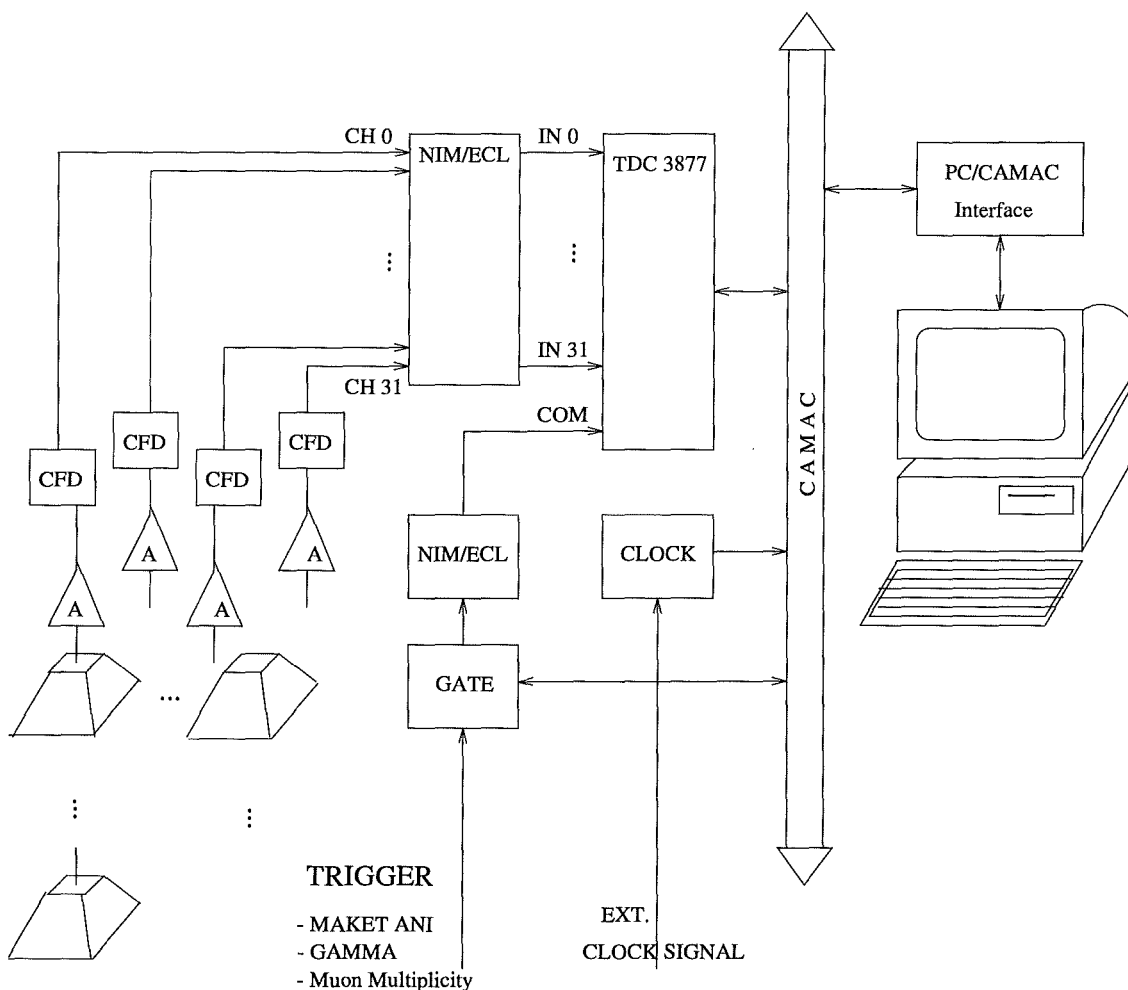


Fig. 5: A block diagram of the electronics needed for a possible first phase (32 detectors instrumented) of the proposed timing experiment.

experiments could be triggered as long as one out of them is busy with the reading of data.

The first solution has to be considered as the best solution whereas the other two can be used only as preliminary ones.

Another important point is the calibration of the timing experiments detectors. It is clear that the efficiency of the scintillator for muons should be near 100 % but on the other side the background rejection has also not to be neglected. Therefore single muon spectra have to be taken from every channel in order to control and to adjust the thresholds of the timing channels.

To have a good timing accuracy all the channel specific delay times have to be measured somehow. They consist of differences in the PMT characteristics (due to different high voltage, ageing effects, thresholds, ...), cable lengths and electronic signal propagation. This must be done not only for a short period even the long term stability of the system has to be monitored.

The calibration of the detectors can be done with different methods:

- Calibration of single detectors using a muon telescope at the detectors position.

This method gives individual ADC and TDC spectra for each detector but is also very time consuming.

- Calibration runs with a local trigger. As local trigger the GAMMA array or the mentioned majority trigger could be used. The individual time offsets of the detectors can be evaluated from a shower plane fit to the measured timing signals. It should be possible to get a new calibration in a reasonable short time, i.e. 12 - 24 hours. In the first time this should be done weekly to prove and check the long term stability of the setup. Later a period of 4 weeks could be sufficient.
- Calibration by using the measured data is also possible. In this case the trigger rate must be sufficiently high to fulfill the above mentioned condition.

Conclusion

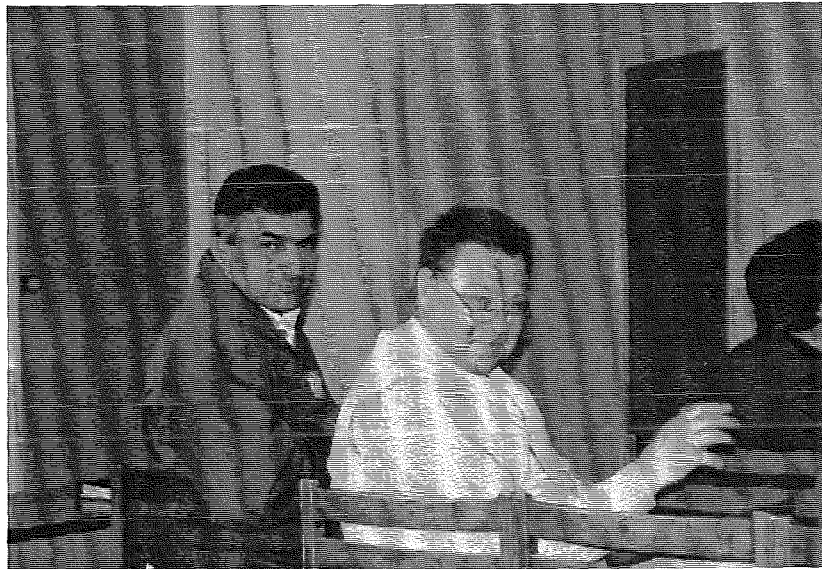
Measuring the arrival times of muons at the ANI observation level offers some interesting perspectives mainly to study the longitudinal EAS development and to compare result at mountain and at sea level. For such an experiment detectors with a timing resolution better than 2 ns are needed. It is shown that with some modifications the present detectors (mainly housing and scintillators) could be used. Nevertheless further tests with the final detector setup have to be carried out to confirm the estimations. From the presented schemes a list of necessary equipment useful for the first step towards a bigger timing experiment could be worked out.

Acknowledgements

The present proposal is based on a pleasant scientific interaction of experts of Forschungszentrum Karlsruhe, National Institute for Physics and Nuclear Engineering of Bucharest and the Yerevan Physics Institute. We thank for the kind hospitality of the Armenian colleagues during the workshop ANI 98.

References

- [1] A.F. Badea et al., ANI 98, this proceedings
- [2] J. N. Capdevielle et al., KfK-Report 4998, Kernforschungszentrum Karlsruhe (1990)
D. Heck et al., FZKA-Report 6019, Forschungszentrum Karlsruhe (1998)
- [3] GEANT: CERN Program Library Long Writeups W5013 (1993)
- [4] M.Z. Zazyan and A. Haungs, ANI 98, this proceedings
- [5] P. Doll et al., KfK-Report 4686, Kernforschungszentrum Karlsruhe (1990)
- [6] G. Hovsepian, internal research report, unpublished (1997)
- [7] J. Zabierowski, H.O. Klages, H. Schieler, KfK-Report 5373, Kernforschungszentrum Karlsruhe (1994)



The universal approach to superhigh energy hadron production

H.J. Drescher¹, M. Hladik¹, K. Werner¹, and S. Ostapchenko²

¹ *SUBATECH, Université de Nantes – IN2P3/CNRS – EMN, Nantes, France*

² *Moscow State University, Institute of Nuclear Physics, 119899 Moscow, Russia*

We develop the universal model for soft and hard hadron production in hadron-hadron, hadron-nucleus and nucleus-nucleus interactions as well as in electron-positron annihilation and deep inelastic scattering. The main algorithms are tested versus the data on different reactions. This allows to fix the corresponding uncertainties and to ensure the reliable extrapolation of the model for the description of heavy ion collisions at ultrarelativistic energies.

Introduction

Monte Carlo models of hadronic interactions are now widely used for experimental data analysis and interpretation both at accelerators and in cosmic ray physics. Nevertheless, with the energy of incident particle growing up model predictions become less and less constrained by the initial conditions fixed by hadron-hadron and hadron-nucleus reaction data at low and intermediate energies. On the other hand, the very problem of model calibration at intermediate energies is rather ambiguous due to the limited accuracy of the corresponding measurements and considerable gaps in the data available, especially in the forward region. Thus, the construction of a reliable scheme requires it to be universal, i.e. allowing the model application for the description of reactions different from hadron-hadron (hadron-nucleus) one, like electron-positron annihilation into hadrons or deep inelastic lepton-proton scattering (DIS), where a bulk of data, measured with a high precision, can be used for testing and calibration of the model algorithms. Besides that, the model is to be based on the solid theoretical ground in order to ensure the reliable extrapolation up to energies few orders of magnitude higher than the ones for current experiments.

There are two serious assumptions behind that strategy. The first one, more or less generally accepted, is the universality hypothesis, i.e. that relevant aspects of the interaction dynamics are the same in different reactions. The second assumption is that current theoretical knowledge and the experimental information available are sufficient to construct the basis for the description of hadronic interactions even at ultrahigh energies, so that possible new mechanisms can be taken into account as corrections above the **underlying interaction**, described by the basic model. This idea is supported by the success of Gribov-Regge models in describing the data measured both at accelerators and in cosmic ray experiments [1,2].

The model construction

It is generally expected, both theoretically and experimentally, that hadronic interaction at ultrahigh energies is dominated by multiple processes of hard parton-parton scattering, giving rise to the production of high transverse momentum jets of secondary particles [3,4]. Those binary hard parton processes, characterized by some high momentum trans-

for Q_B^2 , are preceded by cascades of partons of smaller virtualities $Q^2 \ll Q_B^2$, resulting in the production of a bulk of additional hadrons with moderate and small p_t . As perturbative description can only be used to describe the parton emission processes with relatively large momentum transfer $Q^2 Q_0^2$, where Q_0^2 – some cutoff for QCD being applicable, one can employ the perturbative formalism for the part of the cascade between Q_0^2 and Q_B^2 and describe the beginning of the cascade (below Q_0^2) phenomenologically, on the basis of Regge theory [5] - fig.1.

In that case one has to consider two contributions into the nonperturbative region - from the soft Pomeron emission, which results in the parton i (a sea quark or a gluon) distribution at the scale Q_0^2 , behaving asymptotically like

$$E_{soft P}^i(x, \vec{b}) \sim x^{-\alpha_P}, \quad x \rightarrow 0, \quad (1)$$

and the Reggeon contribution, corresponding to the case of valence quark being involved into the hard rescattering:

$$E_{soft R}^i(x, \vec{b}) \sim x^{-\alpha_R} \delta_q^i, \quad x \rightarrow 0, \quad (2)$$

where x is the parton share of the parent hadron light cone momentum $p^\pm = E \pm p_z$, \vec{b} - its impact parameter position, and $\alpha_P \simeq 1.07$, $\alpha_R \simeq 0.5$ are the Pomeron and Reggeon trajectory intercepts correspondingly.

Thus, we define the contribution of the **semihard Pomeron** exchange, corresponding to an elementary semihard rescattering, as a convolution of soft Pomeron (Reggeon) couplings to the initial hadrons $C_{P(R)}$, soft evolution part $E_{soft P(R)}^i$, the operator E_{QCD}^{ij} , describing QCD evolution of the initial parton i , chosen at the scale Q_0^2 , into the final parton j at the scale Q_B^2 , and the final (Born) parton-parton scattering differential cross section $d\sigma_{Born}^{jl}/dQ_B^2$ [6] - fig.1

$$G_{semi} \sim \int dQ_B^2 \sum_{P_1, R_1, P_2, R_2} \sum_{ijkl} C_{P_1(R_1)} \otimes E_{soft P_1(R_1)}^i \otimes E_{QCD}^{ij} \otimes \frac{d\sigma_{Born}^{jl}}{dQ_B^2} \otimes E_{QCD}^{kl} \otimes E_{soft P_2(R_2)}^k \otimes C_{P_2(R_2)}, \quad (3)$$

where for the convolution over light cone momentum shares we used the notation

$$f \otimes g = \int \frac{dz}{z} f(z) g\left(\frac{x}{z}\right) \quad (4)$$

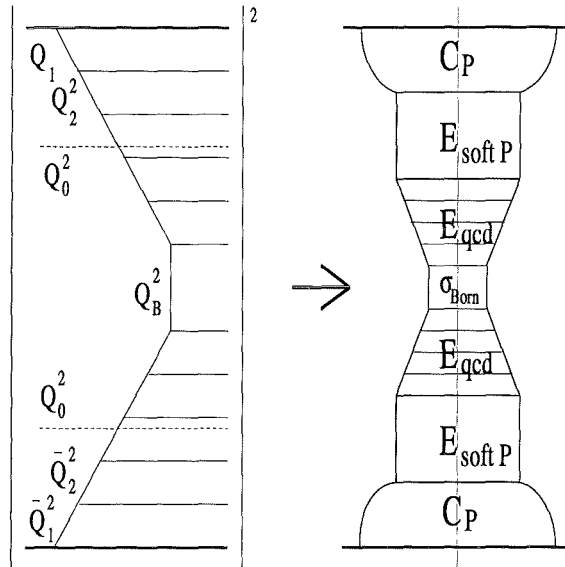


Fig. 1: Parton cascade picture of hard scattering process and its description by the semihard Pomeron exchange.

In general hadron-hadron inelastic interaction may contain a number of partial semi-hard interactions; in addition, one has to account for virtual semihard Pomeron exchanges, described by the same expression (3), where all the partons after the scattering are gathered together back to their parent hadrons. Still, even at very high energies, the contribution of pure soft processes (corresponding to the case of parton cascade being developed below the cutoff Q_0^2), described by the usual soft Pomeron amplitude, remains sizable, whereas at low energies it dominates the interaction [1]. Considering the complete hadron-hadron scattering amplitude, applying the AGK technique [7], and summing up virtual soft and semihard rescatterings, one can get both total and inelastic interaction cross sections and the probabilities for particular configurations of the interaction (for given numbers of **real** soft and semihard processes). Thus, the simulation of hadron-hadron (hadron-nucleus and nucleus-nucleus) inelastic collision includes the generation of the numbers of partial soft and semihard interactions, the sharing of the initial energy-momentum between them, and the separate treatment of hadron production in those processes.

An important feature of our approach is the proper treatment of the sharing of the energy-momentum between both real (cut) and virtual (uncut) Pomerons, corresponding to the nonplanar structure of the relevant diagrams. More clearly, both all real and virtual Pomerons are emitted at the same time and the available energy-momentum is shared between them. In contrary, in the planar picture Pomerons would be emitted one after another, each one having the total energy of the interaction. As discussed in [8], in the correct procedure the AGK cancellations are fulfilled in the whole kinematical region of the interaction.

Hadron production from the semihard pomeron

In our description of the QCD parton evolution (spacelike parton cascading) from the initial scale Q_0^2 to Q_B^2 we take into account only "resolvable" parton emissions, corresponding to the production of final partons of transverse momenta larger than some cutoff $p_{t,res}^2$ [9]. The emission of collinear partons of $p_t^2 < p_{t,res}^2$ is assumed to contribute to the formation of color flow, connecting the final parton jets to each other. The generated final partons are characterized by some initial offshellness and undergo further time-like splitting - s -channel parton cascade. There one considers again only resolved parton branchings. In turn, the soft evolution, described as soft Pomeron (Reggeon) emission, is assumed to form the color flow, connecting the ends of the Pomeron - quark and antiquark (valence quark and diquark in the Reggeon case) - to the produced jets. Finally one ends with the configuration of on-shell partons flying apart and stretching the color field, connecting them to each other. The breaking of the color flow gives rise to the production of final hadrons. The suitable framework for the description of that process is provided by so-called "kinky string" model - different kinky strings follow the color flow and connect quarks and antiquarks (diquarks) via a number of intermediate gluons; usual soft Pomeron strings are then obtained as no-kink limit. The hadronization of those objects is entirely determined by the string dynamics.

The best laboratory for testing the timelike parton cascade and the hadronization procedure is the e^+e^- -annihilation reaction, where one starts with the evolution of a color connected quark-antiquark pair and gets after the perturbative cascading either one kinky string with a number of gluon kinks or a few strings if some additional quark-antiquark

pairs have been generated. The available data allow to compare model predictions with the experiment both at the parton level (numbers of resolved jets) and the hadron level (final hadron spectra).

Similarly, the structure of the semihard Pomeron and the spacelike parton cascade can be tested in the process of deep inelastic electron-proton scattering. The generation procedure for DIS reaction includes the simulation of the proton light cone momentum share given to the whole semihard Pomeron and to the perturbative part of it (to the first parton in the QCD evolution), and the modeling of the parton cascade - from the initial virtuality Q_0^2 till the maximal one. After that the timelike cascading of partons, the formation and hadronization of kinky strings are performed on the basis of the procedures already tested in e^+e^- -annihilation.

The description of hadron production from the semihard Pomeron in hadron-hadron and nucleus-nucleus collisions is quite analogous, except that the modeling of the space-like parton cascade is performed from both ends of the Pomeron.

Acknowledgements

The authors would like to acknowledge their collaboration with the KASCADE group (Forschungszentrum Karlsruhe). This work was supported in part by IN2P3/CNRS (grant PICS-580) and Russian Foundation of Basic Researches (grant 98-02-22024).

References

1. K. Werner, Phys. Rep. 232 (1993) 1983
2. N.N. Kalmykov, S.S. Ostapchenko, A.I. Pavlov, Nucl. Phys. B (Proc. Suppl.) 52 (1997) 17
3. L.V. Gribov, E.M. Levin, M.G. Ryskin, Phys. Rep. 100 (1983) 1
4. G.J. Alner et al., UA5 Collaboration, Phys. Rep. 154 (1987) 247
5. K. Werner et al., Proc. of the "3rd Int. Conf. on Physics and Astrophysics of Quark-Gluon Plasma" (Jaipur) 1997, to be published
6. H.J. Drescher et al., Proc. of the "Workshop on Nuclear Matter in Different Phases and Transitions" (Les Houches) 1998, to be published
7. V.A. Abramovskii, V.N. Gribov, O.V. Kancheli, Yad. Fiz. (Rus) 18(1973) 595
8. V.A. Abramovskii, G.G. Leptoukh, Yad. Fiz. (Rus) 55 (1992) 1646
9. G. Marchesini and B.R. Webber, Nucl.Phys. B 238 (1984) 1

On the differences in high energy hadronic interaction models and their influence on the calculated EAS characteristics

N. Kalmykov and S. Ostapchenko

Moscow State University, Institute of Nuclear Physics, 119899 Moscow, Russia

The differences in existing Monte Carlo models for the simulation of high energy hadron-nucleus and nucleus-nucleus interactions are discussed in connection to their effect on the predicted characteristics of extensive air showers. A special attention is paid to the role of Pomeron structure functions used in the simulations. The projection of the corresponding uncertainties on the resulted superhigh energy EAS parameters and, correspondingly, on the conclusions concerning the primary cosmic ray mass composition is investigated.

Introduction

Microscopic models of high energy hadronic interactions are now widely used in the field of cosmic ray physics. Nevertheless, due to large uncertainties in the model parameters and algorithms, arising mainly from the unknown physics of hadronic interactions at ultrahigh energies, on one side, and from the large gaps in the data on hadron-hadron and hadron-nucleus interactions at moderate energies, on the other side, those models differ in their predictions [1].

In the current work we analyze the differences between the models widely used in EAS studies, like MOCCA [2], SYBILL [3], and the family of Gribov-Regge models, represented by DPMJET [4], QGSJET [5,6], and VENUS [7], and draw attention to the model parameters, which are of special importance for model applications to EAS simulations.

Different approaches to the interaction dynamics

The simplest of the mentioned models, MOCCA, is essentially based on the idea that the dynamics of hadronic interactions scales with the energy. The invalidity of that hypothesis had been already proved experimentally [8]. Nevertheless, there are no direct measurements which would allow to estimate the power of the scaling violation in the fragmentation region. Consequently, there exist two main strategies to treat high energy interactions – mini-jet approach [9] and Gribov-Regge theory [10,11,7].

In the first case, represented by SYBILL model, all deviations from the

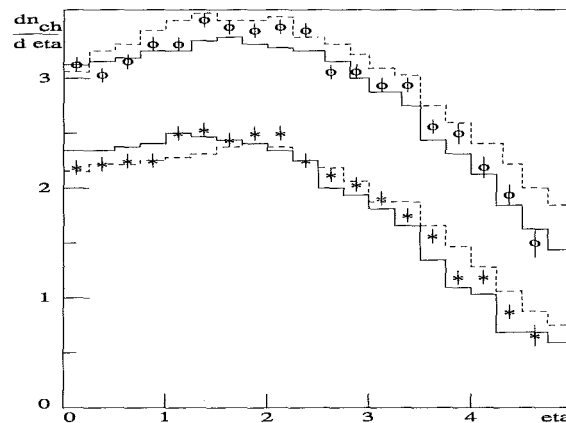


Fig. 1: *Pseudorapidity distribution of charged particles in $\bar{p}p$ -interaction. UA5 data [8]: * – $\sqrt{s} = 200$ GeV, o – $\sqrt{s} = 900$ GeV. QGSJET calculations for $\alpha_R = 0.5$, 0.95 - full and dashed histograms correspondingly.*

scaling behavior are attributed to the perturbative minijet physics [3]. Correspondingly, for the particle production in hadron-hadron interaction one considers two essential sources: the hadronization of a pair of color strings stretched between the valence quarks and the diquarks (antiquark for a meson hadron), which is essentially the scaling type contribution, and the fragmentation of binary jet pairs produced in the central rapidity region. The latter contribution grows rapidly with the interaction energy and gives rise to the increasing particle production at **small values of Feynman x** in the hadron-hadron center of mass system but does not influence significantly the hadron spectra in the fragmentation region.

The characteristic feature of Gribov-Regge models is the allowance for multiple soft rescattering, resulting in the production of a number of "soft" color strings stretched between the interacting hadrons. The powerlike increase of the number of strings with the energy gives rise to the violation of the Feynman scaling even if the perturbative contributions are neglected. Furthermore, supplementing those models with the account for semihard processes one gets much greater increase of the inelasticity and multiplicity of the interaction with the energy due to the additional soft particle production, coming from the color connections of the partons, undergoing hard scattering, to their parent hadrons [5,12].* As it was already mentioned in [12], the main effect is not due to the high p_t jet production itself, but rather due to the appearance of those additional chains of secondary particles of soft origin, which are extended **till the fragmentation region** (without any rapidity gap between the leading baryon and high p_t jets). Here the overall effect of semihard interactions depends on their partial rate, which is influenced

by the model assumptions concerning parton distributions in hadrons, the imposed cutoffs in the QCD evolution etc. Nevertheless, that rate, or mean number of semihard rescatterings at given energy, is essentially constrained by fitting the model predictions for total hadron-hadron interaction cross sections and for elastic scattering slopes to corresponding measured values.

Influence of the pomeron structure functions

It turned out, however, that the picture, described above, is rather dependent on the assumptions concerning the Pomeron (soft strings) momentum distributions. As the sharing of the initial hadron energy-momentum between (anti-)quarks, positioned at the ends of the strings, is governed by nonperturbative soft mechanism, it is generally assumed that the momentum distributions of string ends are defined by the asymptotics of correspond-

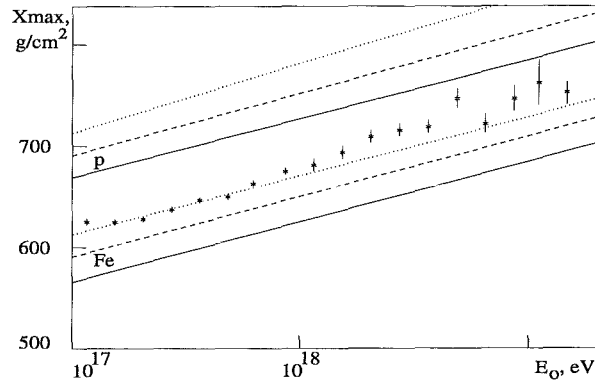


Fig. 2: *EAS maximum depth versus primary energy*: * – *Fly's Eye data* [13], *full and dashed curves* – *QGSJET calculations for $\alpha_R = 0.5, 0.95$ correspondingly*, *dotted curves* – *SYBILL results* [3]; *p* – *primary proton*, *Fe* – *primary iron nucleus*.

*Although particular realizations of that mechanism are model dependent.

ing Regge trajectories [10]:

$$f_q(x^\pm) \sim (x^\pm)^{-\alpha_R}, \quad (1)$$

where x^\pm are the shares of the initial hadron light cone momenta $p^\pm = E \pm p_z$ and $\alpha_R \simeq 0.5$.

Nevertheless, there exist also arguments for a different choice of the string distributions, which could be obtained by taking into account contributions of more complicated (so-called enhanced) Regge diagrams, not considered consistently in the current generation of Monte Carlo models [11]:

$$\tilde{f}_q(x^\pm) \sim \frac{1}{x^\pm} \quad (2)$$

So one may think of choosing an effective value for the parameter α_R : $\frac{1}{2} < \alpha_R < 1$. For a choice of larger α_R some changes of the string hadronization procedure are required to keep the consistency with the measured secondary particle spectra in hadronic interactions, more clearly, one has to assume larger density of produced hadrons per rapidity unit of the string. In the limit $\alpha_R \rightarrow 1$ one gets in average rather short strings (in the rapidity space), centered at the mid rapidity region, and the particle production dynamics becomes similar to the one of SYBILL model.

To investigate quantitatively the effect of that modification we compared the predictions of QGSJET model for the default value $\alpha_R = 0.5$ and rather large value $\alpha_R = 0.95$ (with the proper change of some hadronization parameters). To illustrate that hadron-hadron interaction data alone does not allow to constrain the mentioned arbitrariness we plot at Figure 1 the calculated pseudorapidity spectra of charged particles for $\bar{p}p$ -interactions at different energies for the two choices of the parameters. Of cause, a reasonable fit to the data could be obtained for an intermediate value of α_R . At the same moment the two cases considered result in quite different energy behavior of the main characteristics of hadron-hadron and hadron-nucleus interactions. Naturally, this difference projects itself on the calculated characteristics of extensive air showers – Figures 2,3. In particular, the calculated energy dependence for the EAS maximum depth for the second option of the model comes closer to the SYBILL model predictions. It was shown in [6] that the default QGSJET model allows to describe consistently a great variety of EAS data with the same assumptions concerning primary cosmic radiation. The obtained results allow to suggest that possibly a different (and still consistent) fit could be obtained for a different value of α_R parameter and **different parametrization** for the

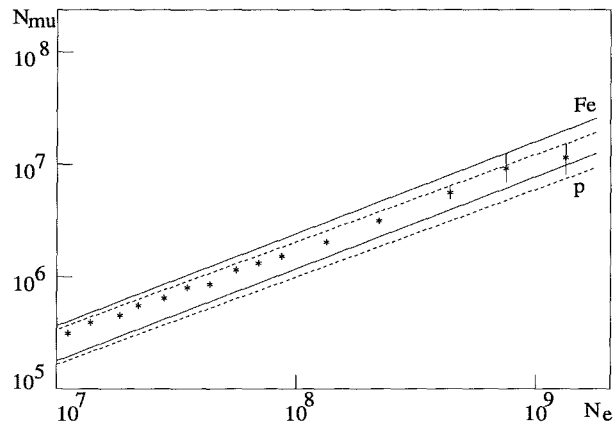


Fig. 3: EAS muon number ($E_\mu 1 \text{ GeV}$) at the sea level versus shower size: * – Akeno data [14], full and dashed curves – QGSJET calculations for $\alpha_R = 0.5, 0.95$ correspondingly; p – primary proton, Fe – primary iron nucleus. $\sec\theta < 1.1$.

primary cosmic ray composition, in particular, larger abundance of heavy nuclei in the PCR above the knee of the spectrum should be assumed.

Conclusions

It was shown that the predictions of Gribov-Regge models of hadronic interactions depend on the assumptions concerning the Pomeron string momentum distributions. The existing ambiguity can be partly removed by simultaneous measurements of different components of extensive air showers and model discrimination on the basis of combined fit to the data. It has been shown in [15] that measuring the hadron component of EAS provides a very useful tool due to its sensitivity to the forward particle spectra in hadron-air nucleus interactions. But the ultimate solution of the problem requires the development of a universal interaction model allowing to fix the existing arbitrariness on the basis of the reactions different from hadron-hadron one, first of all, using electron-positron annihilation and deep inelastic lepton-proton scattering data.

Acknowledgements

This work was supported in part by Russian Foundation of Basic Researches (grant 98-02-22024). One of the authors (S.O.) would like to acknowledge his collaboration with K. Werner.

References

1. J. Knapp, D. Heck, and G. Schatz, Nucl.Phys. B (Proc.Suppl.) 52 (1997) 136
2. A.M. Hillas, Proc. 24th ICRC (Rome) 1995, 1, 270
3. R.S. Fletcher et al., Phys. Rev. D 50 (1994) 5710
4. J. Ranft, Phys. Rev. D 51 (1995) 64
5. N.N. Kalmykov, S.S. Ostapchenko, A.I. Pavlov, Bull. Russ. Acad. Sci., Phys. Ser. 58 (1994) 21
6. N.N. Kalmykov, S.S. Ostapchenko, A.I. Pavlov, Nucl. Phys. B (Proc. Suppl.) 52 (1997) 17
7. K. Werner, Phys.Rep. 232 (1993) 1983
8. G.J. Alner et al., Phys. Rep. 154 (1987) 247
9. L. Durand, H. Pi, Phys. Rev. Lett. 58 (1987) 303
10. A.B. Kaidalov and K.A. Ter-Martirosyan, Phys. Lett. B 117 (1982) 247
11. A. Capella et al., Phys. Rep. 236 (1994) 225
12. S. Ostapchenko, T. Thouw, K. Werner, Nucl. Phys. B (Proc. Suppl.) 52 (1997) 113
13. D.J. Bird et al., Proc. 23rd ICRC (Calgary) 1993, 2, 38
14. N. Hayashida et al., J.Phys. G 21 (1995) 1101
15. J. Hörandel et al., ANI workshop 98, these proceedings

Test of high–energy hadronic interaction models using the hadronic shower core measured with the KASCADE calorimeter

J.R. Hörandel* for the KASCADE collaboration

Universität und Forschungszentrum Karlsruhe, P.O. Box 36 40, D–76 021 Karlsruhe, Germany

The fine segmented hadron calorimeter of the KASCADE experiment allows to study the hadronic component of extensive air showers. Several hadronic observables are compared with predictions of air shower simulations, using the interaction models VENUS, QGSJET and SIBYLL with the objective to test the hadronic interaction models. Results of the comparison are presented.

Introduction

To investigate cosmic rays in the PeV region and above, one is forced to use indirect measurements, observing extensive air showers (EAS) induced in the atmosphere. To interpret the secondary particles at ground level, the measured data are compared with results from Monte Carlo calculations, describing the development of the EAS in the atmosphere and the response of the individual detectors.

One of the principle goals of the investigations is to estimate the mass and the energy of the primary particle. Starting with a given energy and mass of the primary, the development of the EAS in the atmosphere was calculated using the program CORSIKA [1] with different hadronic interaction models. The response of the secondary particles in the detectors at ground level are simulated to obtain the energy deposit and arrival time of each particle in the individual detectors. To reconstruct observables from the detector signals, the same procedures are used for measured and simulated data and comparing simulations and measurements we estimate the primary's mass and energy.

The particle interactions within the detectors are well studied at accelerators. In contrast to the latter, our knowledge of the high–energy hadronic interactions in the atmosphere above a few TeV is very poor. The cosmic–ray energies are much higher than the corresponding CMS energies at colliders, and the forward kinematic range important for EAS physics cannot be investigated in detail. Hence, in the simulation chain the hadronic interaction models in air shower calculations are the weakest point. The question of validity of the interaction models is especially important concerning the origin of the *knee*. The latter could be related to astrophysical or particle physical reasons.

Mostly soft hadronic interactions are important for the EAS development. Due to the energy dependence and the absolute value of the parameter α_s of the strong interaction, the interactions cannot be evaluated by QCD calculations via perturbation theory. Instead, one is obliged to use phenomenological descriptions. In the program CORSIKA, different hadronic interaction models are at the users disposal. In the following, the results of VENUS, QGSJET and SIBYLL calculations are compared with measurements in order

*Corresponding author: E–mail: joerg@ik1.fzk.de

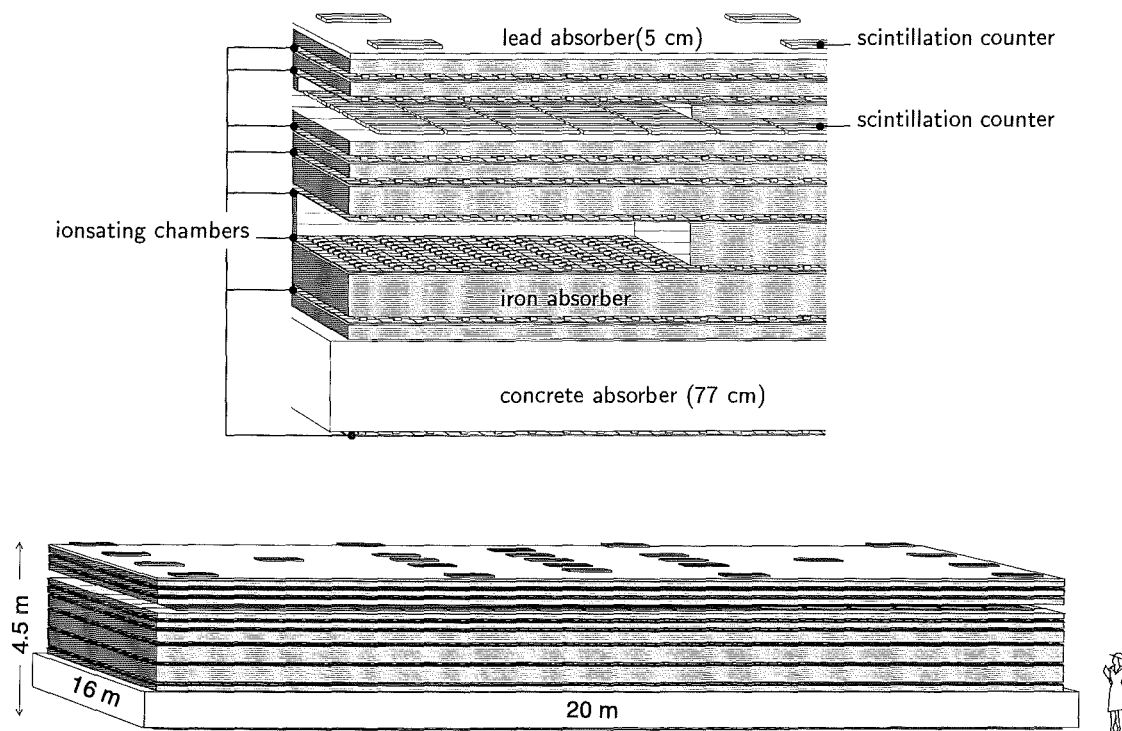


Fig. 1: Schematic view of the KASCADE central calorimeter. Top: detailed sketch, bottom: total view.

to test the models.

Experimental Setup

The interaction models are tested by investigating individual hadrons in the core of EAS. The fine segmented hadron calorimeter of the KASCADE experiment allows to distinguish two hadrons and to determine their energies separately with an energy threshold of 50 GeV in a distance of at least 40 cm [2]. At this energy the reconstruction efficiency for hadrons amounts to 50% growing to nearly 100% for an energy of 100 GeV. For showers in the PeV range, the number of not found hadrons typically amounts to 10% and is nearly constant with energy.

The calorimeter consists of iron slabs with increasing thickness from 12 cm up to 36 cm, as sketched in Figure 1. Between the absorber seven layers of liquid ionisation chambers are interspersed. Behind the third iron layer, scintillation counters for fast-trigger purposes are located. A 5 cm lead absorber on top of the first iron layer serves to suppress electromagnetic punch-through. A last layer of ionisation chambers is situated below the concrete ceiling, which acts as a tail catcher. The total depth of the calorimeter for vertical protons amounts to 11.5 interaction lengths ensuring a reasonable shower containment up to 25 TeV. At this energy on average 97.5% of the energy are deposited in the calorimeter. Each ionisation chamber consists of four independent electronic channels with a size of $25 \times 25 \text{ cm}^2$ as shown in Figure 2. They are inserted in a stainless steel box and positioned by ceramic spacers. A ceramic feed-through allows to apply high voltage to the electrodes and to read out their signals independently ensuring the fine segmentation. The chambers are filled either with the room temperature liquid tetramethylsilane (TMS)

or tetramethylpentane (TMP). These liquids show electron conduction, which allows to detect excess electrons emitted in the ionisation process.

The electrons and muons are detected in an array of 252 stations of scintillation counters. The muon detectors are positioned directly below the electron scintillators and are shielded by slabs of lead and iron corresponding to 20 radiation lengths in total. A detailed description can be found in [3].

Energy Calibration

It is not possible to test the absolute amount of energy deposition due to the lack of calibration possibilities at accelerators. We, therefore, use a two step calibration procedure. Firstly, each ionisation chamber is calibrated with the signal of throughgoing muons. The second step is an indirect calibration using detailed detector simulations. We determine the longitudinal and lateral profiles of energy deposition and compare the measured distributions with simulation results, using the GEANT [4] package with the FLUKA [5] code.

As an example, the longitudinal development of single hadrons from 0.5 TeV up to 10 TeV in the calorimeter is shown in Figure 3. At the higher energies, the simulations reproduce the experimental data quite well. At lower energies the cascades seem to enter deeper into the absorber. However, this is probably an artifact caused by instrumental effects. At these energies the energy deposition in a chamber is low and still in the MeV region where the amplifier noise cannot be neglected. In the simulation it is taken into account as a mean value with a Gaussian distribution. This may not be realistic enough to simulate the data correctly. Consequently, the slight differences should not be taken as major discrepancies. At the lower energies measurements of the transition curves with a prototype calorimeter have shown good agreement with FLUKA calculations [6].

Measurements and Simulations

From October 1996 up to May 1998 about $7 \cdot 10^7$ events were collected. In

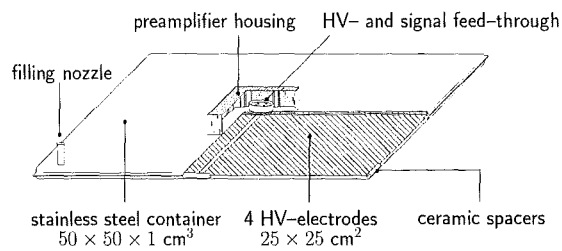


Fig. 2: Sketch of a liquid ionisation chamber.

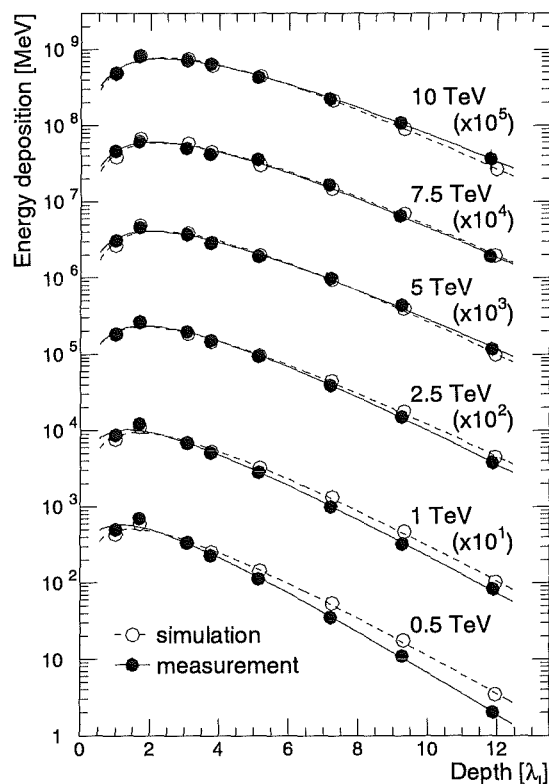


Fig. 3: Experimental transition curves of single hadrons compared to simulated transition curves using the FLUKA code.

$4 \cdot 10^6$ events we reconstructed at least one hadron. Events accepted for the present analysis had to fulfill the following requirements: At least three hadrons with a threshold energy of 50 GeV had been reconstructed. The zenith angle of the shower was less than 30° , and the shower core was located inside the calorimeter. After this cuts 28000 events remained for the further analysis.

EAS simulations were performed with the program CORSIKA, versions 5.2 and 5.62. We calculated 2000 proton and iron induced showers for SIBYLL and 7000 p and Fe events for QGSJET. For VENUS 2000 showers were generated, each for p, He, O, Si and Fe primaries. The showers were distributed in the energy range 0.1 PeV up to 31.6 PeV according to a power law with an index of -2.7 . All secondary particles at ground level are passed through a detector simulation program using the GEANT package to determine the signals in the individual detectors.

Results

The cosmic-ray mass composition is poorly known above 0.5 PeV. Therefore, the interaction models can be tested only by comparing their predictions for the extreme primary masses, namely protons and iron nuclei. If the measured observables lie in between these predictions, the corresponding model is compatible with the data, otherwise we have to exclude it.

When comparing measurements and simulations, it is necessary to divide the data into intervals of fixed shower size. For our investigations we use shower size parameters of all three components, i. e., the number of electrons and muons as well as the hadronic energy sum. For the muonic shower size we use a muon number obtained by integration of the muon lateral distribution in the range from 40 to 200 m. Simulations show that this value N'_μ is a reasonably mass independent energy estimator. We investigated several hadronic observables [7], some of them are discussed in the following.

Firstly, the relation between the electromagnetic and hadronic component is presented in Figure 4. Plotted is the

number of hadrons with an energy threshold of 50 GeV versus the number of electrons N_e as measured by the scintillator array. The measured data are compared with results for proton and iron induced showers calculated with the models VENUS and QGSJET. The energy range corresponds to approximately 0.2 PeV up to 20 PeV. Within this range QGSJET is compatible with our measurements. VENUS generates a steeper increase than the measurements indicate, and especially for higher energies the data are significant below the predictions. Similar discrepancies for VENUS show up in other observables, when electrons and hadrons are compared with each other.

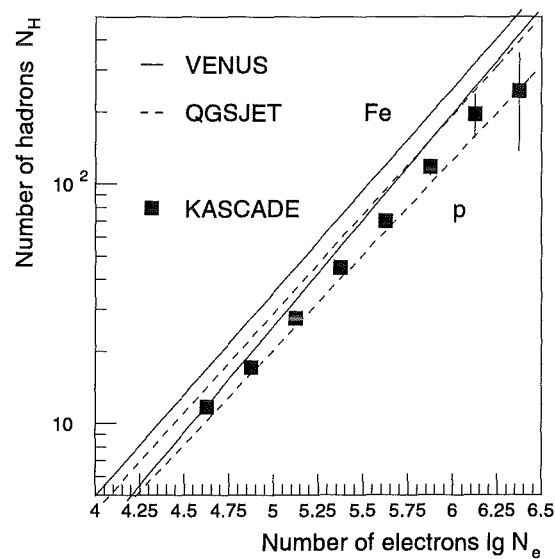


Fig. 4: Number of hadrons ($E_H > 50$ GeV) versus number of electrons.

A second example is presented in Figure 5. The graph shows frequency distributions of the energy of each hadron normalized to the energy of the most energetic hadron in the shower. The measurements are compared with predictions for primary protons and iron nuclei, calculated with the models QGSJET and SIBYLL for two muon size intervals corresponding to approximately 3 PeV and 10 PeV. The upper two graphs show the low energy bin below the *knee*. The measured data are in between the range given by the QGSJET model in contrast to the SIBYLL predictions, which are not able to describe the measurements. Like in this example, SIBYLL cannot reproduce the measurements in other observables, especially when grouping the data into muon shower size bins. This might be due to a wrong muon number as generated by SIBYLL [8]. In the energy range above 10 PeV, as shown in the third graph, the data are outside the acceptable range also for the QGSJET simulation. It seems as if QGSJET produces correct distributions of the hadronic energy fraction below the *knee*, but there are discrepancies describing the data above. On the other hand, there exist observables like the lateral distribution of hadrons or their differential energy spectrum for which the QGSJET predictions are compatible with the measurements below and above the *knee*. These inconsistencies need more detailed investigations, but may be a hint that the hadronic interaction models fail for energies above the *knee*.

As a last example, Figure 6 presents the spatial distribution of the individual hadrons in a 15 PeV proton induced shower core. The points show the impact coordinates at the top of the calorimeter and their size represents the corresponding energy in a logarithmic scale. To investigate the structure of the core a *minimum spanning tree* is constructed. For this objective all hadrons are connected by lines with each other and their distance is divided by the sum of their energies. The *minimum spanning tree* is that connection pattern which minimizes the total sum of weighted distances. Figure 6 shows the connecting lines for a particular shower core.

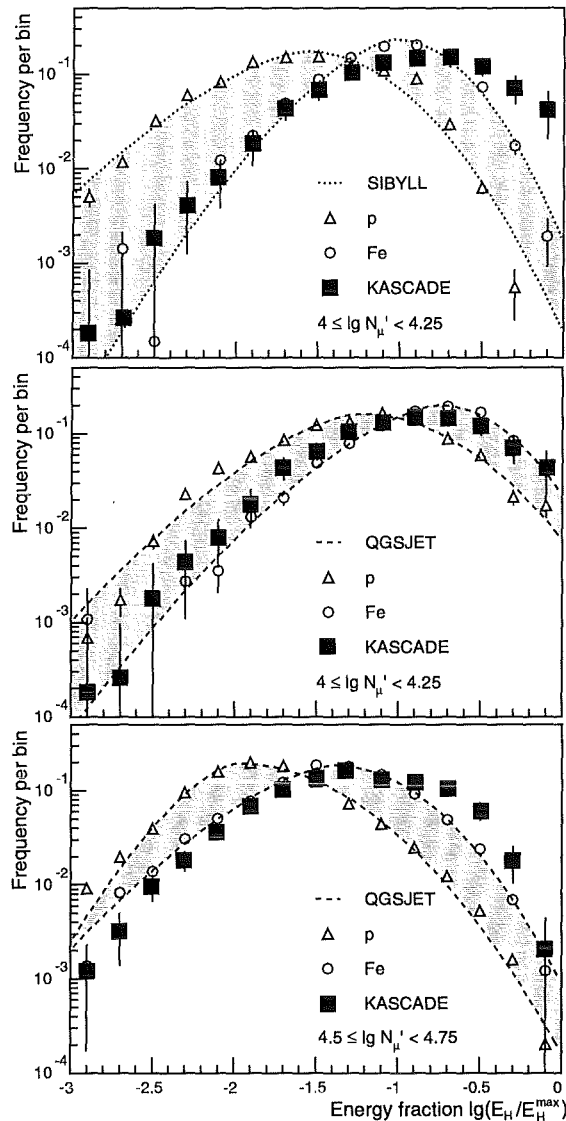


Fig. 5: Frequency distributions of energy fraction for different interaction models and energy ranges. The curves connecting the simulated data points are fitted to guide the eye.

Frequency distributions of all distances in the *minimum spanning tree* are shown in Figure 7. Results are shown for showers in two muon size bins, corresponding to an energy below and above the *knee*. In the upper graph, below the *knee*, the KASCADE data are between the simulations for primary protons and iron nuclei, which means that QGSJET is compatible with the measurements. However, above the *knee*, as shown in the lower graph, a disagreement between data and simulations is observed. Further investigations are necessary to clarify the differences.

Conclusions

Several observables of the hadronic component of EAS have been investigated. The lateral distribution, the lateral energy density, the differential energy spectrum, the distance distribution, the number of hadrons and their energy sum, the maximum hadron energy, and the fraction of the energy of each hadron to the maximum hadron energy in each shower. All observables are investigated for five different thresholds of hadron energy from 50 GeV up to 1 TeV and the showers are divided into shower size intervals of all components, the number of electrons and muons as well as the hadronic energy sum. Out of these only a few examples have been discussed presenting the principle findings.

The model SIBYLL has problems to describe the data, especially when the data are classified according to the muon shower size. It is possible, that a new release [8] will fit the data better. The model VENUS fits the data reasonable well, but there are deviations when binning the data in intervals of the electron number.

QGSJET describes the data well. Es-

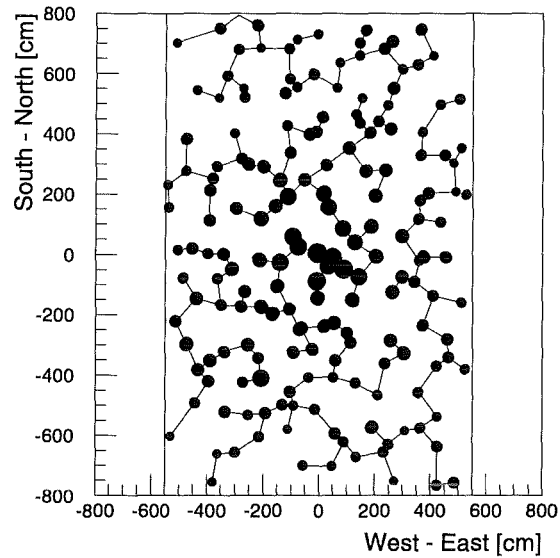


Fig. 6: *Spatial distribution of hadrons in the calorimeter for a shower induced by a 15 PeV proton. The distances between the hadrons are measured by a minimum spanning tree.*

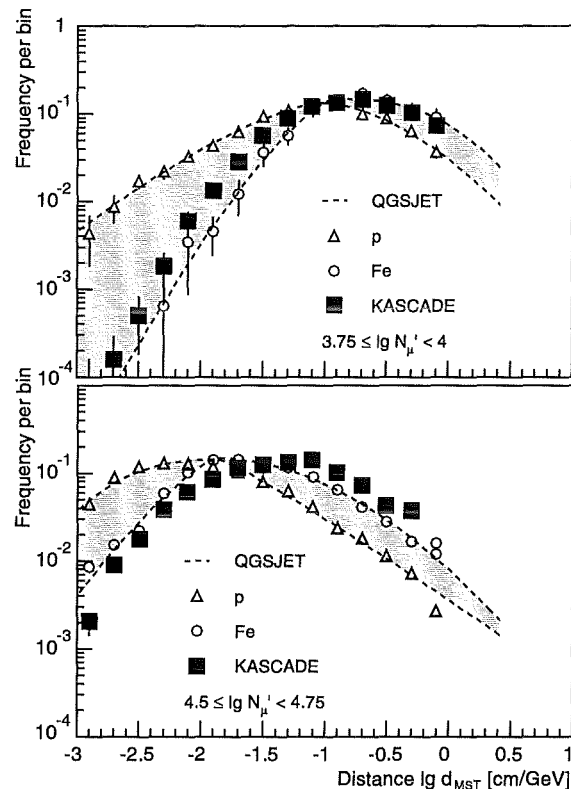
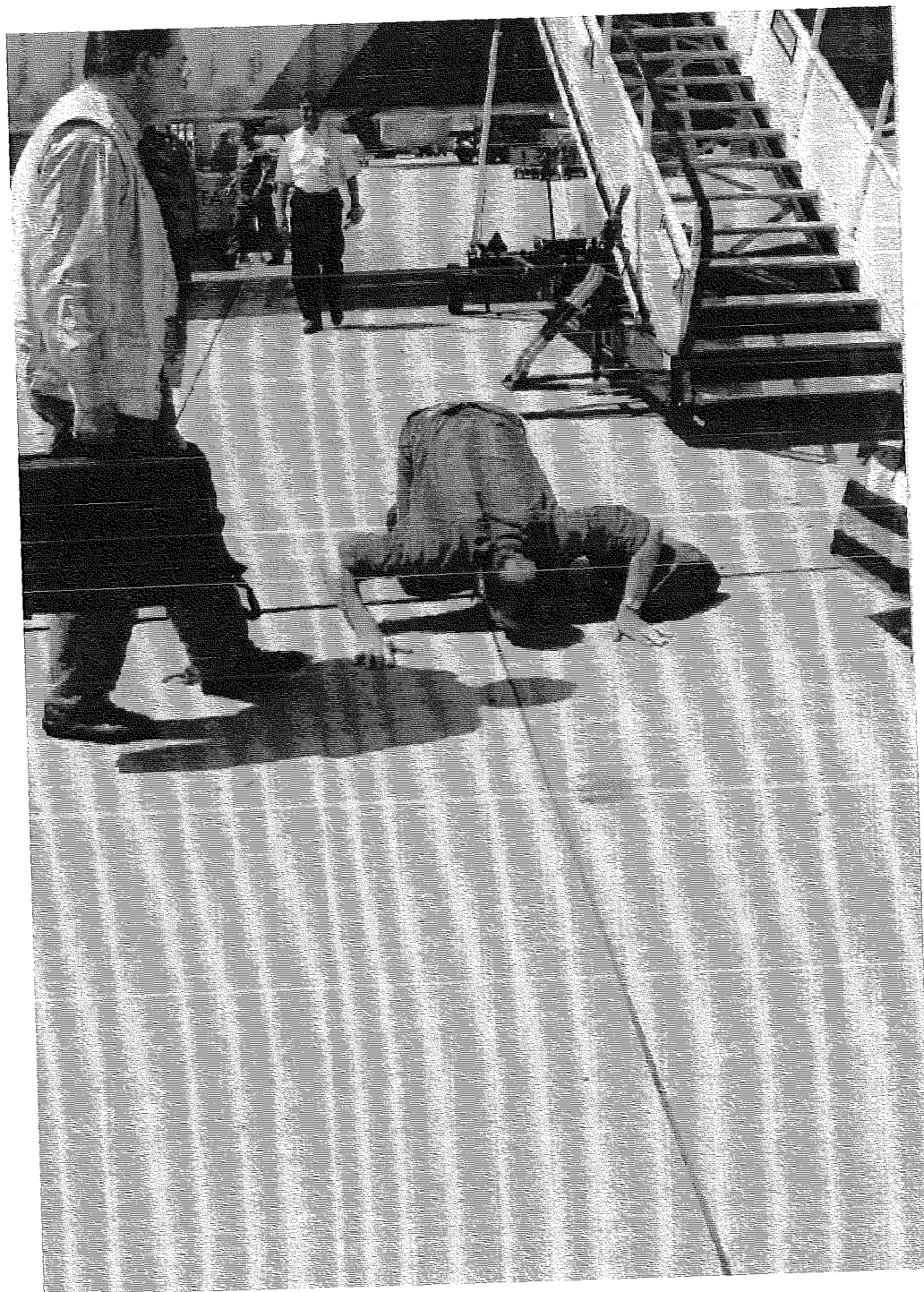


Fig. 7: *Frequency distributions of all distances in a minimum spanning tree. The curves connecting the simulated data points are fitted to guide the eye.*

pecially below the *knee* ($E_0 < 5$ PeV) compatibility between its predictions and measurements were found. Above the *knee* deviations in several observables are seen, which need further investigations. To sum up, it can be concluded that the results are a confirmation of the Gribov Regge theory, on which the models VENUS and QGSJET are based, and which is obviously able to describe the hadronic interactions in extreme forward region up to energies of at least 5 PeV.

References

- [1] D. Heck, J. Knapp et al., FZKA 6019, Forschungszentrum Karlsruhe (1998)
- [2] J. Engler et al., A Warm-Liquid Calorimeter for Cosmic Ray Hadrons, submitted to Nucl. Instr. and Meth. (1998)
- [3] H.O. Klages et al., Nucl. Phys. B (Proc. Suppl.), 52 B (1997) 92
- [4] GEANT 3.15, Detector Description and Simulation Tool, CERN Program Library Long Writeup W5013, CERN (1993)
- [5] P.A. Armio et al., FLUKA user's guide, Technical Report, TIS-RP-190, CERN (1987, 1990)
- [6] H.H. Mielke et al., Nucl. Instr. and Meth., A 360 (1995) 367
- [7] J.R. Hörandel, FZKA 6015, Forschungszentrum Karlsruhe (1998) (in German)
- [8] T. Stanev, Proc. Xth International Symposium on Very High Energy Cosmic Ray Interactions, Laboratori Nazionali del Gran Sasso, 1998, to be published



Verification of the CORSIKA code in the 0.01-500 TeV energy range

S.V. Ter-Antonyan* and L.S. Haroyan

Yerevan Physics Institute, Alikhanyan Br.2, 375036 Yerevan, Armenia

Comparisons of the world experimental data for the near-horizontal muon energy spectra in the .01-500 TeV energy range and the vertical hadron energy spectrum at the mountain level in the 1-10 TeV energy range with corresponding calculations performed by the CORSIKA simulation code are presented. The results point out on the correctness of the CORSIKA code with QGSJET and VENUS interaction models at least up to 10^3 TeV primary energies.

Introduction

The main purpose of the investigation is to make a verification of the CORSIKA Extensive Air Shower (EAS) simulation code in the primary energy range .01-500 TeV, where an information about primary energy spectrum and an elemental composition is quite known on the basis of satellites and balloons experiments. The CORSIKA code has been worked out in Karlsruhe (Germany) [1,2] and allows to simulate interactions and decays of nuclei, hadrons, muons, electrons and photons in the atmosphere up to energies of some 10^{20} eV. It gives the type, energy, location, direction and arrival times of all secondary particles that are created in an air shower and reach an observation level. The interpretation of EAS measurements relies strongly on the model of shower development in the Earth's atmosphere. Such models are used to simulate the transport of particles through the atmosphere, their interaction with air nuclei and the production of secondary particles. For high energy hadronic interactions we used two different models (VENUS and QGSJET) [2] based on Gribov-Regge theory. Inelastic reactions are simulated by cutting Pomerons, thus, creating two color strings per Pomeron which subsequently fragment into colorless hadrons. Low energy hadronic interactions are simulated with the GHEISHA code [2].

Near-horizontal muon energy spectra

The calculations of the expected absolute near-horizontal muon flux are carried out by means of the CORSIKA-HORIZONT code [1]. The standard CORSIKA program models the Earth's atmosphere as a flat disc where the density of the air decreases with the height following the U.S. standard atmosphere. The shower simulation under large zenith angles (greater than 75°) is carried out the same as for vertical showers traveling through an atmospheric profile corresponding to the desired angle. The modified profiles are stored in special files [1].

We have made a comparison of the muon differential energy spectra $\partial N(E_\mu, \theta)/\partial E_\mu$ which are measured directly in experiments DEIS [3] at the sea level and Aragats [4] at the

*corresponding author: e-mail: samvel@jerewan1.yerphi.am

mountain level for large zenith angles with the adequate calculations by the CORSIKA-HORIZONT simulation code. The calculations are carried out according to the expression

$$\frac{\partial N(E_\mu, \theta)}{\partial E_\mu} = \int \sum_A \frac{\partial \mathcal{S}_0(E_0, A)}{\partial E_0} \frac{\partial \Omega_\mu(E_0, A, E_\mu, \theta)}{\partial E_\mu} dE_0 \quad (1)$$

where $\partial \mathcal{S}_0(E_0, A)/\partial E_0$ - are the absolute primary energy spectra of nuclei of mass A ($A = 1, 4, 16, 28, 56$) [5],

$\partial \Omega_\mu(E_0, A, E_\mu, \theta)/\partial E_\mu$ - is the differential muon energy spectrum at observation level generated by the primary nucleus with the energy E_0 , the mass A and the zenith angle θ . The values of Ω_μ functions are calculated by the CORSIKA code.

The results of calculations (small symbols and dotted lines) and the experimental data [3,4] (large symbols) are shown in Fig. 1,2 for the QGSJET and VENUS models correspondingly. The good agreement of experimental data and theoretical predictions by the CORSIKA in a whole zenith angle range points out on a correctness of the employed models.

The presented results are based on 10^7 simulated muon events by the CORSIKA520-HORIZONT code at the $20 - 5 \times 10^5$ GeV primary energy interval. The average primary energies for the generation of muons with energies more than of 2 GeV are equal to .1-1 TeV at zenith angles $\theta \in 75 - 90^\circ$ correspondingly.

The same calculations are performed for the muon energy interval 10-50 TeV using the CORSIKA561-HAS code and the QGSJET interaction model. The corresponding primary energies are simulated in the $15 - 2 \times 10^3$

TeV interval. The results of calculations of the differential muon energy spectra at different zenith angles (filled symbols) and experimental data [6] (empty circles) are illustrated in Fig.3. The line in Fig. 3 corresponds to the calculation data from [7].

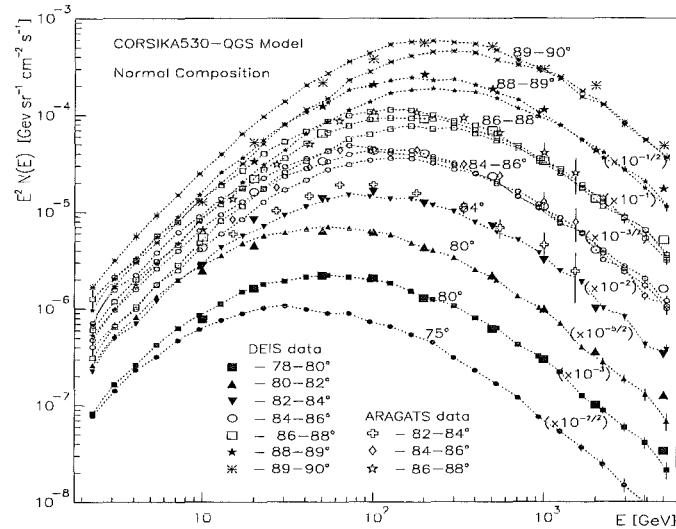


Fig. 1: Muon differential energy spectrum at different zenith angles (QGSJET model).

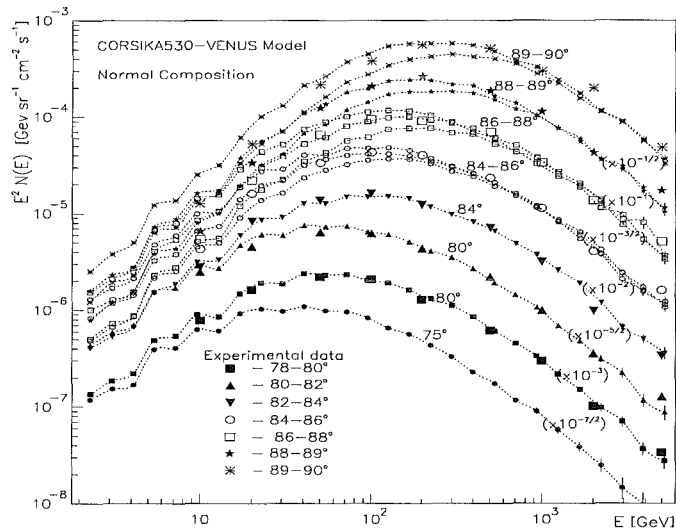


Fig. 2: The same as Fig.1 (VENUS model).

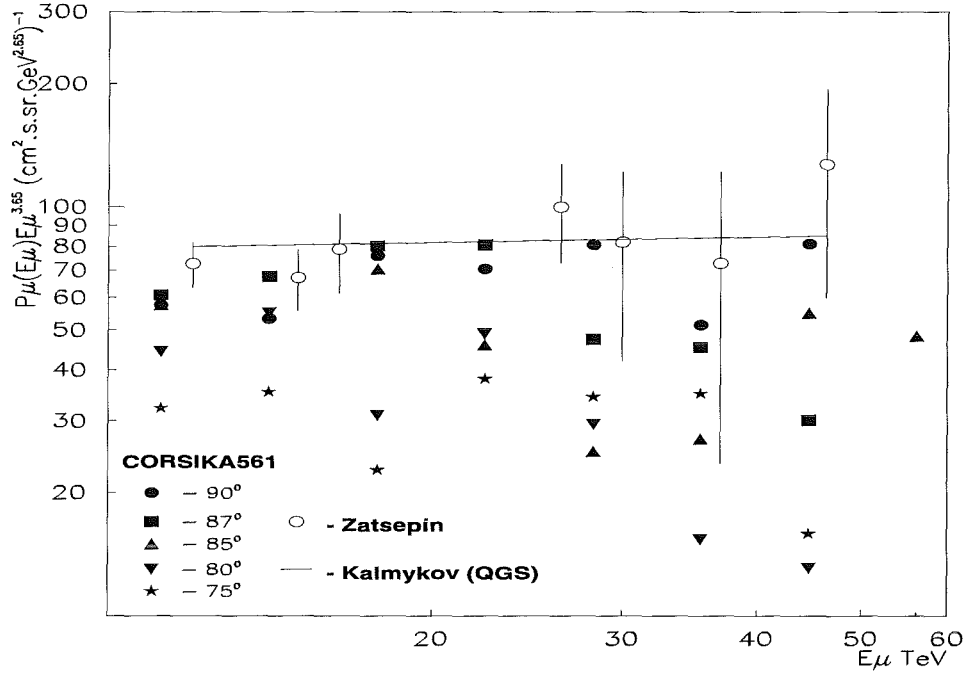


Fig. 3: Muon differential energy spectrum at different zenith angles. The filled symbols are the result of calculations by the CORSIKA with QGSJET model, the empty circles are experimental data from [6], line is calculation data [7].

High energy hadron flux

Further verification of the CORSIKA code is performed in the 1-500 TeV primary energy range by the comparison of the precise PION experimental data [8,9] with corresponding CORSIKA predictions. The PION experiment was carried out in 1976-1986 and was aimed to measure hadron energy spectra in the 1-10 TeV energy range. (Armenia, Aragats mountain, 3200 m above the sea level).

The PION setup consisted of an ionization calorimeter with iron absorbers (12 layers) and cylindrical Ar filled ionization chambers. The calorimeter's effective area was $(3.2 \times 3.2)m^2$. The thickness of the iron absorbers equaled 10 cm. The hadron energy and coordinate resolutions in the experiment were $\sigma(\ln E) = .15$ and $\sigma(x, y) = 5$ cm correspondingly. The detailed information about the PION experiment and the measurement accuracies is presented in [9].

The calculation of the expected vertical hadron differential energy spectrum have been performed applying the CORSIKA530 code according to the expression

$$\frac{\partial I(E)}{\partial E} = \int \sum_A \frac{\partial \mathcal{S}_0(E_0, A)}{\partial E_0} \frac{\partial \Omega_h(E_0, A, E)}{\partial E} dE_0 \quad (2)$$

where $\partial \mathcal{S}_0(E_0, A)/\partial E_0$ - are the primary energy spectra of nuclei of mass A ($A=(1,4)$ [10], (16, 28, 56) [5]) and $\partial \Omega_h(E_0, A, E)/\partial E$ - is the differential hadron energy spectrum on the observation level is generated by the primary nucleus with the energy E_0 , mass A and zenith angle equal to 0. The values of Ω_h functions were calculated by the CORSIKA code. The results of the calculations with the CORSIKA for QGSJET, VENUS, HDPM and SIBYLL models (filled symbols) with Aragats (empty circles) and Tien-Shan (empty triangles) data [11] are shown in Fig. 4. The better agreement between PION data and the

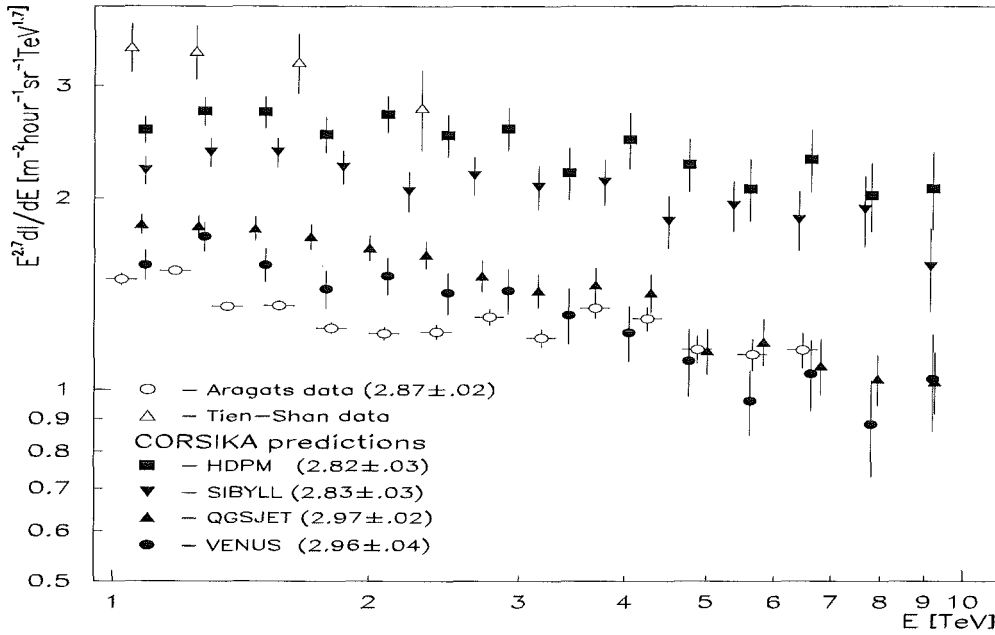


Fig. 4: Hadron absolute differential energy spectrum at Aragats level. The filled symbols are the results of calculation by the CORSIKA with different models and the JACEE93 primary composition [10] for H and He nuclei. The empty symbols are Tien-Shan and Aragats data. The values of corresponding spectral indexes are shown in parentheses.

CORSIKA prediction is obtained with the VENUS and QGSJET models.

The hadron zenith angle distributions on the Aragats level at energies more than 1 and 2 TeV are shown in Fig.5. The experimental data are approximated in the form

$$\frac{\partial I(E, \theta)}{\partial \cos \theta} = \frac{\partial I(E, \theta = 0)}{\partial \cos \theta} \cos^\rho \theta \quad (3)$$

where the power index $\rho = 6.6$ at $E \geq 1$ TeV and $\rho = 6.5$ at $E \geq 2$ TeV. One can see that at $E \geq 2$ TeV hadron energy, the CORSIKA predictions agree with PION data very well. After including the low energy hadrons an underestimation of Aragats spectra is noticed. This can be explained by the approaching to the energy threshold ($E \geq 0.5$ TeV) for a PION calorimeter.

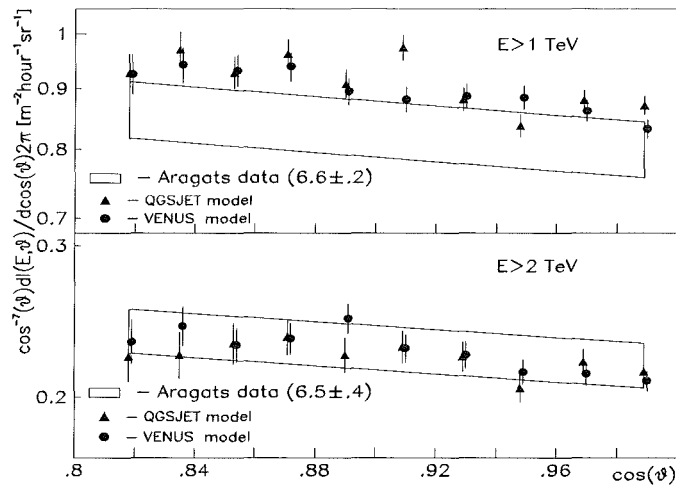


Fig. 5: Zenith angular distribution of the high energy hadrons at different energy thresholds.

Conclusion

The results of the comparison for both the hadron differential energy spectrum on the

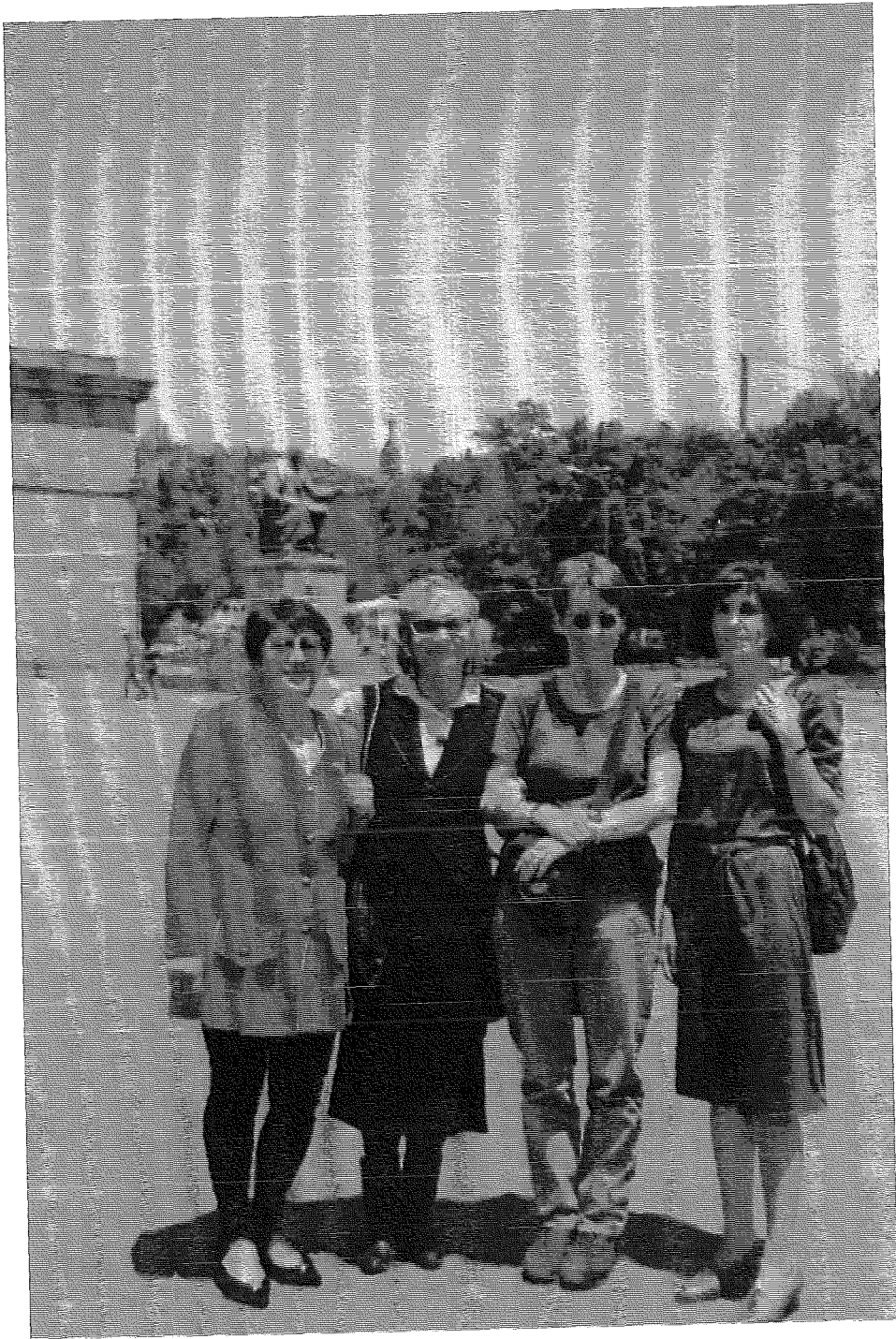
mountain altitudes and the absolute near-horizontal muon energy spectra at different zenith angles point out on the correctness of the CORSIKA code with QGSJET and VENUS models at least in the $10 - 10^6$ GeV energy range.

Acknowledgements

We thank H. Rebel, J. Knapp and D. Heck from Forschungszentrum Karlsruhe for providing the CORSIKA code, and we are grateful to A.A.Chilingarian for significant comments. We would like to thank the ISTC A116 grant for the support of the investigations.

References

1. D. Heck et al., *Report FZKA 6019* (1998) Forschungszentrum Karlsruhe
2. J. Knapp, D. Heck, G. Schatz. *Report FZKA 5828* (1996) Forschungszentrum Karlsruhe
3. O.C. Allkofer, G. Bella, B.M. Bleichert et al., *16th ICRC*, (Kyoto) 1979, **10**, 50
4. T.L. Asatiani et al., *Proc. 14th ICRC*, 1975, **6**, 2024
5. B. Wiebel-Sooth, P.L. Biermann and H. Meyer, *Proc. 24th ICRC*, (Rome) 1995, **2**, 656
6. G.T. Zatsepinet et al., *Izv. Akad. Nauk Ser. Fiz.*, 1994, **58** 119
7. N.P.II'ina, N.N.Kalmykov et al., *Proc. 24th ICRC*, (Rome) 1995, **1**, 524
8. V.V. Avakian et al., *Proc. 21th ICRC* (Adelaide) 1990, **8**, 206
9. V.V.Avakian, *Thesis, Doctor of Science*, YerPhI, 1988, Yerevan
10. K. Asakimori et al., *Proc. 23th ICRC* (Calgary) 1993, **2**, 25
11. A.P. Chubenko and S.I. Nikolsky, *Proc. 21th ICRC* (Adelaide) 1990, **8**, 202



The charge ratio of cosmic ray muons

I. M. Brâncuş¹, B. Vulpescu¹, J. Wentz², H. Rebel², A. F. Badea¹, H. Bozdog¹, M. Duma¹, A. Haungs², H.-J. Mathes², M. Petcu¹ and M. Roth²

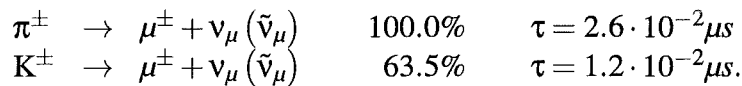
¹National Institute of Physics and Nuclear Engineering – Horia Hulubei, Bucharest, Romania

²Forschungszentrum Karlsruhe, Institut für Kernphysik, Germany

The aspects of the measurements of the muon charge ratio, in particular at low energies, are illustrated by a recent experimental study using an improved “delayed coincidence” method with a compact sampling calorimeter. Using the CORSIKA program for the simulation of extended air showers, the muon energy spectrum and the charge ratio have been investigated and compared with experimental data in the range < 1000 GeV.

Introduction

Our earth is continuously bombarded by primary cosmic ray particles, which are dominantly charged particles, highly energetic protons, alpha particles and heavier nuclei, with individual energies up to tremendous values of 10^{20} eV. Entering the atmosphere, a primary cosmic particle interacts with the air nuclei generating an immense number of secondary particles by successive interactions, phenomenon called extended air shower (EAS) [1]. Cosmic ray muons observed with detectors placed at the ground level originate from the decay of mesons produced by interactions of high energy cosmic ray primaries with air nuclei in high altitudes. Their origin is mainly due to the decay of charged particles pions and kaons, processes which lead also to the production of atmospheric neutrinos:



Muons have a relative large lifetime, $2.2 \mu\text{s}$, so they can reach the Earth before they decay in

$$\mu^\pm \rightarrow e^\pm + \nu_e (\tilde{\nu}_e) + \tilde{\nu}_\mu (\nu_\mu).$$

Taking into account the nature of the processes in which muons appear, it can be easily seen that the ratio of positive to negative cosmic muons, called the muon charge ratio $R_\mu = N_{\mu^+}/N_{\mu^-}$, could bring valuable informations in both problems of debate, the hadronic interactions and the atmospheric neutrinos.

Hadronic interactions and muon charge ratio

The identification of hadronic interaction effects and of the nature of the primary by EAS studies requires a detailed modelling of the shower development by Monte Carlo methods, (CORSIKA code [2]) following each individual particle from production to destruction, decay or passage through the plane of observation and displaying the fluctuations arising from stochastic processes. In order to describe EAS showers by MC simulations in a

realistic way, the interpretation of the observations of the earth detectors need the knowledge of basic interactions of these high-energy particles (the parameters on interaction lengths, particle production multiplicities, the elasticity and the reaction kinematics and their energy dependence). It is important to look for observables which enable some tests or provide experimental constraints of the constructed models, such kind of observable being the charge ratio of cosmic muons.

Many experimental studies carried out above a few GeV muon energy have used magnetic spectrographs, in which the charge particle trajectories are determined before and after traversing the magnetic field. This type of instruments has a long tradition. A typical example of an advanced instrument is the spectrograph devise for measurements on the observatory on Mt. Aragads. In 1975 at the ICRC in Munich, Tina Asatiani presented measurements of horizontal atmospheric muons using this instrument [3]. The determination of muon charge ratio in measurements performed with expensive magnetic spectrometers involving a lot of systematic errors due to different acceptance and detection efficiencies shows an excess of positive muons, a value about 1.25 for low energy muons and a slow increase with the muon energy.

The explanation of the positive charge excess could be found in the production of pions and kaons which is determined by the intrinsic momentum distribution of the quarks in the projectile. The proton has two up quarks (positive charge $+2/3$) and only down quark (negative charge $-1/3$). Hence in the formation of the positive pion, the configuration (ud) is favored. This valence quark argument leads also to a significant asymmetry for muons with kaons parents, since $K^+ = (s\bar{u})$ does not contain the original valence quark. In nucleons collisions kaons are produced in pairs or associated with strange baryons (which carry negative strangeness), whereby the positive kaon carries the positive strangeness. Taking into account the secondary interactions of the pions and kaons, the theoretical studies [4] stress the importance of weighted energy momenta in the expression of inclusive cross-sections demonstrating that the production of positive pions and kaons are favoured. Thus the charge ratio of cosmic muons reflects the properties of the hadronic interactions and of the inclusive production cross-sections indicating the asymmetry in the production of pions and kaons.

Atmospheric neutrinos and the muon charge ratio

The determination of muon charge ratio is important also in giving new information about an important topics under debate, called "the atmospheric neutrino problem" As it was shown above, muon neutrinos and electron neutrinos are generated through the decay of secondary pions, kaons and muons:

$$R(e/\mu) = \frac{\nu_e + \bar{\nu}_e}{\nu_\mu + \bar{\nu}_\mu}$$

From the decay chains one can immediately see that the expected flavour ratio, neutrinos and antineutrinos summed up, is about 2. Atmospheric neutrino fluxes have been calculated with various degrees of sophistication, but the results for the absolute fluxes are considered to have considerable uncertainties ($\pm 30\%$) while the ratio is quoted with better accuracy ($\pm 5\%$). Atmospheric neutrino fluxes are determined by large absorber detectors as KAMIOKANDE [5] and KARMEN [6]. Though the experimental situation is by far not clarified, there seems to be a considerable deficit of the muon neutrinos and/or an

excess of electron neutrinos, summed over particles and antiparticles. The experimental ratio tends to be only about ($\pm 60\%$) of the predicted value, such result inducing speculations about flavour oscillations of the neutrinos. If neutrinos do have a finite rest mass and if different flavors are mixed, then a certain fraction of one type could be converted to another one.

However such interpretation is subject to many uncertainties, beyond insufficient statistical accuracies. For the understanding of the observed events in the water Cerenkov detectors, the expected fluxes must be folded with the detector response, using the respective cross sections and excitation functions. It is known that the neutrino scattering cross sections are different for different flavours, and for neutrinos and antineutrinos as well. In addition any neutrino oscillation effect would be opposite for neutrinos and antineutrinos. In conclusion, there is a strong interest in the atmospheric muon charge ratio for relative low energies, which reflects the expected ratio of electron neutrinos to electron antineutrinos.

The determination of the muon charge ratio

Motivated by such background, a Romanian-German experiment have been performed with the electromagnetic calorimeter WILLI (Weakly Ionising Lepton Lead Interactions) built in NIPNE Bucharest, consisting in 20 modules, each of 1cm Pb and 3cm NE114 scintillator on a support of 1.2cm Al, see Fig. 1. Our method to determine the charge ratio of positive to negative muons [7] is based on the different behaviour of positive and negative muons stopped in the calorimeter layers. While positive muons decay with their natural lifetime, the negative muons are captured in atomic orbits and form muonic atoms. Due to the strong overlap of the atomic orbits of muonic atoms with the nucleus, negative muons are often absorbed. This leads effectively to a shorter lifetime of the negative muons in matter, which is known from precise measurements. The WILLI device measures the effective lifetime of the stopped muons for both charge states by observing the timely appearance of decay electrons and positrons with the scintillator layers after the muon stop. Fig. 2 shows an individual event from the off-line computer event display containing the ADC and MTDC information of the lowest 16 scintillator layers (32 photomultipliers). The continuous muon track is seen as zero time signals down to a stopping layer and the decay electron as a short delayed track in the vicinity of the stopping layer. From the measured value the charge ratio can be deduced, since the lifetime for each separate state is known. The measured time spectra are a superposition of different decay curves, the parameters being determined by simulating the detector response based on GEANT code [8].

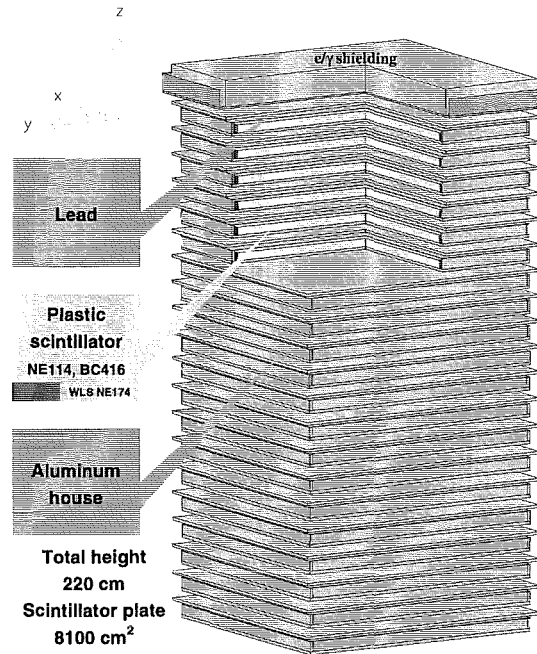


Fig. 1: The WILLI detector.

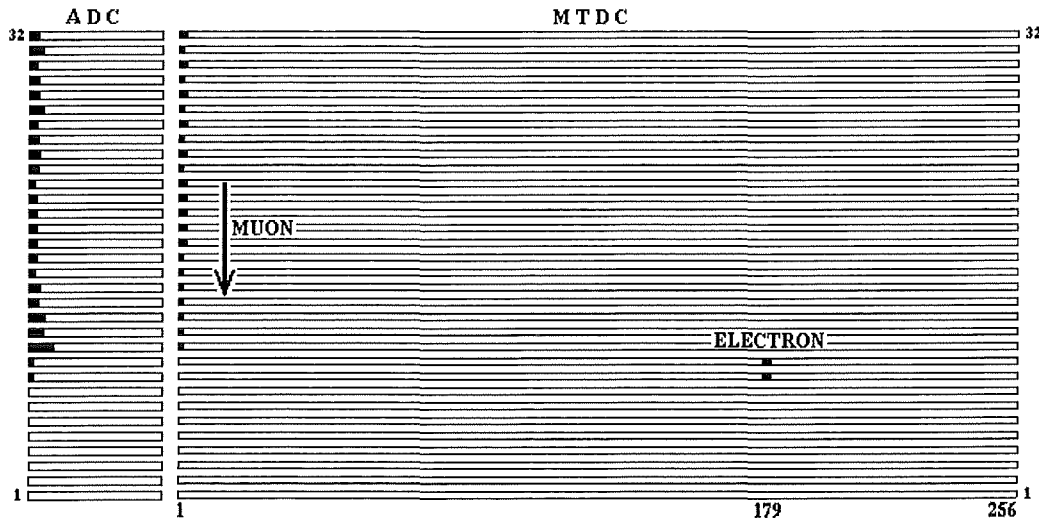


Fig. 2: Event display: ADC and MTDC image of a muon decay event. The ADC scale corresponds to the 0 – 4095 channel range and the MTDC comprises 256 bins of 20 ns width. The muon stops after penetrating 4 + 11 active layers and the electron is seen in the next layer.

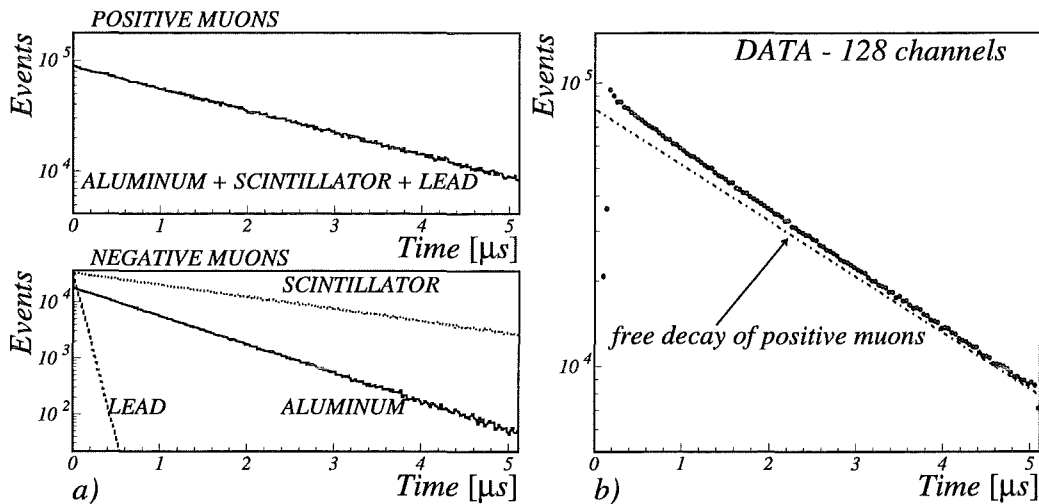


Fig. 3: MC simulation results on different materials contribution to the total decay curve (a); experimental data decay curve (b).

$$\Delta N(t_i, t_i + \Delta t) = N_+ c_0 \delta_0 \exp\left(-\frac{t_i}{\tau_0}\right) + N_- \left[\sum_{j=1}^3 c_j^* \delta_j \exp\left(-\frac{t_i}{\tau_j}\right) \right].$$

In Fig. 3a the detector efficiency constants c_0 and c_i^* , $i = 1, 2, 3$ determined by the MC simulations, are used to illustrate the four exponentials which have to be deconvoluted from the total decay curve. Fig. 3b displays experimental data for about 5.3 million events. The first 10 channels could not be evaluated mainly because of the 80 ns second trigger condition. The free decay curve ($\tau = 2.2 \mu\text{s}$, adequately normalized) is plotted for comparison. The analysis of experimental data using a calibration set of 600000 events leads to the

value of the charge ratio of : $R(\mu^+/\mu^-) = 1.30 \pm 0.05$ for cosmic muons with a mean momentum of 0.86 GeV/c and a mean zenith angle of 26° .

Model interpretation of the muon charge ratio

The experimental determination of the cosmic muons charge ratio provides relevant information for the study of the air shower development, as the muon production reflects the nature and the multiplicity of the parents particles produced in the interactions of the primary cosmic particles with the atmospheric nuclei. An additional problem of interest is the influence of the terrestrial magnetic field on the energy spectrum of charged particles, which could be determined by measuring the muon charge ratio at different inclinations in the East-West geomagnetic plane. The phenomenon of the splitting of the values of muon charge ratio in measurements on different East-West direction is called the East-West effect. From the present experimental data it is known that the geomagnetic deviation decreases the muon charge ratio in the East direction and increases in the West direction [9]. For the analyses of such features theoretical models have been developed, based on the modification of the muons trajectories in the atmosphere due to the magnetic field.

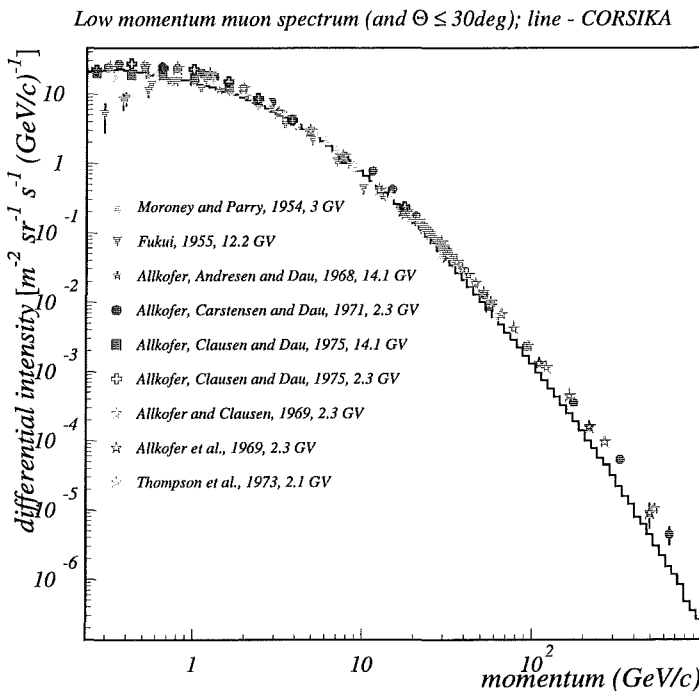


Fig. 4: Muon flux in the 0.23 to 1000 GeV/c range calculated for muon angle of incidence less than 30° .

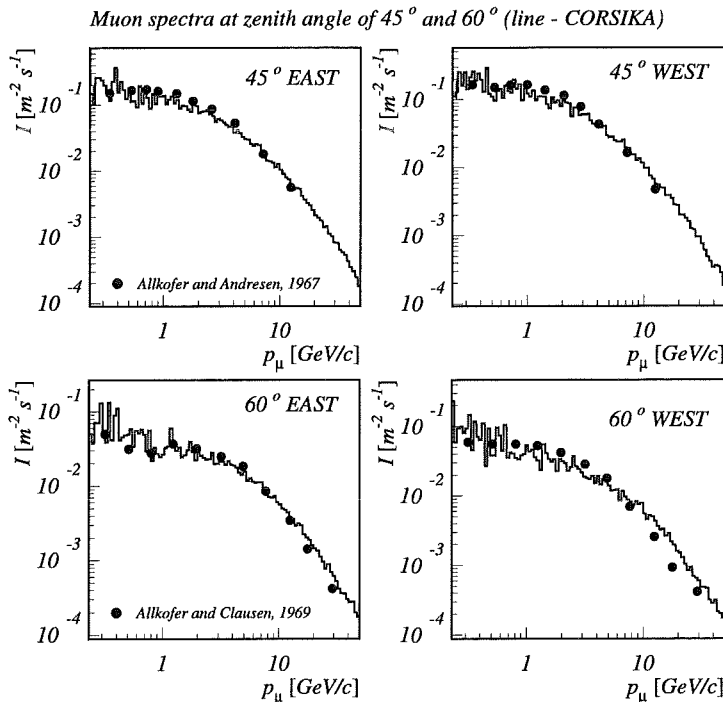


Fig. 5: Muon intensity in the East-West plane at 30° , 45° and 60° .

This effect changes the proportion of the probabilities for decay and of interaction. The initial conditions contain the characteristics of the hadronic interactions and of the multiplicities of pions and kaons. In the low energy range where we perform measurements on the muon charge ratio these effects are increasing significantly.

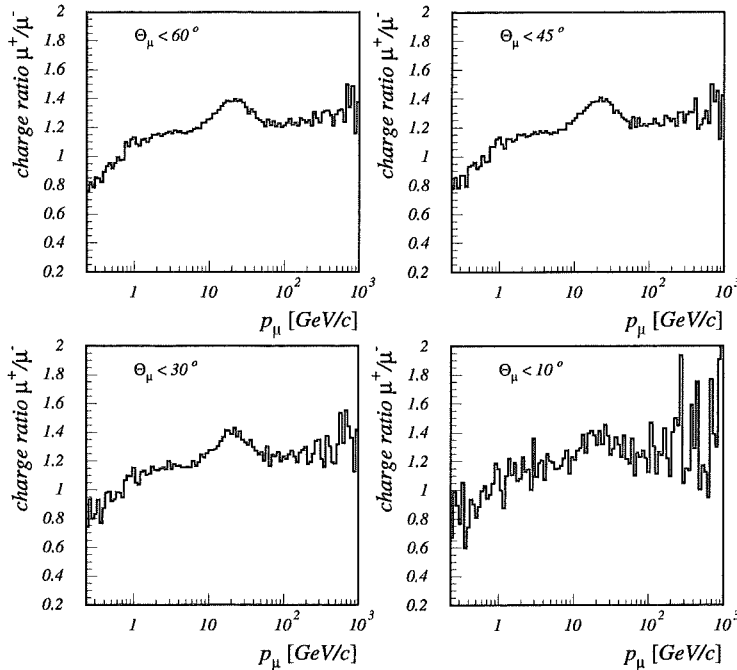


Fig. 6: Charge ratio of positive to negative muons for different limits in the zenith angle.

Using the CORSIKA program [2] developed for the KASCADE experiment to simulate extensive air showers, the muon flux at low energies, the energy spectrum and the muon charge ratio have been investigated. The simulation results have been weighted according to primary cosmic ray spectra from recent measurements. In order to simulate primary nuclei heavier than protons, a superposition model have been assumed. First, the primary energy range which contributes mainly to the muon flux has been investigated. The primary energy per nucleon in the simulations has been divided in 8 bins covering the range from 3 GeV/nucleon to 20 TeV/nucleon. Fig. 4 presents the resulting muon momentum spectrum from simulations in good agreement with the experimental data. The upper limit in the primary energy reduces high energy muon production which can be noticed in the spectra. Simulations of muon flux in the East-West plane have been performed at different zenith angles, as presented in Fig. 5.

The main goal of our investigations being the cosmic ray muons charge ratio, the energy spectra of the positive and negative muons as well as the charge ratio have been calculated in the overall primary energy range. Fig. 6 shows the charge ratio of positive to negative muons for different ranges of the zenith angle.

A cut at 80 GeV/nucleon has been applied to the primary energy in order to separate features of two interaction models, GHEISHA [10] for low energy and VENUS [11] for high energy, respectively. Figs. 7,8 show the charge ratio dependence on the muon energy reflecting a different behaviour of the two interaction models in producing muons of both signs.

Finally the CORSIKA predictions of the muon charge ratio have been compared in Fig. 9 with the experimental data from the literature, including our result. One can recognise that for vertical measurements the simulations generate values consistently smaller than the measured results for muon energies less than 1 GeV. That decrease of the charge ratio at very low energies is associated with peculiarities of the interaction models.

Using the CORSIKA program [2] developed for the KASCADE experiment to simulate extensive air showers, the muon flux at low energies, the energy spectrum and the muon charge ratio have been investigated. The simulation results have been weighted according to primary cosmic ray spectra from recent measurements. In order to simulate primary nuclei heavier than protons, a superposition model have been assumed. First, the primary energy range which contributes mainly to the muon flux has been investigated. The primary energy per nucleon in the simulations has been divided in 8 bins covering the range from 3 GeV/nucleon to 20 TeV/nucleon. Fig. 4 presents the resulting muon momentum spectrum from simulations in good agreement with the experimental data. The upper limit in the primary energy reduces high energy muon production which can be noticed in the spectra. Simulations of muon flux in the East-West plane have been performed at different zenith angles, as presented in Fig. 5.

Concluding remarks

A) With instrumental – methodical aspects the study demonstrates a simple and efficient procedure, reaching accuracies in the order of few percent and excluding systematic errors of magnetic spectrometers. The reported result is due to five months measuring time. The method has been already used by large-volume detectors, the KARMEN detector of the Karlsruhe neutrino experiment and the KAMIOKANDE detector. In contrast to these setups, our device is easily transportable, suitable for balloon flights for measuring profiles in altitudes. Actually due to different interaction and decay lengths of the parent pions and kaons and different penetration of the cosmic particles in the atmosphere, a variation is expected.

B) What concerns the model interpretation, we emphasise some important features:

- The simulations of the differential energy spectra of different primary particles observed at the top of the atmosphere and of the the muon flux in 0.23-1000 GeV/c range calculated with CORSIKA code are in good agreement with experimental data.
- The calculations of the muon spectra for different zenith angle in the East and West direction using CORSIKA code are also in agreement with the measurements.

• We additionally mention that the comparison of calculated values with measurements in the East-West plane shows that CORSIKA reproduces well the East-West effect, i.e. the asymmetry in the charge ratio, dependent on the muon energy < 10 GeV.

• For vertical measurements the CORSIKA simulations predict smaller results than the

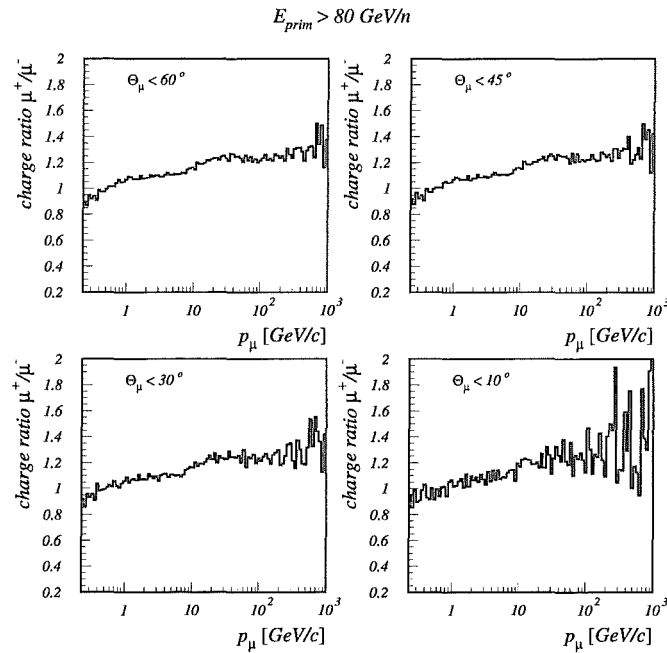


Fig. 7: Charge ratio of positive to negative muons for different limits in the zenith angle for primary energy > 80 GeV/nucleon.

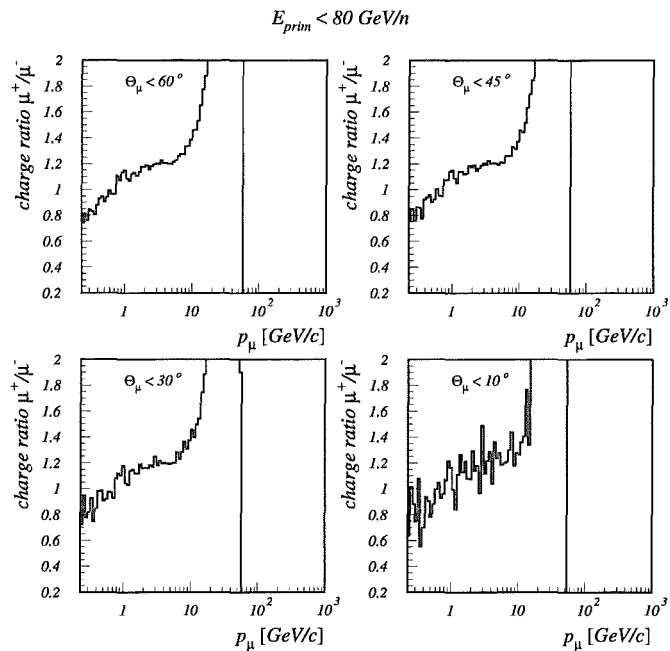


Fig. 8: Charge ratio of positive to negative muons for different limits in the zenith angle for primary energy < 80 GeV/nucleon.

measurements. This decrease of the charge ratio at very low energies could be associated with peculiarities of the interaction models. The present studies have opened a field of interest in view of improving different interaction models, e.g. GHEISHA which is dedicated for the low energy region.

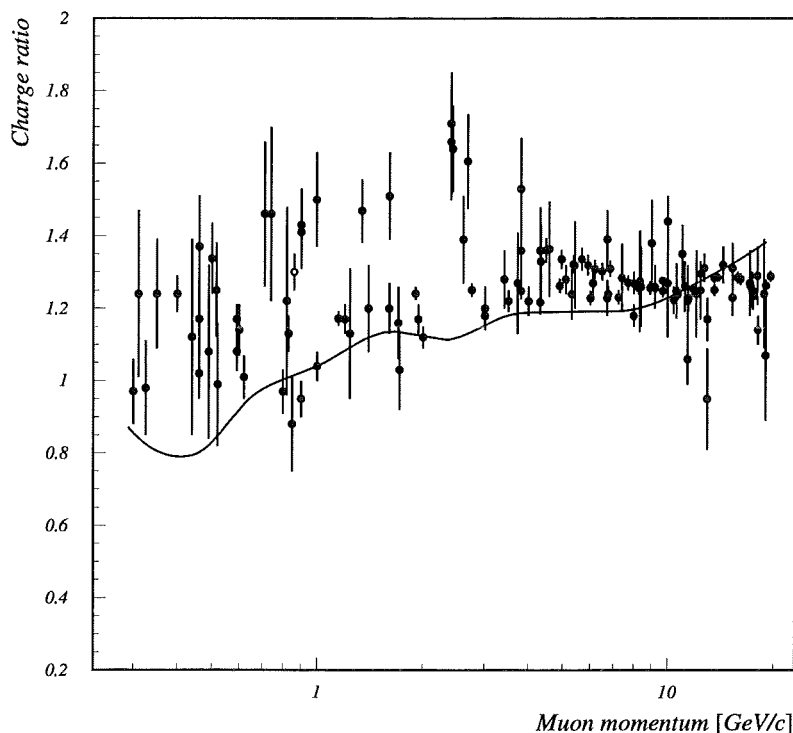


Fig. 9: Charge ratio of vertical muons. From the CORSIKA simulations muons have been collected from $0^\circ - 10^\circ$ zenith angle. Circle – our result. Full list of references in [7].

In conclusion, till the Large Hadron Collider will get into operation in the middle of the next decade, cosmic ray investigations are the only way to extend our knowledge about hadronic interactions to “Terra incognita”. Muon charge ratio spectroscopy, a kind of investigations being still in its infancy, has an interesting information potential for various aspects, about hadronic interactions and about the ratio electron- antineutrinos to electron- neutrinos in the atmospheric flux.

Acknowledgements

The present investigations are embedded in a collaboration between IPNE Bucharest and FZK Karlsruhe, based on the WTZ cooperation understanding of the governments of Romania and Germany and especially supported by the Volkswagen foundation.

We acknowledge gratefully this help and the kind hospitality of the Armenian colleagues during the workshop on Mt.Aragats.

References

- [1] H. Rebel: Proc. Int. Conf. Astrophysics and Cosmology, Calcutta, India, Dec. 20 – 23, 1993, Eds. B. Sinha, p.121;
I. M. Brancus, H. Rebel: Proc. Tours Symp. on Nucl. Phys., France, Aug. 30 – Sept. 2, 1994, Ed. H. Utsunomiya, M. Ohta, J. Galin, G. Münzenberg, World Scientific, Singapore, p.78
- [2] J. N. Capdevielle et al.: KfK-Report 4998 (1992);
D. Heck et al.: FZKA-Report 6019 (1998)
- [3] T. Asatiani et al.: Proc. 14th ICRC, München, Germany, Aug. 15 – 29, 1975, Vol.6, p.2024

- [4] P. Lipari: *Astropart. Phys.* 1 (1995) 195
- [5] M. Yamada et al.: *Phys. Rev. D*44 (1991) 617
- [6] W. Grandegger: KfK-Report 5122 (1993);
T. E. Jannakos, FZKA-Report 5520 (1995)
- [7] B. Vulpescu et al.: FZKA Report 6071 (1998);
Nucl. Instr. and Meth. A 414 (1998) 205
- [8] W. Lohmann et al.: CERN-Report 85-03 (1985)
- [9] O. C. Allkofer and R. D. Andresen, *Nuovo Cimento* 51 (1967) 229;
O. C. Allkofer and K. Klausen, *Acta. Phys. Acad. Scien. Hun.* 29 Suppl. 2 (1970)
698
- [10] H. Fesefeldt, GHEISHA: Report PITHA 85/02, RWTH Aachen, Germany (1985)
- [11] K. Werner, VENUS: *Phys. Rep.* 232 (1993) 87



COLLABORATION LISTS

The ANI collaboration

K.M.Avakian^a, A.A.Chilingarian^a, A.V.Daryan^a, V.S.Eganov^a, A.P.Garyaka^a, G.V.Gharagozyan^a, G.G.Hovsepien^a, V.A.Ivanov^a, N.V.Kabanova^b, S.S.Kazarian^a, E.A.Mamidjanian^a, R.M.Martirosov^a, L.G.Melkumian^a, N.M.Nikolskaya^b, S.I.Nikolsky^b, V.A.Romakhin^b, S.O.Sokhoyan^a, V.V.Subbotin^b, S.V.Ter-Antonian^a, M.Z.Zazian^a

^aYerevan Physics Institute, Yerevan, Republic of Armenia

^bP.N.Lebedev Physical Institute, Moscow, Russian Federation



The KASCADE collaboration

T. Antoni^c, W.D. Apel^c, A.F. Badea^d, K. Bekk^c, K. Bernlöhr^c, E. Bollmann^c, H. Bozdog^d, I.M. Brancus^d, A. Chilingarian^e, K. Daumiller^f, P. Doll^c, J. Engler^c, F. Feßler^c, H.J. Gils^c, R. Glasstetter^f, R. Haeusler^c, W. Hafemann^c, A. Haungs^c, D. Heck^c, J.R. Hörandel^c, K.-H. Kampert^{c,d}, H. Keim^c, J. Kempa^g, H.O. Klages^c, J. Knapp^d, H.J. Mathes^c, H.J. Mayer^c, J. Milke^c, D. Mühlenberg^c, J. Oehlschläger^c, M. Petcu^d, H. Rebel^c, M. Risse^c, M. Roth^c, G. Schatz^c, F.K. Schmidt^c, T. Thouw^c, H. Ulrich^c, A. Vardanyan^e, B. Vulpescu^d, J. Weber^c, J. Wentz^c, T. Wibig^e, T. Wiegert^c, D. Wochele^c, J. Wochele^c, J. Zabierowski^h, S. Zagromski^c

^cInstitut für Kernphysik, Forschungszentrum Karlsruhe, Germany

^dInstitute of Physics and Nuclear Engineering, Bucharest, Romania

^eCosmic Ray Division, Yerevan Physics Institute, Yerevan, Armenia

^fInstitut für Experimentelle Kernphysik, Univ Karlsruhe, Germany

^gUniversity of Lodz, Institute of Physics, Lodz, Poland

^hSoltan Institute for Nuclear Studies, Lodz, Poland

The ANI-TIME collaboration

A.F. Badeaⁱ, H. Bozdogⁱ, I.M. Brancusⁱ, A. Chilingarian^j, H.J. Gils^k, A. Haungs^k, G.G.Hovsepian^j,
V.A.Ivanov^j, R.M.Martirosov^j, H.J. Mathes^k, M. Petcuⁱ, H. Rebel^k, M. Roth^c

ⁱInstitute of Physics and Nuclear Engineering, Bucharest, Romania

^jCosmic Ray Division, Yerevan Physics Institute, Yerevan, Armenia

^kInstitut für Kernphysik, Forschungszentrum Karlsruhe, Germany